R. & M. No. 2952
(5,668, 6,290, 5,917)
A.R.C. Technical Report

MINISTRY OF SUPPLY

AERONAUTICAL RESEARCH COUNCIL
REPORTS AND MEMORANDA

Spring Tab Flutter

PART I

A Theoretical Investigation on Wing–Aileron–Tab Flutter

By
R. A. FRAZER, B.A., D.Sc., and W. P. JONES, M.A.
of the Aerodynamics Division, N.P.L.

PART II

Experiments on Binary Aileron–Tab Flutter

By
C. SCRUTON, B.Sc., J. WILLIAMS, B.Sc., and C. J. W. MILES
of the Aerodynamics Division, N.P.L.

LONDON : HER MAJESTY'S STATIONERY OFFICE
1955
PRICE £1 5s 0d NET

Spring Tab Flutter

Parts I and II

By

R. A. FRAZER, B.A., D.Sc., W. P. JONES, M.A., C. SCRUTON, B.Sc.,
J. WILLIAMS, B.Sc., and C. J. W. MILES,
of the Aerodynamics Division, N.P.L.

Reports and Memoranda No. 2952
July, 1942

CONTENTS

PART I

A Theoretical Investigation on Wing–Aileron–Tab Flutter

CONTENTS—*continued*

PART I—*continued*

Section II. Numerical Applications to Binary Flutter

Section III. Numerical Applications to Ternary Flutter

Section IV. Approximations to Some Binary Inertia-Stiffness Diagrams

PART II

Experiments on Binary Aileron–Tab Flutter

PART I

A Theoretical Investigation on Wing–Aileron–Tab Flutter

By

R. A. FRAZER, B.A., D.Sc., and W. P. JONES, M.A.

Summary.—A theoretical discussion is given of wing–aileron–tab flutter, with special reference to the influence of spring tab control. Numerical applications of the theory are made to two representative types of spring tab, and with the aid of special stability diagrams certain conclusions are drawn regarding the conditions for flutter prevention.

In relation to binary aileron–tab flutter it is shown that certain restrictions on the aileron–tab density ratio should be observed, and that when a balancing mass for the tab is fitted its arms should be limited to a certain length. Calculations relating to ternary flutter indicate that the possibility of ternary flutter occurring when all the possible binary types are absent is very remote.

Introduction.—(*a*) *Scope of the Paper.*—The paper gives a theoretical discussion of wing–aileron–tab flutter with special reference to the influence of spring tab control on the flutter. Section I describes the analytical and graphical methods used, which are based on vortex strip-theory. Section II deals with the calculated binary flutter characteristics of a particular wing system (referred to as aeroplane S), the basic data for which are derived by simplifying assumptions from those of a modern fighter aeroplane. Section III gives numerical applications to ternary flutter, and approximate methods are considered in Section IV. To avoid unnecessary complication of the main text, the derivation of the numerical data is explained in three appendices.

The main purpose of the paper is to indicate the general rules which should be observed in the design of spring tabs in order that flutter may be avoided. Numerical values for critical speeds are occasionally given, but they are intended only to illustrate tendencies and should not be interpreted as attempts to predict the critical speeds of any existing aeroplane. The graphical methods on which the final conclusions of the paper are based, are briefly explained under headings (*h*) and (*i*) of this Introduction. The conclusions reached relate solely to non-preloaded spring tabs.

(*b*) *Spring Tabs Considered.*—The possible advantages in control to be gained from spring tabs have been discussed by Gates[1] and Brown[2]. One form of spring tab is shown in Figs. 1a and 1b: the two diagrams correspond respectively to the cases in which preloading of the spring is absent, and present. Another device which has been fitted experimentally to a *Spitfire* and tested in flight is shown in Fig. 2.

The two devices just mentioned have different elastic characteristics, and will be distinguished as spring tabs Nos. 1 and 2. Both have in common a casing and a spring constrained plunger. With spring tab No. 1 the operating force is applied to the casing, which is mounted in the main wing and connected by a link FM to the tab lever TM; the plunger is attached to the aileron lever AI. With spring tab No. 2, which contains a single compression spring, the casing is mounted in the aileron, and the operating force is applied to a lever BCH. This lever is connected directly to the plunger and also to the tab lever by a link FM.

In the theory two fundamental constants n, N, which are in the nature of gear ratios, are introduced. They are defined by $n = (\mathrm{AF} - \mathrm{AI})/\mathrm{TM}$ and $N = \mathrm{AF}/\mathrm{TM}$ in the case of spring tab No. 1, and by $n = 0$ and $N = \mathrm{HQ} \times \mathrm{CS}/\mathrm{HC} \times \mathrm{TM}$ in the case of spring tab No. 2. If the angular co-ordinates are chosen to be ξ (aileron angle relative to main wing) and β (tab angle relative to aileron) the constant n is the ratio β/ξ when the tab–aileron system is displaced but the spring is assumed centralised and locked. The constant N is the ratio β/ξ when the system is displaced but the control point H is held undisplaced in the direction of the operating force.

(*c*) *The Elastic Cross-Stiffness.*—When ξ and β are adopted as the angular co-ordinates, an elastic cross-stiffness is present with both types of spring tab. This cross-stiffness is the sum of two parts—the first proportional to n times the spring tab stiffness σ, and the second proportional to N times the effective stiffness σ_0 of the control circuit.

(*d*) *Barred Co-ordinates and Dynamical Coefficients.*—The presence of an elastic coupling is a great inconvenience in flutter analysis, and it is generally preferable to choose angular co-ordinates in such a way that such couplings are avoided. For example, with flexure–torsion flutter, the reference centre for the definition of the flexural co-ordinate is usually chosen to be the flexural centre with this special object in view. In the case of the spring tab it is necessary to use a linear transformation of the co-ordinates ξ and β. Amongst the infinite number of possible transformations by means of which the cross-stiffness can be removed, there is a particular one which offers the very great advantage that it depends only on the gear ratios n and N, and not on σ and σ_0. The new angular co-ordinates $\bar{\xi}$, $\bar{\beta}$ are connected with ξ, β by the relations $\xi = \bar{\xi} + \bar{\beta}$ and $\beta = n\bar{\xi} + N\bar{\beta}$. The dynamical coefficients resulting from the transformation, which are of course linear combinations of the original coefficients, are referred to as the ' barred coefficients '. One of the barred direct elastic stiffnesses for the aileron–tab combination is directly proportional to σ_0, the other is proportional to σ, and the cross-stiffness is zero. With normal spring tabs the values of the barred aileron and tab moments of inertia, and of the barred product of inertia, are all roughly of the same order. To reduce the barred product of inertia to zero, the tab would have to be provided with a prohibitive degree of mass overbalance.

(*e*) *The Complete Dynamical System.*—The complete system (Fig. 3) consists of the port and starboard wing–aileron–tab combinations together with the control column and the interconnections. When the springs are not preloaded the possible varieties of flutter are symmetrical flutter (control column locked) and antisymmetrical flutter (control column free). Each variety can involve wing flexure and torsion and displacements of the tab and aileron, but as usually the simpler binary and ternary types will mainly be considered in numerical applications. With antisymmetrical flutter the stiffness σ_0 is not operative. In the case of preloaded spring tabs symmetrical and antisymmetrical oscillations can occur, and more general varieties are perhaps also possible.

(*f*) *Suffix Notation for Dynamical Co-ordinates and Coefficients.*—In view of the large number of parameters involved in the theory, it is convenient to adopt a single suffix notation for the angular co-ordinates and a double suffix notation for the coefficients. Thus the usual angles ϕ, θ, ξ, β denoting wing flexure, wing torsion and the aileron and tab angles, are replaced respectively by q_1, $(l/c_0)q_2$, $(l/c_0)q_3$, $(l/c_0)q_4$, where c_0 denotes the root chord and l is the spanwise distance of the reference section from the root. The typical inertial coefficient then is A_{ij}, and the corresponding non-dimensional coefficient is a_{ij}. For example, a_{33}, a_{44}, a_{34} are the non-dimensional aileron and tab moments of inertia, and the product of inertia. Similarly $\bar{a}_{33}$. $\bar{a}_{44}$, $\bar{a}_{34}$ are the barred coefficients corresponding to the transformed co-ordinates $\bar{q}_1(= q_1)$, $\bar{q}_2(= q_2)$, $\bar{q}_3$, $\bar{q}_4$.

A somewhat similar scheme of notation is used to describe the type and variety of flutter. Thus symmetrical torsion–aileron flutter is indicated concisely as (23s) flutter, antisymmetrical flexure–aileron–tab flutter as (134a) flutter, and so on.

(*g*) *Air-Load Coefficients.*—In flutter analysis attention is usually restricted to critical conditions and to a single complex constituent motion. In the present paper, in order to accord with a notation which has now been standardised for matrices[3], the complex amplitudes corresponding to q_1, q_2, q_3, q_4, are denoted by k_1, k_2, k_3, k_4, so that the critical flexural motion for instance is $q_1 = k_1 e^{2\pi i f t}$, where f denotes the critical frequency.

Now suppose Q_1, Q_2, Q_3, Q_4 to denote the non-dimensional aerodynamic moment coefficients. On the hypothesis of small oscillations the complex amplitudes of each moment coefficient must be linear in k_1, k_2, k_3, k_4 so that Q_1, for example, is given by an expression of the form

$$Q_1 = -(\mathscr{A}_{11}k_1 + \mathscr{A}_{12}k_2 + \mathscr{A}_{13}k_3 + \mathscr{A}_{14}k_4)e^{2\pi i f t},$$

and similarly for the remaining moments. The complex coefficients $\mathscr{A}_{ij} \equiv C_{ij} + iB_{ij}$ are termed the *air-load coefficients*. From dimensional considerations it is evident that, if scale effect is

absent (as is assumed), the air-load coefficients can depend only on the value of the non-dimensional frequency parameter referred to some datum length, *e.g.*, on $\omega \equiv 2\pi f c_0/V$, where V denotes the critical speed and c_0 the root chord.

In the numerical applications the values of the air-load coefficients for aeroplane S are calculated by simple vortex strip-theory, in which the theoretical two-dimensional coefficients are integrated over the span and allowance is made for the distortion modes.

(*h*) *Inertia-Stiffness Diagrams**.—When the flutter is binary and no elastic cross-stiffness is present, the influence of the two moments of inertia and of the two direct elastic stiffnesses can be discussed very conveniently by a graphical method similar to that applied for flexure–torsion flutter by Cicala[4]. The method makes use of a ' base curve ' and a ' frequency parameter curve ', (*e.g.*, Fig. 4), which depend only on the air-load coefficients and the product of inertia and are for convenience usually plotted on separate sheets. The sheet with the base curve is referred to as the inertia-stiffness diagram, and is used as follows. The current values of the moments of inertia are plotted in the third quadrant, and through the inertia point I so obtained the stiffness line IP is drawn having for its slope the ratio of the two elastic stiffness coefficients. Then if P_1 is any intersection of IP with the base curve, and if IM_1 and PM_1 are parallel to the co-ordinate axes, PM_1 is inversely proportional to the square of the critical frequency, and so $\omega^2 PM_1$ is inversely proportional to the square of the corresponding critical speed. The appropriate value of ω^2 is read from the frequency parameter curve. If two such intersections occur there are two critical speeds, and if no intersections occur flutter is avoided. Examples of binary inertia–stiffness diagrams in which the product of inertia also is varied are provided by Figs. 8 to 16. With some additional complications the method can be extended to ternary flutter.

(*i*) *Prevention of Binary Aileron–Tab Flutter.*—In the case of (34) flutter and spring tab No. 2, if N is kept constant and the barred product of inertia $\bar{p}$ ($\equiv \bar{a}_{34}$) is varied, the base curves resemble a set of parallel wedges pointing towards the right and with their vertices in the third quadrant (*see* Figs. 13, 15 and 16). With practical distributions of mass, the values of $\bar{a}_{33}$ and $\bar{a}_{44}$ do not differ greatly from $\bar{p}$, and it is found that the inertia point I always lies near the vertex of the appropriate curve. In order that flutter may be prevented absolutely (*i.e.*, for all values of σ and σ_0) it is necessary that no stiffness line through I shall intersect the base curve. Since the slope of the stiffness line is always positive, the abscissa of I (namely $\bar{a}_{44}$) is required to be less than the numerically smallest abscissa of the curve. Now it is found that this abscissa plots linearly against $\bar{p}$ (Fig. 17). Hence if, in this new diagram, the vertical scale is adopted for $\bar{a}_{44}$, all points J ($\bar{p}$, $\bar{a}_{44}$) lying above the line represent inertial conditions for which flutter is possible, whereas all points below the line represent conditions for which flutter is prevented absolutely. The disadvantages of a low aileron–tab density ratio will be clear from the small sketches in Fig. 17 indicating the type of covering. In para. 16 it is also shown by simple arguments that any addition of mass to the main aileron will result in the inertia point J being displaced in a direction which will improve the stability. On the other hand, addition of mass to the tab ahead of the hinge axis will produce an advantageous displacement of J only when the offset of the mass from the hinge axis is restricted within a certain limit.

The general conclusions regarding the absolute prevention of binary aileron–tab flutter with non-preloaded spring tabs of type No. 2 are stated in para. 16. In paras. 18 and 19 it is shown that the same conclusions are also valid for the more general spring tab type No. 1.

(*j*) *Prevention of Ternary Flutter.*—The problem of ternary flutter prevention is considered in paras. 20 to 23, but owing to the complicated nature of the inertia–stiffness diagrams simple stability conditions similar to those for binary flutter cannot be obtained. It is shown that both flexure–aileron–tab and torsion–aileron–tab flutter are possible under certain conditions when aileron–tab flutter is absent. Flexure–aileron–tab flutter is eliminated by static balance of the aileron ($a_{13} = 0$), but torsion–aileron–tab flutter is still possible. This also is prevented by balancing the aileron dynamically ($a_{23} = 0$). The possibility of ternary flutter occurring when all the binary types are absent is very remote.

* A description of inertia-stiffness diagrams based on classical derivative theory is given in para. 10.

Acknowledgements.—The writers wish to express their indebtedness to Miss S. Skan, Mrs. J. Muir and Miss J. Francis, of the Aerodynamics Division, who carried out the greater part of the numerical work of the investigation.

Section I. General Theory

1. *Elastic Constraints.*—(*a*) *Spring Tabs.*—It is assumed first that the preloaded spring tab No. 1 (*see* Fig. 1b) is fitted, and that $\xi = 0$, $\beta = 0$ when the plunger is centralized. When both the aileron and the tab are given small displacements the rearward displacement of the plunger from its initial position is $\mathrm{AI}\xi$, and the corresponding displacement of the casing is $\mathrm{AF}\xi - \mathrm{TM}\beta$. Thus the right-hand spring will be picked up if

$$\mathrm{AI}\xi > \mathrm{AF}\xi - \mathrm{TM}\beta ,$$

i.e., if

$$r\beta > R\xi ,$$

where $r \equiv \mathrm{TM}$ and $R \equiv \mathrm{AF} - \mathrm{AI}$. In this case, if P_0 denotes the preloading force in the spring, and σ denotes the stiffness rate, the strain energy is given by

$$2W_1 = \sigma\left(r\beta - R\xi + \frac{P_0}{\sigma}\right)^2 . \qquad .. \quad .. \quad .. \quad .. \quad .. \quad (1.1)$$

On the other hand, if $r\beta < R\xi$, the left-hand spring will be engaged, and the strain energy is then given by

$$2W_1 = \sigma\left(R\xi - r\beta + \frac{P_0}{\sigma}\right)^2 . \qquad .. \quad .. \quad .. \quad .. \quad .. \quad (1.2)$$

If spring tab No. 2 is fitted (*see* Fig. 2) the additional spring compression when $\beta > 0$ is $(\mathrm{CK} \times \mathrm{TM/CS})\beta$. Hence if σ denotes the stiffness rate and P_0 the preloading force, the strain energy is given by

$$2W_1 = \sigma\left(r\beta + \frac{P_0}{\sigma}\right)^2 , \qquad .. \quad .. \quad .. \quad .. \quad .. \quad .. \quad (1.3)$$

where $r \equiv (\mathrm{CK} \times \mathrm{TM/CS})$. On comparison of (1.1) and (1.3) it is seen that the theory for spring tab No. 2 is covered by that for the particular case $R = 0$ of spring tab No. 1.

(*b*) *Control Circuit.*—In Fig. 3 the connections to the control column are represented by segments of cables tensioned by springs, each of stiffness σ_0. To simplify the diagram further, the actual control column is replaced by a nominal column $\mathrm{C_0}$ mounted in the plane of the wings, and the movements are shown transmitted to the tabs through levers $\mathrm{L_p}$, $\mathrm{L_s}$.

The flexural and torsional wing displacements do not (in general) contribute to the strain energy of the control connections. Thus the effective variables to be considered are ξ_p, β_p (the port aileron and tab angles), ξ_s, β_s (the corresponding starboard angles), and lateral displacement Y of the points of attachment of the control cables to $\mathrm{C_0}$.

Suppose first that spring tabs No. 1 are fitted. Then in a general displacement of the complete system the rearward displacement of the point H in Fig. 1b for the port wing is $\mathrm{AF}\xi_p - \mathrm{TM}\beta_p$. Hence the corresponding displacement of the point $\mathrm{H_p}'$ of the lever $\mathrm{L_p}$ in Fig. 3, measured inwards along the span is

$$R'\xi_p - r'\beta_p ,$$

where $R' \equiv \nu\mathrm{AF}$, $r' \equiv \nu\mathrm{TM}$, and ν is a gearing constant. Similar considerations apply for the starboard wing. It readily follows that the strain energy of the control connections (excluding spring tabs) is given by

$$\begin{aligned} 2W_2 = {} & 2\sigma_0\{(R'\xi_p - r'\beta_p)^2 + (R'\xi_s - r'\beta_s)^2 + 2Y^2\} \\ & + 4\sigma_0 Y\{(R'\xi_p - r'\beta_p) - (R'\xi_s - r'\beta_s)\} . \qquad .. \quad .. \quad .. \quad .. \quad (1.4) \end{aligned}$$

The same expression applies for spring tabs No. 2 (Fig. 2), except that for this case $R' \equiv \nu\mathrm{HQ}$ and $r' \equiv \nu(\mathrm{HC} \times \mathrm{TM/CS})$.

(*c*) *Complete System.*—The total strain energy, obtained by the addition of W_1 and W_2 and the usual terms arising from wing flexure and wing torsion, is given by

$$\begin{aligned} 2W = {} & l_\phi(\phi_p^2 + \phi_s^2) + m_\theta(\theta_p^2 + \theta_s^2) \\ & + \sigma\left\{\left(r\beta_p - R\xi_p \pm \frac{P_0}{\sigma}\right)^2 + \left(r\beta_s - R\xi_s \pm \frac{P_0}{\sigma}\right)^2\right\} \\ & + 2\sigma_0\{(R'\xi_p - r'\beta_p)^2 + (R'\xi_s - r'\beta_s)^2 + 2Y^2\} \\ & + 4\sigma_0 Y\{R'\xi_p - r'\beta_p) - (R'\xi_s - r'\beta_s)\}\,. \qquad .. \quad .. \quad .. \quad .. \quad (1.5) \end{aligned}$$

In each of the round brackets containing ambiguities of sign, the positive or negative sign is to be taken according as $r\beta > R\xi$ or $< R\xi$ for the relevant wing.

The complete set of elastic moments on the port wing–aileron–tab combination, obtained by differentiation of the strain energy function, can be expressed by matrices as

$$\begin{aligned} \{L_{ep}, M_{ep}, H_{ep}, T_{ep}\} &= \left\{\frac{\partial}{\partial\phi_p}, \frac{\partial}{\partial\theta_p}, \frac{\partial}{\partial\xi_p}, \frac{\partial}{\partial\beta_p}\right\} W \\ &= E\chi_p \pm P_0\tilde{\omega} + 2\sigma_0\vartheta Y\,, \qquad .. \quad .. \quad .. \quad .. \quad .. \quad (1.6) \end{aligned}$$

where

$$\chi_p \equiv \{\phi_p, \theta_p, \xi_p, \beta_p\}\,,$$

$$E \equiv \begin{bmatrix} l_\phi & 0 & 0 & 0 \\ 0 & m_\theta & 0 & 0 \\ 0 & 0 & \sigma R^2 + 2\sigma_0 R'2 & -\sigma Rr - 2\sigma_0 R'r' \\ 0 & 0 & -\sigma Rr - 2\sigma_0 R'r' & \sigma r^2 + 2\sigma_0 r'^2 \end{bmatrix},$$

$$\tilde{\omega} \equiv \{0 \quad 0 \quad -R \quad r\}\,,$$

$$\vartheta \equiv \{0 \quad 0 \quad R' \quad -r'\}\,.$$

The corresponding starboard elastic moments are

$$\{L_{es}, M_{es}, H_{es}, T_{es}\} = E\chi_s \pm P_0\tilde{\omega} - 2\sigma_0\vartheta Y\,, \qquad .. \quad .. \quad .. \quad .. \quad .. \quad (1.7)$$

and the restoring force on the ' control column ' (mass M_0) is

$$\begin{aligned} \frac{\partial W}{\partial Y} &= 2\sigma_0 R'(\xi_p - \xi_s) - 2\sigma_0 r'(\beta_p - \beta_s) + 4\sigma_0 Y \\ &= 2\sigma_0\vartheta'(\chi_p - \chi_s) + 4\sigma_0 Y\,, \qquad .. \quad .. \quad .. \quad .. \quad .. \quad (1.8) \end{aligned}$$

where ϑ' denotes the transposed of ϑ, *i.e.*, the row $[0, 0, R', -r']$.

(*d*) *Spring Tab Gear Ratios.*—The constants defined by

$$n \equiv R/r \qquad N \equiv R'/r' \quad .. \quad .. \quad .. \quad .. \quad .. \quad (1.9)$$

play an important part in the theory. They will be referred to as the *spring tab gear ratios.*

The first constant n measures the ratio of tab angle to aileron angle when the system is moved but the spring is assumed centralized and locked. The second constant N measures the ratio of tab angle to aileron angle when the system is moved but the control point H is held undisplaced in the direction of the operating force (*see* Figs. 1 and 2). With spring tab No. 2, the first gear ratio $n = 0$.

2. *The Dynamical Equations.*—It will first be assumed that the plungers of the spring tabs are in central position when the system is in equilibrium.

Let $U_p \equiv \{L, M, H, T\}_p$ and $U_s \equiv \{L, M, H, T\}_s$ denote the columns of the increments of aerodynamical moment on the port and starboard sides in the disturbed motion : also let A denote the inertia matrix appropriate to each wing system, and E, $\tilde{\omega}$, ϑ be the matrices defined for equations (1.6). Then the dynamical equations are as follows.

Port Wing

$$\left(A\frac{d^2}{dt^2} + E\right)\chi_p \pm P_0\tilde{\omega} + 2\sigma_0\vartheta Y = U_p \,. \quad .. \quad .. \quad .. \quad .. \quad .. \quad (2.1)$$

Starboard Wing

$$\left(A\frac{d^2}{dt^2} + E\right)\chi_s \pm P_0\tilde{\omega} - 2\sigma_0\vartheta Y = U_s \,. \quad .. \quad .. \quad .. \quad .. \quad .. \quad (2.2)$$

Control Column (of effective mass M_0)

$$M_0\frac{d^2Y}{dt^2} + 2\sigma_0\vartheta'(\chi_p - \chi_s) + 4\sigma_0 Y = 0 \,. \quad .. \quad .. \quad .. \quad .. \quad .. \quad (2.3)$$

To express these equations in the non-dimensional form a new time variable τ, and modified dynamical co-ordinates q are introduced, defined by

$$\left.\begin{array}{llll} \tau \equiv tV/c_0\,; & q_0 \equiv Y/l & & \\ q_1 \equiv \phi\,; & q_2 \equiv (c_0/l)\theta\,; & q_3 \equiv (c_0/l)\xi\,; & q_4 \equiv (c_0/l)\beta \end{array}\right\} \,. \quad .. \quad .. \quad (2.4)$$

The last four relations can be expressed by matrices as

$$\chi = (l/c_0)\mu q$$

where $q \equiv \{q_1, q_2, q_3, q_4\}$ and

$$\mu \equiv \begin{bmatrix} c_0/l & 0 & 0 & 0 \\ 0 & 1 & 0 & 0 \\ 0 & 0 & 1 & 0 \\ 0 & 0 & 0 & 1 \end{bmatrix} \,. \quad .. \quad .. \quad .. \quad .. \quad .. \quad (2.5)$$

On application of the preceding transformations to (2.1), premultiplication of the resulting equations by μ to retain symmetry of the inertial and elastic matrices, and division throughout by $\rho V^2 l c_0^2$, we obtain

$$(aD^2 + e)q_p \pm p_0\tilde{\omega} + n_0\vartheta q_0 = Q_p \,, \quad .. \quad .. \quad .. \quad .. \quad (2.6)$$

in which

$$D \equiv \frac{d}{d\tau}\,; \qquad a \equiv \mu A\mu/\rho l c_0^4\,; \qquad e \equiv \mu E\mu/\rho V^2 l c_0^2$$

$$p_0 \equiv P_0/\rho V^2 l^2 c_0\,; \qquad n_0 \equiv 2\sigma_0/\rho V^2 l c_0 \,,$$

and

$$Q_p \equiv \frac{\mu U_p}{\rho V^2 l^2 c_0} = \left\{\frac{L}{\rho V^2 l^3}\,,\ \frac{M}{\rho V^2 l^2 c_0}\,,\ \frac{H}{\rho V^2 l^2 c_0}\,,\ \frac{T}{\rho V^2 l^2 c_0}\right\}_p .$$

A similar treatment of (2.2) yields

$$(aD^2 + e)q_s \pm p_0\tilde{\omega} - n_0\vartheta q_0 = Q_s \,, \quad .. \quad .. \quad .. \quad .. \quad (2.7)$$

while (2.3), expressed non-dimensionally, can be written

$$(m_0 D^2 + 2c_0 n_0)q_0 + n_0\vartheta'(q_p - q_s) = 0 \,, \quad .. \quad .. \quad .. \quad .. \quad (2.8)$$

where $m_0 \equiv M_0/\rho c_0^2 l$.

In (2.6) the upper or the lower sign for $\tilde{\omega}$ must be taken according as $rq_{4p} - Rq_{3p} > 0$ or < 0. Similarly in (2.7) the upper or lower signs are taken according as $rq_{4s} - Rq_{3s} > 0$ or < 0. With non-preloaded springs these restrictions do not arise since $p_0 = 0$. The dynamical equations with

the simplification $p_0 = 0$ are also valid for small disturbed motions and preloaded or non-preloaded springs, if the controls are assumed to be non-centralized and the force applied to the control column is kept steady. In this case the dynamical co-ordinates and the aerodynamical moments represent the deviations from the equilibrium values.

The full expressions for the non-dimensional inertial and elastic coefficients a_{ij}, e_{ij} are given by

$$a \equiv \begin{bmatrix} A_{11}/\rho l^3 c_0^2 & A_{12}/\rho l^2 c_0^3 & A_{13}/\rho l^2 c_0^3 & A_{14}/\rho l^2 c_0^3 \\ A_{21}/\rho l^2 c_0^3 & A_{22}/\rho l c_0^4 & A_{23}/\rho l c_0^4 & A_{24}/\rho l c_0^4 \\ A_{31}/\rho l^2 c_0^3 & A_{32}/\rho l c_0^4 & A_{33}/\rho l c_0^4 & A_{34}/\rho l c_0^4 \\ A_{41}/\rho l^2 c_0^3 & A_{42}/\rho l c_0^4 & A_{43}/\rho l c_0^4 & A_{44}/\rho l c_0^4 \end{bmatrix}, \quad .. \quad .. \quad .. \quad .. \quad (2.9)$$

$$e \equiv \begin{bmatrix} l_\phi/\rho V^2 l^3 & 0 & 0 & 0 \\ 0 & m_\theta/\rho V^2 l c_0^2 & 0 & 0 \\ 0 & 0 & (\sigma R^2 + 2\sigma_0 R'^2)/\rho V^2 l c_0^2 & -(\sigma R r + 2\sigma_0 R' r')/\rho V^2 l c_0^2 \\ 0 & 0 & -(\sigma R r + 2\sigma_0 R' r')/\rho V^2 l c_0^2 & (\sigma r^2 + 2\sigma_0 r'^2)/\rho V^2 l c_0^2 \end{bmatrix}. \quad (2.10)$$

3. *Classical Derivative Theory and Vortex Theory.*—The aerodynamic moments can be expressed either by derivative coefficients or by the more general air-load coefficients of vortex theory. It is necessary to explain the different viewpoints.

(*a*) *Classical Derivative Theory.*—Here the moment coefficients Q are represented by expressions which are linear in the accelerations, velocities, and displacements. Thus say

$$-Q = (\hat{a}D^2 + \hat{b}D + \hat{c})q$$

where $D \equiv d/d\tau$ and $\hat{a}$, $\hat{b}$, $\hat{c}$ are the matrices of the constant derivative coefficients. An important consequence of this assumption is the linearization of the dynamical equations. The most general disturbed motion can then be represented by a superposition of a finite number of exponential constituent motions $q = k\,e^{\lambda\tau}$, and the relevant values of λ are the roots of the usual determinantal equation. Moreover, the free constants are determined uniquely by the displacements and velocities which define the initial disturbance. In this theory the aerodynamic moments corresponding to the typical constituent are given by

$$-Q = (\hat{a}\lambda^2 + \hat{b}\lambda + \hat{c})k\,e^{\lambda\tau} \equiv \mathscr{A}k\,e^{\lambda\tau}, \text{ say.} \quad .. \quad .. \quad .. \quad .. \quad (3.1)$$

In particular, with a simple harmonic constituent of frequency f, the appropriate value of λ is $i\omega$, where ω denotes the frequency parameter $\omega = 2\pi f c_0/V$, and then

$$\mathscr{A} = -\hat{a}\omega^2 + \hat{c} + i\hat{b}\omega\,. \quad .. \quad .. \quad .. \quad .. \quad .. \quad .. \quad (3.2)$$

(*b*) *Vortex Theory.*—In this theory only the critical type of motion $q = k\,e^{i\omega\tau}$ is usually considered. Then

$$-Q = \mathscr{A}k\,e^{i\omega\tau} \equiv (C + iB)k\,e^{i\omega\tau}, \text{ say,} \quad .. \quad .. \quad .. \quad .. \quad .. \quad (3.3)$$

where $\mathscr{A}$ is the matrix of the 'air-load coefficients'. These coefficients are functions of ω only.

A theory restricted to simple harmonic oscillations is sufficient for calculations of critical speeds, but is inadequate for a proof of the familiar resolution theorems concerning symmetrical and antisymmetrical oscillations. Nor can it be applied with problems such as the discussion of the stability of steady oscillations in the case of preloaded spring tabs. The appropriate generalizations will be indicated without any attempt at formal proof.

The essential necessary assumptions are that the most general motion is expressible by the superposition of exponential constituents $q = k\,e^{\lambda\tau}$, where $\lambda \equiv \mu + i\omega$ is in general complex, and that the moment coefficients corresponding to that constituent are

$$-Q = \mathscr{A} k\, e^{\lambda\tau}, \qquad \ldots \qquad (3.4)$$

in which $\mathscr{A}$ depends on λ only. The damping parameter μ and the frequency parameter ω are here defined in terms of the true damping factor μ_0 and the true frequency f by the relations $\mu \equiv \mu_0 c_0/V$ and $\omega \equiv 2\pi f c_0/V$.

Now consider the small motions of a quite general aerodynamic system given by

$$(aD^2 + e)q = Q\,,$$

where, as previously, $D \equiv d/d\tau$. The trial solution $q = k\,e^{\lambda\tau}$, in conjunction with (3.4) here leads to the condition

$$(a\lambda^2 + e + \mathscr{A})k = 0\,,$$

so that the permissible values of λ are given by the determinantal equation

$$|a\lambda^2 + e + \mathscr{A}| = 0\,. \qquad \ldots \qquad (3.5)$$

The corresponding equation obtained by classical derivative theory would be

$$|(a + \hat{a})\lambda^2 + \hat{b}\lambda + e + \hat{c}| = 0\,. \qquad \ldots \qquad (3.6)$$

If the system has n degrees of freedom (3.6) has $2n$ roots; on the other hand, (3.5) has an infinite number, since $\mathscr{A}$ is in general a matrix of transcendental functions of λ. Hence, according to classical theory, a disturbed motion is fully determined by $2n$ conditions, *e.g.*, n displacements and n velocities at a given starting instant. Whereas, in vortex theory, the term ' initial disturbance ' is strictly speaking meaningless. For example, suppose a wing to be moved inexorably in any manner before $t = 0$, and to be released at $t = 0$ with known velocities and displacements. Then, according to classical theory, the ensuing motion is quite independent of the movements before $t = 0$. On the other hand, vortex theory would take into account the antecedent air disturbances.

In the present paper vortex theory is adopted in preference to the simpler classical theory, since in the particular numerical applications considered all the air-load coefficients required can be calculated directly.

4. *Symmetrical and Antisymmetrical Oscillations.*—With non-preloaded spring tabs, or with preloaded spring tabs oscillating about a non-central equilibrium position, equations (2.6), (2.7) and (2.8) are applicable with the simplification $p_0 = 0$. In this case, if a typical constituent motion is denoted by $\{k_p, k_s, k_0\}e^{\lambda\tau}$ and the aerodynamic moments are defined by (3.4), the equations require that

$$\begin{aligned}(a\lambda^2 + e + \mathscr{A})k_p + n_0\vartheta k_0 &= 0\,,\\ (a\lambda^2 + e + \mathscr{A})k_s - n_0\vartheta k_0 &= 0\,,\\ (m_0\lambda^2 + 2c_0n_0)k_0 + n\vartheta'(k_p - k_s) &= 0\,.\end{aligned}$$

These may be written

$$\begin{aligned}(a\lambda^2 + e + \mathscr{A})(k_p + k_s) &= 0\,,\\ (a\lambda^2 + e + \mathscr{A})(k_p - k_s) + 2n_0\vartheta k_0 &= 0\,,\\ (m_0\lambda^2 + 2c_0n_0)k_0 + n\vartheta'(k_p - k_s) &= 0\,,\end{aligned}$$

and elimination of the complex amplitudes leads to the determinantal equation

$$\begin{vmatrix} a\lambda^2 + e + \mathscr{A} & 0 & 0 \\ 0 & a\lambda^2 + e + \mathscr{A} & 2n_0\vartheta \\ 0 & n\vartheta' & m_0\lambda^2 + 2c_0n_0 \end{vmatrix} = 0\,.$$

The permissible values of λ are thus given either by

$$|a\lambda^2 + e + \mathscr{A}| = 0 \quad .. \quad .. \quad .. \quad (4.1)$$

in conjunction with $k_p = k_s$ and $k_0 = 0$ (symmetrical oscillations): or by

$$\begin{vmatrix} a\lambda^2 + e + \mathscr{A} & 2n_0\vartheta \\ n_0\vartheta' & m_0\lambda^2 + 2c_0n_0 \end{vmatrix} = 0 \quad .. \quad .. \quad .. \quad (4.2)$$

in conjunction with $k_p = -k_s$ (antisymmetrical oscillations).

When, as will be assumed throughout, the inertia of the control column can be neglected ($m_0 = 0$), (4.2) simplifies to

$$|a\lambda^2 + \varepsilon + \mathscr{A}| = 0 \quad .. \quad .. \quad .. \quad (4.3)$$

where

$$\varepsilon \equiv e - \frac{n_0}{c_0}\vartheta\vartheta' .$$

The matrix ε, giving the elastic stiffnesses appropriate to the antisymmetrical oscillations, is then defined similarly to e (*see* (2.10)) but with the terms dependent on σ_0 omitted.

In the more complicated case where the spring tabs are preloaded and oscillate about the central position, both symmetrical and antisymmetrical oscillations can occur, but a formal proof that these yield the most general motion has not yet been devised. The symmetrical oscillations (in which $q_p = q_s$, $q_0 = 0$ and the terms involving p_0 have the same signs) are given by

$$(aD^2 + e)q \pm p_0\tilde{\omega} = Q ,$$

where the upper or the lower sign is taken according as $rq_1 - Rq_3 > 0$ or < 0. The antisymmetrical oscillations are given similarly by

$$(aD^2 + \varepsilon)q \pm p_0\tilde{\omega} = Q .$$

5. *Elimination of the Elastic Cross-Stiffness.*—For a discussion of the stability it is convenient to remove the cross-stiffnesses which are present in the elastic matrices e and ε. This requires a change of the aileron and tab co-ordinates q_3, q_4 to new ' barred ' co-ordinates q_3, q_4, as explained in the Introduction. If a general transformation is assumed, say

$$q_3 = u\bar{q}_3 + v\bar{q}_4 .$$
$$q_4 = w\bar{q}_3 + z\bar{q}_4 ,$$

it is readily shown that the cross-stiffness will be absent in the transformed Langrangian equations provided

$$\sigma r^2(nu - w)(nv - z) + 2\sigma_0 r'^2(Nu - w)(Nv - z) = 0 , \quad .. \quad .. \quad .. \quad (5.1)$$

where n ($\equiv R/r$) and N ($\equiv R'/r'$) denote the gear ratios (*see* (1.9)). This condition is satisfied for all values of σ and σ_0 if the free constants are chosen to be $u = v = 1$, $w = n$, $z = N$. The relations connecting the original and the modified co-ordinates then are

$$\left.\begin{aligned} q_3 &= \bar{q}_3 + \bar{q}_4 , \\ q_4 &= n\bar{q}_3 + N\bar{q}_4 , \end{aligned}\right\} \quad .. \quad .. \quad .. \quad .. \quad .. \quad .. \quad (5.2)$$

to which for symmetry may be added $q_1 = \bar{q}_1$, $q_2 = \bar{q}_2$. When this transformation is applied, the equations for symmetrical oscillations become

$$(aD^2 + \bar{e} + \bar{\mathscr{A}})\bar{q} = 0 , \quad .. \quad .. \quad .. \quad (5.3)$$

where the new inertial coefficients $\bar{a}_{ij}$ are given by

$$\begin{bmatrix} a_{11} & a_{12} & a_{13}+na_{14} & a_{13}+Na_{14} \\ a_{21} & a_{22} & a_{23}+na_{24} & a_{23}+Na_{24} \\ a_{31}+na_{41} & a_{32}+na_{42} & a_{33}+n(a_{34}+a_{43})+n^2a_{44} & a_{33}+Na_{34}+na_{43}+nNa_{44} \\ a_{31}+Na_{41} & a_{32}+Na_{42} & a_{33}+na_{34}+Na_{43}+nNa_{44} & a_{33}+N(a_{34}+a_{43})+N^2a_{44} \end{bmatrix}, \quad (5.4)$$

the new elastic coefficients $\bar{e}_{ij}$ are given by

$$\begin{bmatrix} l_\phi/\rho V^2 l^3 & 0 & 0 & 0 \\ 0 & m_0/\rho V^2 l c_0^2 & 0 & 0 \\ 0 & 0 & 2\sigma_0 r'^2(N-n)^2/\rho V^2 l c_0^2 & 0 \\ 0 & 0 & 0 & \sigma r^2(N-n)^2/\rho V^2 l c_0^2 \end{bmatrix}, \quad (5.5)$$

and the new air-load coefficients $\bar{\mathscr{A}}_{ij} \equiv \bar{C}_{ij} + i\bar{B}_{ij}$ are defined similarly to (5.4).

The results just stated are also applicable for the antisymmetrical oscillations except that $\sigma_0 = 0$ in (5.5).

From (3.3) and (5.3) it is seen that for critical conditions of the system

$$|-\bar{a}\omega^2 + \bar{e} + \bar{C} + i\bar{B}| = 0\,. \quad (5.6)$$

For the further treatment of (5.6) it is convenient to introduce the further symbols

$$X' = \bar{e}_{11}, \quad Y' = \bar{e}_{22}, \quad Z' = \bar{e}_{33}, \quad W' = \bar{e}_{44}, \quad (5.7)$$

$$\left.\begin{aligned} X'/\omega^2 &\equiv X + \bar{a}_{11} = l_\phi/4\pi^2\rho l^3 c_0^2 f^2\,, \\ Y'/\omega^2 &\equiv Y + \bar{a}_{22} = m_0/4\pi^2\rho l c_0^4 f^2\,, \\ Z'/\omega^2 &\equiv Z + \bar{a}_{33} = 2\sigma_0 r'^2(N-n)^2/4\pi^2\rho l c_0^4 f^2\,, \\ W'/\omega^2 &\equiv W + \bar{a}_{44} = \sigma r^2(N-n)^2/4\pi^2\rho l c_0^4 f^2, \end{aligned}\right\} \quad (5.8)$$

$$\bar{D}_{ij} \equiv -\bar{a}_{ij}\omega^2 + C_{ij}\,, \quad (5.9)$$

$$x \equiv X' + \bar{D}_{11}; \quad y \equiv Y' + \bar{D}_{22}; \quad z \equiv Z' + \bar{D}_{33}; \quad w \equiv W' + \bar{D}_{44} \quad (5.10)$$

The determinant (5.6), expressed at length, is then

$$\begin{vmatrix} x+i\bar{B}_{11} & \bar{D}_{12}+i\bar{B}_{12} & \bar{D}_{13}+i\bar{B}_{13} & \bar{D}_{14}+i\bar{B}_{14} \\ \bar{D}_{21}+i\bar{B}_{21} & y+i\bar{B}_{22} & \bar{D}_{23}+i\bar{B}_{23} & \bar{D}_{24}+i\bar{B}_{24} \\ \bar{D}_{31}+i\bar{B}_{31} & \bar{D}_{32}+i\bar{B}_{32} & z_{33}+i\bar{B}_{33} & \bar{D}_{34}+i\bar{B}_{34} \\ \bar{D}_{41}+i\bar{B}_{41} & \bar{D}_{42}+i\bar{B}_{42} & \bar{D}_{43}+i\bar{B}_{43} & w+i\bar{B}_{44} \end{vmatrix} = 0\,. \quad (5.11)$$

The preceding definitions, and equations are also applicable for antisymmetrical oscillations, with the simplification $Z' = 0$. They can also be applied for divergence speeds, which correspond to $\omega = 0$. In this case there is the simplification $\bar{B}_{ij} = 0$.

6. *Natural Frequencies in Vacuo and in Still Air.*—In the present theory a distinction is drawn between the natural frequencies f_v appropriate to oscillations *in vacuo* and the frequencies f_a appropriate to oscillation in still 'perfect air'. The equation giving the frequencies f_v can be

deduced from (5.11) by omission of the air-load coefficients and division of the rows by ω^2. If X, Y, Z, W are as defined by (5.8), the required equation is

$$\begin{vmatrix} X_v & -\bar{a}_{12} & -\bar{a}_{13} & -\bar{a}_{14} \\ -\bar{a}_{21} & Y_v & -\bar{a}_{23} & -\bar{a}_{24} \\ -\bar{a}_{31} & -\bar{a}_{32} & Z_v & -\bar{a}_{34} \\ -\bar{a}_{41} & -\bar{a}_{42} & -\xi_{43} & W_v \end{vmatrix} = 0 \ldots \quad \ldots \quad \ldots \quad \ldots \quad (6.1)$$

To obtain the corresponding equation for oscillations in still air, use is made of the asymptotic expressions for the air-load coefficients. When $\omega \to \infty$ $(V \to 0)$ it is found that

$$\bar{C}_{ij}/\omega^2 \to -\bar{\gamma}_{ij}\,; \qquad \bar{B}_{ij}/\omega^2 \to 0\,, \qquad \ldots \quad \ldots \quad \ldots \quad \ldots \quad (6.2)$$

where $\bar{\gamma}_{ij}$ are positive constants such that $\bar{\gamma}_{ij} = \bar{\gamma}_{ji}$, which represent the aerodynamic (or 'apparent additional') moments and products of inertia of the system in still air. The limiting form of (5.11), when the rows are divided by ω^2 and $\omega \to \infty$, is

$$\begin{vmatrix} X_a - \bar{\gamma}_{11} & -\bar{a}_{12} - \bar{\gamma}_{12} & -\bar{a}_{13} - \bar{\gamma}_{13} & -\bar{a}_{14} - \bar{\gamma}_{14} \\ -\bar{a}_{21} - \bar{\gamma}_{21} & Y_a - \bar{\gamma}_{22} & -\bar{a}_{23} - \bar{\gamma}_{23} & -\bar{a}_{24} - \bar{\gamma}_{24} \\ -\bar{a}_{31} - \bar{\gamma}_{31} & -\bar{a}_{32} - \bar{\gamma}_{32} & Z_a - \bar{\gamma}_{33} & -\bar{a}_{34} - \bar{\gamma}_{34} \\ -\bar{a}_{41} - \bar{\gamma}_{41} & -\bar{a}_{42} - \bar{\gamma}_{42} & -\bar{a}_{43} - \bar{\gamma}_{43} & W - \bar{\gamma}_{44} \end{vmatrix} = 0\,. \quad \ldots \quad (6.3)$$

7. *The Inertial Coefficients.*—In past theoretical investigations the control surfaces have usually been treated as rigid and provided with two pivots only. However, on modern aeroplanes control surfaces with three or more pivots, or even with a continuous 'piano' type of hinge, are not uncommon. In the present analysis it is supposed that both the aileron and the tab are provided with hinges which are effectively continuous along the span and capable of bending deformation with the wing. On the other hand, since some limitation is necessary on the number of degrees of freedom, the control surfaces are treated as rigid in torsion. The assumption of continuous hinges ensures continuous connection between the control surfaces in all wing sections, and is necessary for a satisfactory calculation of the air-load coefficients.

Now suppose the port wing, for example, to be given a general displacement ϕ, θ, ξ, β and let z_{w-a-t}, z_{a-t}, z_t denote, respectively the vertical displacements of a general point of the main wing, of the main aileron, and of the tab. The terms 'main wing' and 'main aileron' here mean the parts of the wing that remain when the aileron and tab are removed, and the part of the aileron that remains when the tab is removed. Then

$$z_{w-a-t} = \phi l f(\eta) + \theta x F(\eta)\,, \quad \ldots \quad \ldots \quad \ldots \quad \ldots \quad \ldots \quad \ldots \quad \ldots \quad \ldots \quad (7.1)$$

where, as usual $\eta = y/l$, and $f(\eta)$, $F(\eta)$ are the flexural and torsional distortion modes of the wing proper. These functions are assumed chosen such that $f(\eta) = F(\eta) = 1$ at the reference section $\eta = 1$.

Again, the twist of the wing proper at section η is $\theta F(\eta)$. Hence the local aileron angle (*i.e.*, the inclination to the wing at section η) is

$$\xi_\eta = \xi + \theta\{1 - F(\eta)\}\,.$$

It follows that, if the aileron hinge axis lies at distance d_a behing OY*,

$$z_{a-t} = \phi l f(\eta) + [x + d_a\{F(\eta) - 1\}]\theta + (x - d_a)\xi\,. \quad \ldots \quad \ldots \quad \ldots \quad \ldots \quad (7.2)$$

Moreover, if the tab hinge axis lies at distance d_t behind OY

$$z_t = z_a + (x - d_t)\beta\,. \quad \ldots \quad \ldots \quad \ldots \quad \ldots \quad \ldots \quad \ldots \quad \ldots \quad \ldots \quad (7.3)$$

* It is here assumed for simplicity that the hinge-line is parallel to OY.

It should be noted that when $\xi = 0$ (aileron locked central at the reference section) (7.2) does not reduce to (7.1). Thus, in the discussion of flexure–torsion flutter, the distortion modes must be taken as given by (7.1) for points of the main wing, and by (7.2) with $\xi = 0$ for points of the aileron.

The inertial coefficients can be deduced from (7.1), (7.2), (7.3) in the usual way by expansion of the kinetic energy function

$$2T = \Sigma\, m\dot{z}_{w-a-t}^{\,2} + \Sigma\, m\dot{z}_{a-t}^{\,2} + \Sigma\, m\dot{z}_{t}^{\,2}\,,$$

where the summations are taken over the appropriate parts of the system. To express the results conveniently, let $\underset{w}{\Sigma}$, $\underset{a}{\Sigma}$, $\underset{t}{\Sigma}$ denote respectively summations taken over the *complete* wing (including aileron and tab), over the complete aileron (including tab), and over the tab only. Then the inertial coefficients are found to be

$$\left.\begin{aligned}
&A_{11} = \underset{w}{\Sigma}\, ml^2f^2; \qquad A_{22} = \underset{w}{\Sigma}\, mx^2F^2 + \underset{a}{\Sigma}\, m\{(x - d_a + d_aF)^2 - x^2F^2\};\\
&A_{33} = \underset{a}{\Sigma}\, m(x - d_a)^2; \quad A_{44} = \underset{t}{\Sigma}\, m(x - d_t)^2;\\
&A_{12} = A_{21} = \underset{w}{\Sigma}\, mlxfF - \underset{a}{\Sigma}\, mlf(x - d_a)(F - 1);\\
&A_{13} = A_{31} = \underset{a}{\Sigma}\, ml(x - d_a)f; \qquad A_{14} = A_{41} = \underset{t}{\Sigma}\, ml(x - d_t)f;\\
&A_{23} = A_{32} = \underset{a}{\Sigma}\, m(x - d_a)(x - d_a + d_aF); \quad A_{24} = A_{42} = \underset{t}{\Sigma}\, m(x - d_t)(x - d_a + d_aF);\\
&A_{34} = A_{43} = \underset{t}{\Sigma}\, m(x - d_a)(x - d_t)\,.
\end{aligned}\right\} \quad \ldots\ \ldots\ \ldots\ \ldots\ \ldots\ \ldots \quad (7.4)$$

The corresponding non-dimensional coefficients a_{ij} are given by equation (2.9).

In practice both the aileron and the tab would be ' mass-balanced ' on some basis. In the present paper an aileron is described as *uniformly statically balanced* if the centre of mass of the aileron in *every section* lies on the aileron hinge-line. A similar definition applies for the tab. If both conditions are satisfied the combination is said to be uniformly statically balanced. From (7.4) it is seen that with such a system $A_{13} = A_{14} = 0$, $A_{23} = A_{33}$, and $A_{24} = A_{34} = A_{44}$. The inertia matrix then has the simple form

$$a = \begin{bmatrix} a_{11} & a_{12} & 0 & 0 \\ a_{21} & a_{22} & a_{33} & a_{44} \\ 0 & a_{33} & a_{33} & a_{44} \\ 0 & a_{44} & a_{44} & a_{44} \end{bmatrix}. \quad \ldots\ \ldots\ \ldots\ \ldots \quad (7.5)$$

The corresponding barred inertial coefficients are

$$\bar{a} = \begin{bmatrix} a_{11} & a_{12} & 0 & 0 \\ a_{21} & a_{22} & a_{33} + na_{44} & a_{33} + Na_{44} \\ 0 & a_{33} + na_{44} & a_{33} + n(n+2)a_{44} & a_{33} + (Nn + N + n)a_{44} \\ 0 & a_{33} + Na_{44} & a_{33} + (nN + n + N)a_{44} & a_{33} + N(N+2)a_{44} \end{bmatrix}. \quad (7.6)$$

It is readily verified that the aileron–tab barred inertias then satisfy the relation

$$(N + n + 2)\bar{p} = (N + 1)\bar{a}_{33} + (n + 1)\bar{a}_{44}\,, \quad \ldots\ \ldots\ \ldots\ \ldots \quad (7.7)$$

in which $\bar{p} \equiv \bar{a}_{34} = \bar{a}_{43}$. If on the other hand the tab balancing is such that the aileron–tab product of inertia $a_{34} = a_{43} = 0$, the barred inertias for the combination are

$$\left.\begin{aligned} \bar{a}_{33} &= \bar{a}_{33} + n^2a_{44} \\ \bar{p} &= \bar{a}_{33} + nNa_{44} \\ \bar{a}_{44} &= \bar{a}_{33} + N^2a_{44} \end{aligned}\right\}. \quad \ldots\ \ldots\ \ldots\ \ldots\ \ldots \quad (7.8)$$

8. *Binary Inertia-Stiffness Diagrams.*—The graphical treatment of binary problems will be explained in relation to aileron–tab flutter.

The determinantal equation appropriate to (34s) flutter* is (*see* 5.11))

$$\begin{vmatrix} z + i\bar{B}_{33} & \bar{D}_{34} + i\bar{B}_{34} \\ \bar{D}_{43} + i\bar{B}_{43} & w + i\bar{B}_{44} \end{vmatrix} = 0 , \quad .. \quad .. \quad .. \quad .. \quad (8.1)$$

which yields

$$zw = \bar{D}_{34}\bar{D}_{43} + \bar{B}_{33}\bar{B}_{44} - \bar{B}_{34}\bar{B}_{43} \equiv E_{34} , \quad .. \quad .. \quad .. \quad .. \quad (8.2)$$

$$\bar{B}_{44}z + \bar{B}_{33}w = \bar{D}_{34}\bar{B}_{43} + \bar{D}_{43}\bar{B}_{34} \equiv F_{34} . \quad .. \quad .. \quad .. \quad .. \quad (8.3)$$

These equations can be solved for z and w to give the pairs of values

$$\left.\begin{aligned} z_1 &= Z_1' + \bar{D}_{33} = (F_{34} + \sqrt{G_{34}})/2\bar{B}_{44} , \\ w_1 &= W_1' + \bar{D}_{44} = (F_{34} - \sqrt{G_{34}})/2\bar{B}_{33} , \end{aligned}\right\} \quad .. \quad .. \quad .. \quad .. \quad (8.4)$$

or

$$\left.\begin{aligned} z_2 &= Z_2' + \bar{D}_{33} = (F_{34} - \sqrt{G_{34}})/2\bar{B}_{44} , \\ w_2 &= W_2' + \bar{D}_{44} = (F_{34} - \sqrt{G_{34}})/2\bar{B}_{33} , \end{aligned}\right\} \quad .. \quad .. \quad .. \quad .. \quad (8.5)$$

in which

$$G_{34} = F_{34}^2 - 4\bar{B}_{33}\bar{B}_{44}E_{34} . \quad .. \quad .. \quad .. \quad .. \quad .. \quad .. \quad .. \quad (8.6)$$

The roots Z_1', W_1' and Z_2', W_2' represent the critical values of the elastic stiffness coefficients $\bar{e}_{33}$, $\bar{e}_{44}$ appropriate to any chosen frequency parameter ω. The locus described by those roots in the (Z', W')-plane as ω is varied is the analogue of the familiar ' test conic ' of classical derivative theory. In fact, according to that theory, the air-load coefficients—C_{ij}, B_{ij} are, respectively, expressions of the forms $-\hat{a}_{ij}\omega^2 + \hat{c}_{ij}$, $\hat{b}_{ij}\omega$ (*see* (3.2)), and it is easy to show that the (Z', W') locus then is a conic section.

The test conic (or its vortex theory analogue) is convenient when it is desired to find the influence of changes of the elastic stiffnesses on the critical speed and *all the inertias are assigned.* An alternative graphical representation will now be described in which not only the elastic stiffnesses but also both *moments of inertia* are left free to be varied. Inertia-stiffness diagrams of this type have been applied by Cicala[4] to flexure–torsion flutter, and are particularly valuable in the discussion of measures for the prevention of flutter. Use is made of (5.8), (5.9), (8.4). (8.5), which give for the critical values of Z and W

or

$$\left.\begin{aligned} Z_1 &= (z_1 - \bar{C}_{33})/\omega^2 , \qquad W_1 = (w_1 - \bar{C}_{44})/\omega^2 , \\ Z_2 &= (z_2 - \bar{C}_{33})/\omega^2 , \qquad W_2 = (w_2 - \bar{C}_{44})/\omega^2 \end{aligned}\right\} . \quad .. \quad .. \quad .. \quad (8.7)$$

These critical values depend only on the air-load coefficients and on the product of inertia $\bar{p} \equiv \bar{a}_{34} = \bar{a}_{43}$. Accordingly, if Z and W are plotted as ordinate and abscissa, the locus of the critical points, when ω is varied, will be independent of the elastic stiffness coefficients and the moments of inertia. In Fig. 4a, which illustrates such a diagram, the critical locus is called the ' base curve '. Two points of the curve will (in general) correspond to a given value of ω.

To prepare the diagram for use, the current values of the moments of inertia are plotted in the third quadrant, and through the ' inertia point ' I so obtained the ' stiffness line ' IP is drawn, having for slope the stiffness ratio $Z'/W' = 2\sigma_0 r^2/\sigma r^2$ (*see* (5.5) and (5.7)). Let P_1, P_2 be the points

* For notation *see* Introduction (f).

of intersection of this line with the base curve. Then from (5.8) and (8.7) it follows that the critical frequencies f_1, f_2 corresponding to these two points are given by

$$\left.\begin{aligned} Z_1 + \bar{a}_{33} &\equiv 2\sigma_0 r'^2(N-n)^2/4\pi^2\rho l c_0^4 f_1^2 = \mathrm{P_1M_1}\,, \\ Z_2 + \bar{a}_{33} &\equiv 2\sigma_0 r'^2(N-n)^2/4\pi^2\rho l c_0^4 f_2^2 = \mathrm{P_2M_2}\,, \end{aligned}\right\} \quad .. \quad .. \quad .. \quad .. \quad (8.8)$$

or, alternatively, by $W_1 + \bar{a}_{44} = \mathrm{IM_1}$ and $W_2 + \bar{a}_{44} = \mathrm{IM_2}$.

The critical speeds V_1, V_2 corresponding to f_1, f_2 respectively, can be deduced from the relations

$$\left.\begin{aligned} Z_1' &\equiv 2\sigma_0 r'^2(N-n)^2/\rho V_1^2 l c_0^2 = \omega_1^2 \mathrm{P_1M_1}\,, \\ Z_2' &\equiv 2\sigma_0 r'^2(N-n)^2/\rho V_1^2 l c_0^2 = \omega_2^2 \mathrm{P_2M_2}\,, \end{aligned}\right\} \quad .. \quad .. \quad .. \quad .. \quad .. \quad (8.9)$$

where ω_1, ω_2 are the values of the frequency parameter appropriate to the points $\mathrm{P_1}$, $\mathrm{P_2}$. The required values of ω (or its square) can either be read off directly from a scale of ω marked on the base curve, or a supplementary ' frequency parameter diagram ' (Fig. 4b) can be used, in which ω is plotted as ordinate against the abscissa of the base curve. In Figs. 4 the dotted portions of the base curve and frequency parameter curve are assumed to correspond.

With antisymmetrical flutter $Z' = 0$, and the stiffness line is parallel to the axis OW. The critical speeds corresponding to the two intersections $\mathrm{P_1'}$, $\mathrm{P_2'}$ are then given by

$$\left.\begin{aligned} \sigma r^2(N-n)^2/\rho V_1^2 l c_0^2 &= \omega_1'^2 \mathrm{IP_1'}\,, \\ \sigma r^2(N-n)^2/\rho V_2^2 l c_0^2 &= \omega_2'^2 \mathrm{IP_2'} \end{aligned}\right\} . \quad .. \quad .. \quad .. \quad .. \quad .. \quad (8.10)$$

Some of the simpler properties of a base curve may be noted. As already remarked each value of ω generates a pair of points of the curve. Such pairs may be described as ' conjugates ': for example, the points B, B' in Fig. 4a corresponding to B, B' in Fig. 4b are conjugates. However, the conjugates corresponding to the peak A in Fig. 4b coalesce into a single point A on the base curve*. From (8.4), (8.5) and (8.7) it is seen that the chord connecting a pair of conjugates has the slope $-\bar{B}_{33}/\bar{B}_{44}$, which is independent of the product of inertia $\bar{p}$. When ω is kept constant but $\bar{p}$ is varied, the centres of the chords connecting conjugate points are colinear, and the locus of the conjugate points is a conic section.

A complete survey of the flutter characteristics for all possible inertias and stiffnesses would require a specification of the base curves and frequency parameter curves for all values of $\bar{p}$ ranging from $+\infty$ to $-\infty$. A few additional theorems may be mentioned, which aid a general description of this complete family of curves. The first of these concerns the asymptotic form of the base curve. When $|\bar{p}| \to \infty$

$$\left.\begin{aligned} Z/\bar{p} &\to \{\bar{B}_{34} + \bar{B}_{43} \pm \sqrt{(-\bar{\Delta})}\}/2\bar{B}_{44}\,, \\ W/\bar{p} &\to \{\bar{B}_{34} + \bar{B}_{43} \pm \sqrt{(-\bar{\Delta})}\}/2\bar{B}_{33}\,, \end{aligned}\right\} \quad .. \quad .. \quad .. \quad .. \quad .. \quad (8.11)$$

in which

$$\begin{aligned} \bar{\Delta} &\equiv 4\bar{B}_{33}\bar{B}_{44} - (\bar{B}_{34} + \bar{B}_{43})^2 \\ &= (N-n)^2\{4B_{33}B_{44} - (B_{34} + B_{43})^2\} \equiv (N-n)^2\Delta \text{ say.} \quad .. \quad .. \quad .. \quad .. \quad (8.12) \end{aligned}$$

The function Δ will be recognized as the discriminant of the dissipation function, and its sign is (in general) positive when ω is very large. The maximum value of ω attained on the asymptotic base curve is accordingly given by the condition $\Delta = 0$, which is independent of the gear ratios N, n. This value does not, of course, represent the greatest ω attained as $\bar{p}$ varies from $+\infty$ to $-\infty$. The *maximum maximorum* value is, in fact, given by the two conditions $G_{34} = 0$, $\partial G_{34}/\partial\bar{p} = 0$, which yield after considerable reduction

$$\bar{\Delta} - (\bar{C}_{34} - \bar{C}_{43})^2 = (N-n)^2\{\Delta - C_{34} - C_{43})^2\} = 0 \quad .. \quad .. \quad .. \quad .. \quad (8.13)$$

$$2\bar{p}\omega^2\bar{\Delta} = (\bar{C}_{34} - \bar{C}_{43})(\bar{B}_{34}^2 - \bar{B}_{43}^2 + \bar{C}_{34}^2 - \bar{C}_{43}^2)\,. \quad .. \quad .. \quad .. \quad (8.14)$$

* The maximum value of ω is given by the condition $G_{34} = 0$.

From the first of these it follows that the greatest ω attained is independent of N and n. The corresponding value of $\bar{p}$ is, however, not invariant. Similar considerations apply for the minima of ω, which are in general definite and distinct from $\omega = 0$ in the case of aileron–tab flutter. On the other hand, with some types of flutter, the range of ω extends continuously down to $\omega = 0$. It is to be noted also that with (34) flutter the base curves will have horizontal and vertical asymptotes corresponding to the small definite values of ω for which $\bar{B}_{33} = 0$ and $\bar{B}_{44} = 0$. The situations of these asymptotes are independent of $\bar{p}$, but vary with N and n.

An inertia-stiffness diagram can be extended to provide also a graphical representation of natural frequencies. The base curves H_v, H_a corresponding respectively to oscillations *in vacuo* and in still air (*see* para. 6) are the two rectangular hyperbolae

$$(H_v) \ldots\ldots\ldots\ldots \quad ZW = \bar{p}^2 \qquad \ldots\ldots\ldots\ldots\ldots\ldots \quad (8.15)$$

$$(H_a) \ldots\ldots (Z - \bar{\gamma}_{33})(W - \bar{\gamma}_{44}) = (\bar{p} + \bar{\gamma}_{34})^2 . \qquad \ldots\ldots\ldots\ldots\ldots \quad (8.16)$$

These curves are used in the way already explained for critical frequencies. Since $\bar{a}_{33}\bar{a}_{44} > \bar{p}^2$ no inertia point I can lie above the lower branch of H_v.

Finally it may be remarked that if the air-load coefficients accord with classical derivative theory, so that, say, $\bar{C}_{ij} = -\hat{a}_{ij}\omega^2 + c_{ij}$ and $\bar{B}_{ij} = b_{ij}\omega$, the base curve will be a conic section. This curve is an ellipse or a hyperbola according as $\nabla > \text{or} < 0$, where

$$\nabla \equiv 4\hat{b}_{33}\hat{b}_{44}\hat{c}_{34}\hat{c}_{43} - (\hat{c}_{34}\hat{b}_{43} + \hat{c}_{43}\hat{b}_{34})^2. \qquad \ldots\ldots\ldots\ldots\ldots \quad (8.17)$$

Examples of binary inertia-stiffness diagrams are given in Section II.

9. *Ternary Inertia-Stiffness Diagrams.*—The (134) type of flutter will be taken as an example. In this case the determinantal equation (5.11) is

$$\begin{vmatrix} x + i\bar{B}_{11} & \bar{D}_{13} + i\bar{B}_{13} & \bar{D}_{14} + i\bar{B}_{14} \\ \bar{D}_{31} + i\bar{B}_{31} & z + i\bar{B}_{33} & \bar{D}_{34} + i\bar{B}_{34} \\ \bar{D}_{41} + i\bar{B}_{41} & \bar{D}_{43} + i\bar{B}_{43} & w + i\bar{B}_{44} \end{vmatrix} = 0 . \qquad \ldots\ldots \quad (9.1)$$

This gives on expansion

$$xzw - E_{34}x - E_{41}z - E_{13}w + F_{34}\bar{B}_{11} + F_{41}\bar{B}_{33} + F_{13}\bar{B}_{44} + K_0 = 0 , \qquad \ldots\ldots \quad (9.2)$$

and

$$\bar{B}_{11}zw + \bar{B}_{33}wx + \bar{B}_{44}xz - F_{34}z - F_{41}z - F_{13}w + 2\bar{B}_{11}\bar{B}_{33}\bar{B}_{44} - E_{34}\bar{B}_{11} - E_{41}\bar{B}_{33} - E_{13}\bar{B}_{44} + H_0 = 0 , \qquad (9.3)$$

where E_{ij}, F_{ij} are defined by relations similar to (8.2), (8.3) and

$$K_0 + iH_0 = (\bar{D}_{13} + i\bar{B}_{13})(\bar{D}_{34} + i\bar{B}_{34})(\bar{D}_{41} + i\bar{B}_{41}) + (\bar{D}_{31} + i\bar{B}_{31})(\bar{D}_{43} + i\bar{B}_{43})(\bar{D}_{14} + iB_{14}) . \qquad \ldots\ldots \quad (9.4)$$

The critical values of x, z, w, for any assigned value of ω, are thus given by the curve of intersection of the cubic and quadric surfaces (9.2), (9.3).

For the ternary case

$$\left.\begin{aligned} X &= (x - \bar{C}_{11})/\omega^2 = X'/\omega^2 - \bar{a}_{11} \\ Z &= (z - \bar{C}_{33})/\omega^2 = Z'\omega^2 - \bar{a}_{33} \\ W &= (w - \bar{C}_{44})/\omega^2 = W'/\omega^2 - \bar{a}_{44} \end{aligned}\right\} . \qquad \ldots\ldots\ldots\ldots \quad (9.5)$$

The direct analogue of Fig. 4a would be a three-dimensional representation, consisting of a ' base surface ' defined by the critical values of X, Z, W, an inertia point situated in the appropriate octant, and a stiffness line determined by the values of the three elastic stiffness coefficients. This representation must, of course, be replaced by a plane diagram.

The ternary plane diagram is shown in Fig. 5. The curve marked $X = \infty$ corresponds to an infinite value of X' and thus to $l_\phi = \infty$. It is accordingly identical with the base curve in Fig. 4a. The remaining base curves in the ternary diagram correspond to assigned values of X, which are marked against the curves. In the third quadrant two inertia points I ($\bar{a}_{44}$, $\bar{a}_{33}$) and I' ($\bar{a}_{44}$, $\bar{a}_{33} + \bar{a}_{11}$) are plotted, and stiffness lines IP, I'P' are drawn through these points having respectively the slopes Z'/W' and X'/W'. Now suppose P_1 to be the critical point of IP which is appropriate to all three assigned elastic stiffnesses. Then

$$P_1'N = I'N\left(\frac{X'}{W'}\right) = I'N\left(\frac{X + \bar{a}_{11}}{W + \bar{a}_{44}}\right) = X + \bar{a}_{11}\,.$$

But $P_1'N = P_1'M + \bar{a}_{11}$. It follows that P_1 must be chosen to lie on that base curve $X = k$ for which the condition $P_1'M = k$ is satisfied. The critical speed is then obtained from any one of the relations $X' = \omega^2 P_1'N$, $Z' = \omega^2 P_1 M$, $W' = \omega^2 IM$. The required values of ω (or ω^2) can be found from a supplementary frequency parameter diagram.

10. *Simplified Theory of Binary Aileron–Tab Flutter and Comparison with Servo-rudder Flutter.*—To conclude Section I the treatment of (34) flutter will be reviewed independently in the light of classical derivative theory and without the use of non-dimensional coefficients. The equations obtained will be compared with those given for binary servo-rudder flutter by Duncan and Collar[5] in R. & M. 1527. The springs are assumed to be non-preloaded.

(*a*) *Aileron–Tab Flutter.*—As in paras. 1 and 2, let β denote the tab angle and ξ the aileron angle. Then the simplified dynamical equations appropriate to symmetrical flutter, stated in a notation similar to that used in R. & M. 1527, are as follows.

Tab Hinge Moments.

$$d_2\ddot{\beta} + e_2V\dot{\beta} + (f_2V^2 + t_\beta)\beta + p\ddot{\xi} + j_2V\dot{\xi} + (k_2V^2 + t_\xi)\xi = 0\,. \quad .. \quad .. \quad .. \quad (10.1)$$

Aileron Hinge Moments.

$$p\ddot{\beta} + e_3V\dot{\beta} + (f_3V^2 + h_\beta)\beta + g_3\ddot{\xi} + j_3V\dot{\xi} + (k_3V^2 + h_\xi)\xi = 0\,. \quad .. \quad .. \quad .. \quad (10.2)$$

In these d_2, f_2, p denote the inertial constants, e, f, j, k are the aerodynamical derivatives, and (*see* para. 1 (*c*))

$$t_\beta = \sigma r^2 + 2\sigma_0 r'^2\,; \quad t_\xi = h_\beta = -\sigma Rr - 2\sigma_0 R'r'\,; \quad h_\xi = \sigma R^2 + 2\sigma_0 R'^2\,. \quad .. \quad .. \quad (10.3)$$

The equations for antisymmetrical flutter are similar except that $\sigma_0 = 0$.

If, as in para. 5 a general transformation

$$\left.\begin{aligned} \beta &= z\bar{\beta} + w\bar{\xi} \\ \xi &= v\bar{\beta} + u\bar{\xi} \end{aligned}\right\} \quad .. \quad .. \quad .. \quad .. \quad .. \quad .. \quad .. \quad (10.4)$$

is applied, the cross-stiffness is found to be absent from the new dynamical equations provided

$$zwt_\beta + (zu + wv)h_\beta + uvh_\xi = 0\,\ldots \quad .. \quad .. \quad .. \quad .. \quad (10.5)$$

On substitution from (10.3) this condition becomes

$$\sigma(zr - vR)(wr - uR) + 2\sigma_0(zr' - vR')(wr' - uR') = 0\,.$$

The particular transformation given by $z = R'/r' = N$, $w = R/r = n$, $v = u = 1$, is independent of the elastic stiffnesses, and yields the set of barred coefficients given in Table A below.

TABLE A

Barred Dynamical Coefficients

New coefft.	Value in terms of original coefficient	New coefft.	Value in terms of original coefficient
$\bar{d}_2$	$d_2N^2 + 2pN + g_3$	$\bar{p}$	$d_2nN + p(n + N) + g_3$
$\bar{e}_2$	$e_2N^2 + (j_2 + e_3)N + j_3$	$\bar{e}_3$	$e_2nN + j_2n + e_3N + j_3$
$\bar{f}_2$	$f_2N^2 + (k_2 + f_3)N + k_3$	$\bar{f}_3$	$f_2nN + k_2n + f_3N + k_3$
$\bar{p}$	$d_2nN + p(n + N) + g_3$	$\bar{g}_3$	$d_2n^2 + 2pn + g_3$
$\bar{j}_2$	$e_2nN + j_2N + e_3n + j_3$	$\bar{j}_3$	$e_2n^2 + (j_2 + e_3)n + j_3$
$\bar{k}_2$	$f_2nN + k_2N + f_3n + k_3$	$\bar{k}_3$	$f_2n^2 + (k_2 + f_3)n + k_3$
$\bar{t}_\beta$	$t_\beta N^2 + 2h_\beta N + h_\xi = \sigma r^2(N - n)^2$	$\bar{h}_\beta$	0
$\bar{t}_\xi$	0	$\bar{h}_\xi$	$t_\beta n^2 + 2h_\beta n + h_\xi = 2\sigma_0 r'^2(N - n)^2$

The stability can now be discussed either by a test conic, or by means of an intertia-stiffness diagram. In either case use is made of the condition for simple harmonic oscillations. This can be written

$$\begin{vmatrix} -\bar{d}_2\omega^2 + \bar{f}_2 + i\omega\bar{e}_2 + W', & -\bar{p}\omega^2 + \bar{k}_2 + i\omega\bar{j}_2 \\ -\bar{p}\omega^2 + \bar{f}_3 + i\omega\bar{e}_3, & -\bar{g}_3\omega^2 + \bar{k}_3 + i\omega\bar{j}_3 + Z' \end{vmatrix} = 0, \quad \ldots \quad \ldots \quad (10.6)$$

where

$$W' \equiv \bar{t}_\beta/V^2 = \sigma r^2(N - n)^2/V^2,$$
$$Z' \equiv \bar{h}_\xi/V^2 = 2\sigma_0 r'^2(N - n)^2/V^2,$$

and $\omega \equiv 2\pi f/V$, where f denotes the critical frequency*.

To obtain the test conic, ω is eliminated between the two real equations implicit in (10.6), and $W' + \bar{f}_2$, $Z' + \bar{k}_3$ are treated as co-ordinates in a plane. The stiffness line has the slope $Z'/W' = 2\sigma_0 r'^2/\sigma r^2$, and the stiffness point has the co-ordinates $\bar{f}_2$, $\bar{k}_3$.

To obtain the inertia-stiffness diagram use is made of the substitutions

$$\left.\begin{aligned} \omega^2 W &= -\bar{d}_2\omega^2 + W' \\ \omega^2 Z &= -\bar{g}_3\omega^2 + Z' \end{aligned}\right\}, \quad \ldots \quad \ldots \quad \ldots \quad \ldots \quad \ldots \quad \ldots \quad (10.7)$$

The two real equations implicit in (10.6) then are

$$\left.\begin{aligned} (\omega^2 W + \bar{f}_2)(\omega^2 Z + \bar{k}_3) &= E \\ (\omega^2 W + \bar{f}_2)\bar{j}_3 + (\omega^2 Z + \bar{k}_3)\bar{e}_2 &= F \end{aligned}\right\}, \quad \ldots \quad \ldots \quad \ldots \quad \ldots \quad (10.8)$$

where

$$E \equiv (-\bar{p}\omega^2 + \bar{k}_2)(-\bar{p}\omega^2 + \bar{f}_3) + \omega^2(\bar{e}_2\bar{j}_3 - \bar{e}_3\bar{j}_2),$$
$$F \equiv (-p\omega^2 + \bar{k}_2)(\bar{e}_3 + (-p\omega^2 + \bar{f}_3)\bar{j}_2.$$

* Note that in the present form of analysis the ' frequency parameter ' ω is not non-dimensional.

Equations (10.8) can be solved to give

$$\left.\begin{aligned}\omega^2 Z &= -\bar{k}_3 + \frac{F \pm \sqrt{G}}{2\bar{e}_2} \\ \omega^2 W &= -\bar{f}_2 + \frac{F \pm \sqrt{G}}{2\bar{j}_3}\end{aligned}\right\}, \quad \ldots\ldots\ldots\ldots\ldots\ldots \quad (10.9)$$

in which $G \equiv F^2 - 4\bar{e}_2\bar{j}_3 E$. These results correspond to equations (8.4) to (8.7). The locus of points W, Z is the base curve, the inertia point I has the co-ordinates $-d_2$, $-\bar{g}_3$, and the slope of the stiffness line is $2\sigma_0 r'^2/\sigma r^2$. With antisymmetrical flutter $\sigma_0 = 0$. The diagram is used as explained in para. 8 for Figs. 4a and b, except that in the present case $\omega = 2\pi f/V$.

(*b*) *Servo-rudder Flutter.*—Equations (10.1) and (10.2) are applicable for servo-rudder flutter provided β, ξ are taken to denote, respectively, the displacement of the servo-rudder relative to the main rudder, and the displacement of the main rudder relative to the fuselage. The expressions given in R. & M. 1527 for the elastic stiffnesses, converted to the notation of the present report, are*

$$\begin{aligned} t_\beta &= (ef/q) + (e\sigma_\zeta/q) + \sigma_\xi , \\ h_\xi &= \nu^2(ef/q) + (f\sigma_\zeta/q) , \\ t_\xi &= h_\beta = -\nu(ef/q) . \end{aligned}$$

In these, ν is a non-dimensional constant defined solely by the geometry of the servo-control mechanism, e, f, σ_ζ, σ_ξ are independent elastic stiffnesses, and $q \equiv f + \nu^2 e + \sigma_\zeta$. Equation (10.5) here leads to the condition

$$(z - \nu v)(w - \nu u)ef + (zwe + uvf)\sigma_\zeta + zwq\sigma_\xi = 0 . \quad \ldots\ldots\ldots\ldots \quad (10.10)$$

The particular transformation of co-ordinates adopted in R. & M. 1527 leaves the rudder co-ordinate unchanged and is given by $z = 1$, $v = 0$, $u = 1$ with

$$w = \nu ef/(ef + e\sigma_\zeta + q\sigma_\xi) . \quad \ldots\ldots\ldots\ldots\ldots\ldots \quad (10.11)$$

The new direct stiffnesses are then

$$\begin{aligned} \bar{t}_\beta &= t_\beta = (ef/q) + (e\sigma_\zeta/q) + \sigma_\xi \\ h_\beta &= f\{(\nu^2 e + \sigma_\zeta)\sigma_\xi + e\sigma_\zeta\}/(ef + e\sigma_\zeta + q\sigma_\xi) . \end{aligned}$$

This transformation, although relatively simple, has the disadvantage that the value of w given by (10.11) depends on the elastic stiffnesses. Hence if a test conic is calculated by means of the transformed dynamical co-ordinates appropriate to a given w, it should strictly only be used for stiffness variations restricted by the condition (10.11)†.

In general, a transformation which satisfies (10.10) and is independent of all four stiffnesses e, f, σ_ξ, σ_ζ, does not exist. However, in the important special case where $\sigma_\zeta = 0$ (direct spring constraint at rudder hinge axis absent) the required conditions are satisfied by $z = \nu$, $w = 0$, $v = u = 1$, and these yield

$$\bar{t}_\beta = \nu^2\sigma_\xi ; \qquad \bar{h}_\xi = \nu^2(ef/q) . \quad \ldots\ldots\ldots\ldots\ldots\ldots \quad (10.12)$$

It will be seen that the theory is then the same as that for aileron–tab flutter with $n = 0$. The correspondence is indicated below.

Servo-rudder Flutter	Aileron–Tab Flutter
$\sigma_\zeta = 0$	$R = 0$ $(n = 0)$
ν (= OA/AS in R. & M. 1527)	N $(= R'/r')$
σ_ξ	σr^2
ef/q	$2\sigma_0 r'^2$

* The symbols β, ξ, t_β, h_ξ, t_ζ, ν, correspond to ξ, ζ, h_ξ, m_ζ, h_ζ, n, of R. & M. 1527.

† This difficulty appears to have been overlooked in R. & M. 1527.

Section II. Numerical Applications to Binary Flutter

11. *Specification of Aeroplane S.*—The numerical applications relate to a particular system which will be referred to as ' aeroplane S '. The dimensions, stiffnesses, and inertias are derived in Appendices 1 and 2 by simplifications from data supplied for the *Spitfire*. Appendix 3 deals with the calculation of the air-load coefficients. A brief specification of the system follows.

(*a*) *Plan-form and dimensions.*—The tapered *Spitfire* wing–aileron–tab combination is replaced by a rectangular combination of constant section, but the effective areas, spans, and mean chords of the components are left unaltered (*see* Appendix I and Fig. 6).

(*b*) *Flexural axis and distortion modes.*—The straight flexure axis is assumed to lie at $0{\cdot}3c$ from the leading edge*. To avoid unessential complications, both the flexural and the torsional displacements are taken to vary linearly with the distance y from the wing root. The two displacements are, respectively, chosen proportional to the distance from the sections $y = 0{\cdot}35s$ and $y = 0{\cdot}2s$, and the displacements inboard of these sections are neglected. These simplified linear modes offer a fair first approximation to the curved modes adopted by Duncan and Lyon[6] for a typical cantilever wing.

(*c*) *Positions of spring tab and reference section.*—In the *Spitfire* tests spring tab No. 2 ($n = 0$) was used, and two alternative lengths of the tab lever TM were available. The short lever corresponded to $N = 5{\cdot}61$ and the long lever to $N = 3{\cdot}03$. The link FM was fitted at about two-thirds of the tab span from the inboard end of the tab. In the calculations the link is for convenience assumed to be placed at the inboard end, and the corresponding wing section is chosen as the reference section (*see* Fig. 6). Rounded values are adopted for the gear ratios, namely $N = 6$ and 3: the cases $N = 2$ and 10 are also investigated.

(*d*) *Elastic and inertial coefficients.*—The results of the calculations are analysed mainly by means of inertia-stiffness diagrams. In the practical interpretation of these diagrams, the values of the stiffnesses and inertias deduced from the *Spitfire* are accepted as the standard of reference, but allowance is made for possible variations due to changes of spring-tab design or to modifications of the weight of outer cover. The numerical values of the elastic stiffnesses are given in Tables 4 and 5, and the inertial coefficients are summarised in Tables 6, 7, and 8 and Fig. 7.

(*e*) *Air-load coefficients.*—Both the aileron and the tab are assumed to be hinged continuously along their leading edges. The air-load coefficients are given in Tables 9.

12. *Flexure–Torsion* (12) *Flutter.*—The tab and aileron are here assumed to be locked in central position to the wing in the reference section. In this first example the steps involved in the calculation of the base curve will be explained in some detail. The case is relatively simple, since barred coefficients are not introduced, and the distinction between symmetrical and anti-symmetrical flutter does not arise.

The equation corresponding to (8.1) is here

$$\begin{vmatrix} x + iB_{11} & D_{12} + iB_{12} \\ D_{21} + iB_{21} & y + iB_{22} \end{vmatrix} = 0 ,$$

where

$$D_{21} = -p\omega^2 + C_{21}; \qquad D_{12} = -p\omega^2 + C_{12}; \qquad p = a_{12} = a_{21} ,$$

and

$$x = \omega^2 X + C_{11}; \qquad y = \omega^2 Y + C_{22} .$$

Also

$$X' = l_\phi/\rho V^2 l^3 , \qquad X'/\omega^2 = X + a_{11} = l_\phi/4\pi^2\rho l^3 c_0^2 f^2 ,$$

$$Y' = m_\theta/\rho V^2 l c_0^2 , \qquad Y'/\omega^2 = Y + a_{22} = m_\theta/4\pi^2\rho l c_0^4 f^2 .$$

* From later information it appeared that the flexural axis on the *Spitfire* lay unusually far forward at about $0{\cdot}27c$. The difference is unlikely to invalidate the conclusions of this report, which are intended to be purely qualitative.

The critical pairs of values of X, Y, corresponding to (8.4), (8.5), (8.6), (8.7), may be written

$$\left.\begin{aligned} X &= \left(\frac{F_{12} \pm \sqrt{G_{12}}}{2B_{22}} - C_{11}\right)\Big/\omega^2 \\ Y &= \left(\frac{F_{12} \mp \sqrt{G_{12}}}{2B_{11}} - C_{22}\right)\Big/\omega^2 \end{aligned}\right\} \quad \ldots \quad (12.1)$$

in which

$$\begin{aligned} E_{12} &\equiv D_{12}D_{21} + B_{11}B_{22} - B_{12}B_{21}\,. \\ F_{12} &\equiv D_{12}B_{21} + D_{21}B_{12}\,, \\ G_{12} &\equiv F_{12}^2 - 4B_{11}B_{22}E_{12}\,. \end{aligned}$$

Now suppose that the base curve corresponding to $j = 0{\cdot}1$ is required. From Table 7 it is seen that the appropriate value of the product of inertia is $p = 2{\cdot}19$. Also the air-load coefficients required are given by the first four columns in Tables 9A and 9B. The calculations of the functions F_{12}, E_{12}, G_{12} are most conveniently arranged in tabular form*, with the first column reserved for the entries ω. To obtain a preliminary rough description of the base curve, the values $\omega = 1, 2, 3, 4, 5$ can first be tried, and spaces can be left for intermediate values, if required later. In the case considered each of the first four trial values of ω leads to a positive value for G_{12}, and consequently to a real pair of points on the base curve (*see* (12.1)). However $G_{12} < 0$ when $\omega = 5{\cdot}0$. The actual maximum permissible ω can be determined by interpolation from a graph of G_{12} against ω. An extension of the calculations to a few lower values of ω (e.g., $\omega = 0{\cdot}4$ and $0{\cdot}2$) yields a perfectly satisfactory plot of the base curve. The total time occupied is a matter of a few hours—provided, of course, the values of the air-load coefficients are known.

Figs. 8a and 8b show the base curves and frequency parameter curves for $p = 0$, $1{\cdot}10$, $2{\cdot}19$, $4{\cdot}39$ (corresponding to $j = 0$, $0{\cdot}05$, $0{\cdot}1$ and $0{\cdot}2$). To illustrate the use of these diagrams in the prediction of critical speeds and critical frequencies, the two moments of inertia are assumed to be $a_{11} = 27{\cdot}5$ and $a_{22} = 1{\cdot}09$, as for aeroplane S in Table 7. These values are plotted in the third quadrant, to give the marked inertia point I. Next, the elastic stiffnesses for aeroplane S taken from Table 5 are $l_\phi/\rho l^3 = 3{\cdot}74 \times 10^6$ and $m_0/\rho l c_0^2 = 1{\cdot}16 \times 10^6$, which yield the value $Y'/X' = 1{\cdot}16/3{\cdot}74 = 0{\cdot}31$ for the slope of the stiffness line IP. The critical frequencies f_1, f_2, when $j = 0{\cdot}1$ for example, can then be found from the relations

$$\begin{aligned} Y_1 + a_{22} &\equiv m_0/4\pi^2\rho l c_0^4 f_1^2 = \mathrm{P_1M_1} = 19{\cdot}09\,, \\ Y_2 + a_{22} &\equiv m_0/4\pi^2\rho l c_0^4 f_2^2 = \mathrm{P_2M_2} = 2{\cdot}68\,. \end{aligned}$$

which yield (when $c_0 = 5{\cdot}87$) $f_1 = 6{\cdot}68$ c.p.s. and $f_2 = 17{\cdot}84$. To obtain the critical speeds V_1, V_2, the ordinates $\omega_1 = 0{\cdot}09$ and $\omega_2 = 0{\cdot}675$ are read from the curve for $j = 0{\cdot}1$ in Fig. 8b. Then

$$\begin{aligned} Y_1' &\equiv m_0/\rho V_1^2 l c_0^2 = \omega_1^2 \mathrm{P_1M_1} = (0{\cdot}09)^2 \times 19{\cdot}09\,, \\ Y_2' &\equiv m_0/\rho V_2^2 l c_0^2 = \omega_2^2 \mathrm{P_2M_2} = (0{\cdot}675)^2 \times 2{\cdot}68\,, \end{aligned}$$

giving

$$\begin{aligned} V_1 &= 2740 \text{ ft/sec (1870 m.p.h.)}, \\ V_2 &= 976 \text{ ft/sec (665 m.p.h.)} \end{aligned}$$

In the present case the equations giving the natural frequencies are

$$X_v Y_v = p^2\,, \quad \ldots \quad (12.2)$$

$$(X_a - \gamma_{11})(Y_a - \gamma_{12}) = p + \gamma_{12})^2\,, \quad \ldots \quad (12.3)$$

where by (23.16) $\gamma_{11} = 2{\cdot}606$, $\gamma_{22} = 0{\cdot}1167$, $\gamma_{12} = 0{\cdot}4079$. These represent the aerodynamic inertias.

* The parameter p should first be left general in the tabulation of F and E if curves are required for a range of values of the product of inertia.

Table 1 illustrates the influence of changes of the product of inertia. The critical speeds and critical frequencies were read from the curves in Figs. 8a and 8b, and the natural frequencies were directly calculated by (12.2) and (12.3). It may be noted that in the three cases leading to flutter the critical frequency corresponding to the lower critical speed is roughly equal to 0·8 of the mean natural frequency *in vacuo*.

13. *Flexure–Aileron* (13) *Flutter.*—The tab is here assumed to be locked in central position to the aileron. Figs. 9 and 10 show the appropriate diagrams, which will be almost self-explanatory after the details given in para. 12.

In Fig. 9a the two inertia points I_1, I_2 represent respectively an unbalanced (complete) fabric aileron and an unbalanced aluminium aileron. An indication of the type of covering is provided by the small rectangles drawn against the inertia points : a plain rectangle signifies fabric, and a shaded rectangle aluminium.

The stiffness lines drawn through I_1 and I_2 and marked by arrows are appropriate to symmetrical flutter, and have the slope (*see* Table 5)

$$\frac{Z'}{X'} = \frac{(2\sigma_0 R'^2/\rho l c_0^2)}{(I_\phi/\rho l^3)} = \frac{4227}{3{\cdot}74 \times 10^6} = 0{\cdot}0112_5 .$$

The stiffness lines for antisymmetrical flutter (not shown in Fig. 9a) are horizontal. In Fig. 10a, which illustrates the advantages of static balance and static overbalance, the curves are shown to a greatly reduced scale.

14. *Torsion–Aileron* (23) *Flutter.*—The appropriate diagrams are Figs. 11a and 11b (for, unbalanced or statically balanced ailerons), and Figs. 12a and 12b (for dynamically balanced ailerons, $a_{23} = 0$). In Fig. 11a the code rectangles drawn against the inertia points are similar to those in Fig. 9a, except that a balancing arm is shown when the aileron is uniformly statically balanced. The points I_1, I_2 relate to fabric covering, and I_3, I_4 to aluminium. In Table 7 the product of inertia appropriate to a balanced aileron with aluminium covering is given as 0·0395. To avoid unnecessary calculations, the base curve already available for $a_{23} = 0{\cdot}037$ is adopted for this case, and the density of the aluminium is assumed reduced by about 6 per cent. Thus I_4 is shown plotted with an ordinate 0·037 instead of 0·0395.

The numerical results appended to Fig. 11a are of some interest. Antisymmetrical flutter occurs with both types of covering, whether the aileron is statically balanced or not. The balancing is definitely advantageous here because it raises the lower critical speed and also tends to compress the speed range leading to flutter. Symmetrical flutter is present only with the metal covering. In this case the static balancing is markedly disadvantageous in the sense that it greatly reduces the lower critical speed, but is advantageous in the sense that it greatly compresses the speed range for flutter. Briefly, *static balancing tends to suppress the antisymmetrical flutter at high speeds and the symmetrical flutter at low speeds.* To effect this pressing out process completely, it is necessary to proceed to true dynamic balance ($a_{23} = 0$), which involves static overbalance. This is shown by Fig. 12a.

15. *Aileron–Tab* (34) *Flutter with Spring Tab No.* 2.—The diagrams relating to aileron–tab flutter were calculated by the formulae given in para. 8. For simplicity those appropriate to spring tab No. 2 were considered first.

Results for $N = 2$.—Table 8 shows that when $N = 2$ the practical range of values for $\bar{p}$ is from about 0·005 to 0·04. It was, however, thought desirable in this first case to extend the calculations to a few higher values of $\bar{p}$, in order to indicate the changes as the asymptotic condition $\bar{p} \to \infty$ is approached. Figs. 13a and 13b show, to a large scale, the parts of the curves for $\bar{p} = 0$ to 0·0125 which are of practical interest. The complete curves for $\bar{p} = 1{\cdot}0$, $10{\cdot}0$ and ∞ are shown to a greatly reduced scale in Figs. 14a and 14b.

The inertia point I_1 in Fig. 13a is appropriate to a fabric aileron and fabric tab (both unbalanced) with $\bar{p} = 0{\cdot}0054$, while I_2 refers to a fabric aileron and aluminium tab (both balanced) with $\bar{p} = 0{\cdot}0128$. As in Fig. 4a the slope of the stiffness line for symmetrical flutter is given by $Z'/W' = 2\sigma_0 r'^2/\sigma r^2$; this is independent of N. If the elastic coefficients for aeroplane S are adopted (Table 5) the slope works out as $29{\cdot}27$, and the line is accordingly nearly parallel to OZ. The stiffness lines corresponding to antisymmetrical flutter (not marked in Fig. 13a) are, of course, parallel to OW.

In practical cases the values of $\bar{a}_{33}$, $\bar{a}_{44}$ and $\bar{p}$ for any given aileron–tab combination do not differ widely, and the inertia point always lies close to the vertex of the base curve. In Fig. 13a both I_1 and I_2 lie wholly to the right of their appropriate base curves, so that in these cases flutter could not occur for any values of the elastic stiffnesses.

The curves in Fig. 14a and 14b are mainly of theoretical interest. One complicating feature is the presence of the vertical and horizontal asymptotes. These are common to all the curves, and correspond to the values $\omega = 0{\cdot}085$ and $0{\cdot}06$ for which the two direct damping air-load coefficients $\bar{B}_{33}$ and $\bar{B}_{44}$ respectively vanish*. From an inspection of the directions along which ω decreases along the base curves (as indicated by the arrows), it is seen that for the smaller values of $\bar{p}$ (*e.g.*, $\bar{p} = 0$ to $1{\cdot}0$) the point of the base curve corresponding to maximum ω is situated on the small sharp indentation of the curve near the origin. The wedge-shaped curves in Fig. 12a are, of course, merely the indentations shown on enlarged scale. As $\bar{p}$ increases from zero, the indentation becomes more and more rounded, and moves away from the origin towards one of the asymptotes†. Eventually it *passes through* the asymptote and thus arrives, greatly modified, in the third quadrant. The curled parts of the branch shown in the third quadrant for $\bar{p} = 10$, though to some extent diagrammatic, illustrate one stage of development.

It is of some interest to compare the curves in Fig. 14a with those which would be obtained on the basis of classical derivative theory. The theoretical air-load coefficients used to construct Fig. 14a can be represented approximately, over the restricted range $\omega = 1{\cdot}0$ to $5{\cdot}0$, by the expressions

$$B_{ij} = \hat{b}_{ij}, \qquad \bar{C}_{ij} = \hat{c}_{ij} - \hat{a}_{ij}\omega^2$$

where

$$10^2\hat{b} = \begin{bmatrix} 0{\cdot}896 & 1{\cdot}00 \\ 0{\cdot}912 & 1{\cdot}03 \end{bmatrix}; \quad 10^2\hat{c} = \begin{bmatrix} 1{\cdot}46 & 2{\cdot}85 \\ 1{\cdot}48 & 2{\cdot}97 \end{bmatrix}; \quad 10^4\hat{a} = \begin{bmatrix} 5{\cdot}56 & 5{\cdot}72 \\ 5{\cdot}72 & 5{\cdot}90 \end{bmatrix}.$$

If these values are adopted for the derivative coefficients the expression defined by (8.17) is found to be negative, so that the new base curves will be hyperbolic. This is illustrated by the dotted curve marked C in Fig. 14a, which is the single hyperbolic branch forming the complete new base curve corresponding to $\bar{p} = 0$. The nose of this hyperbola fits closely into the indentation of the original base curve, as is seen better from Fig. 13a where points calculated for C are represented by black spots.

Results for $N = 3, 6, 10$.—The diagrams for these cases (Figs. 15 and 16) are similar to Figs. 13 and require no separate explanation. For the relevant practical values of the inertias, reference should be made to Table 8. The natural frequencies calculated for $N = 3$ by formulae similar to (12.2) and (12.3) are given in Table 2.

16. *Absolute Prevention of Aileron–Tab Flutter with Spring Tab No. 2.*—With diagrams of the types shown in Figs. 13a, 15a and 16a flutter is prevented absolutely (*i.e.*, for all stiffness ratios) when the inertia point I lies to the right of the vertex of the base curve. The condition to be satisfied is accordingly

$$\bar{a}_{44} < -W_{\max} \quad .. \quad .. \quad .. \quad .. \quad .. \quad .. \quad (16.1)$$

* *See* remarks following (8.14).

† The particular asymptote has not been determined.

where W_{max} denotes the maximum abscissa of the base curve appropriate to the particular values of $\bar{p}$ and N considered*. The values of W_{max} for the various cases are given in Table 3, and plotted against $\bar{p}$ in Fig. 17. To simplify the diagram the actual entries from Table 3 are not marked, but it is found that the points corresponding to any given N lie very closely on straight lines passing just above the origin. If now the vertical scale in the diagram is adopted for $\bar{a}_{44}$, it follows from (16.1) that all points J $(\bar{p}, \bar{a}_{44})$ lying below the line appropriate to a given N represent inertial conditions for which flutter is prevented absolutely. To illustrate this, seven particular points are marked in Fig. 17, all referring to $N = 6$. The pair J_1, J_2 relate to an aluminium aileron–tab combination, J_3, J_4 to a fabric–aluminium combination, and J_5, J_6, J_7 to a fabric–steel combination. An inspection of the positions of these points relative to the line for $N = 6$ shows that a low value for the aileron–tab density coefficient Δ is extremely disadvantageous. In Appendix II, the mass and density coefficients are defined as follows. If μ_a' (slugs) denotes the mass of the unbalanced aileron with the tab removed, and μ_t denotes the mass of the unbalanced tab, then

$$\left.\begin{aligned} \sigma_a \text{ (aileron mass-coefficient)} &\equiv \mu_a'/(s_a c_a^2 - s_t c_t^2)\,, \\ \sigma_t \text{ (tab mass-coefficient)} &\equiv \mu_t/s_t c_t^2\,, \\ \varepsilon_a \text{ (aileron density ratio)} &\equiv \rho/\sigma_a\,, \\ \varepsilon_t \text{ (tab density ratio)} &\equiv \rho/\sigma_t\,, \\ \Delta \text{ (aileron–tab density ratio)} &\equiv \rho_a/\sigma_t = \varepsilon_t/\varepsilon_a\,. \end{aligned}\right\} \quad .. \quad .. \quad .. \quad (16.2)$$

The values for fabric, aluminium, and steel components are estimated respectively as $\sigma = 0{\cdot}03837,\ 0{\cdot}1151,\ 0{\cdot}3125$ (or $\varepsilon = 0{\cdot}06197,\ 0{\cdot}01675,\ 0{\cdot}006197$ with standard air). These give $\Delta = 1{\cdot}0,\ 0{\cdot}27,\ 0{\cdot}1$ for fabric–fabric, fabric–aluminium, and fabric–steel combinations.

The disadvantages of a low aileron–tab density ratio are confirmed if, as an approximation on the safe side, the straight lines in Fig. 17 are replaced by lines actually passing through the origin and the true and approximate values of W_{max} are made to agree closely for the highest value of $\bar{p}$ to be considered. Then W_{max} becomes proportional to $\bar{p}$, so that

$$-W_{max}/\bar{p} = M\,, \quad .. \quad .. \quad .. \quad .. \quad .. \quad .. \quad .. \quad (16.3)$$

where M is a positive constant depending on N only†. The values adopted for M are stated below Table 3, which also compares the true and approximate values of W_{max}. From (16.1) and (16.3) it follows that the stability condition can be replaced safely by

$$\bar{a}_{44}/\bar{p} < M\,. \quad .. \quad .. \quad .. \quad .. \quad .. \quad .. \quad .. \quad (16.4)$$

The values of the ratio $\bar{a}_{44}/\bar{p}$, as calculated for unbalanced tabs from the formulae in Table 6 are shown plotted against Δ in Fig. 18. The points shown as heavy black spots on the curves have for ordinates the appropriate values of M. Hence *the safe values for the density ratio lie to the right of the black spots*. The danger associated with a low density ratio is immediately obvious.

The influence of mass balancing on the stability will next be considered. First, assume any datum inertial condition for the combination, and suppose a mass m to be added to the aileron (but *not* to the tab) at any distance X from the aileron hinge axis. Then the aileron moment of inertia A_{33} will be increased by mX^2, and the other two inertial constants will remain unchanged. From the relations

$$\bar{A}_{33} = A_{33}\,, \qquad \bar{A}_{44} = A_{33} + 2NP + N^2 A_{44}\,, \qquad \bar{P} = A_{33} + NP\,, \quad .. \quad .. \quad (16.5)$$

it follows that $\delta\bar{A}_{44} = mX^2$ and $\delta\bar{P} = mX^2$, so that both these increments are positive and $\delta\bar{A}_{44}/\delta\bar{P} = 1$. Thus also $\delta\bar{a}_{44}/\delta\bar{p} = 1$. Now it is important to note that the gradients of all the lines in Fig. 17 exceed unity. Hence, in the particular mass variation considered, the inertia

* Note that this abscissa is negative in the cases considered.

† It may be noted the M plots almost linearly against N.

point J in the diagram will be moved *downwards* in relation to its appropriate line (*i.e.*, J approaches closer to the line if initially in the unstable region, and away from the line if initially in the stable region). Hence *any addition of mass to the main aileron, and in particular balancing or overbalancing, is beneficial.*

Next, suppose the mass m to be added to the tab instead of to the aileron. Its position is assumed to be at distance $\lambda \equiv \lambda_t c_t$ *forward* of the tab hinge axis and at distance $\Lambda \equiv D - \lambda$ behind the aileron hinge axis, where D denotes the distance between the axes. Then it is readily shown that

$$\delta \bar{A}_{44} = m(N\lambda - \Lambda)^2$$

$$\delta \bar{P} = m\Lambda(\Lambda - N\lambda) .$$

Hence

$$\frac{\delta \bar{A}_{44}}{\delta \bar{P}} = \frac{\delta \bar{a}_{44}}{\delta \bar{p}} = 1 - N\left(\frac{\lambda}{\Lambda}\right).$$

The increment $\delta \bar{A}_{44}$ is always positive, but $\delta \bar{P}$ is positive only when

$$\frac{\Lambda}{\lambda} \equiv \frac{(D/c_t) - \lambda_t}{\lambda_t} > N . \quad .. \quad .. \quad .. \quad .. \quad .. \quad (16.6)$$

The gradient $\delta \bar{A}_{44}/\delta \bar{P}$ is then less than unity, and the displacement of the inertia point J is accordingly in the safe direction. The condition (16.6) requires the tab balancing mass to lie behind the point which divides the distance between the aileron and tab hinge axes in the ratio N. When, on the other hand $\Lambda < N\lambda$, $\delta \bar{P}$ is negative and $\delta \bar{A}_{44}$ is positive as before. J then moves upwards and to the left, and the displacement is in the unsafe direction. In particular, mass-balancing of the tab alone may be expected to be disadvantageous if (16.6) is violated.

If $c_a/c_t = 4{\cdot}35$, as for aeroplane S, the limiting values of λ_t given by (16.6) for $N = 2, 3, 6, 10$ are respectively about $1{\cdot}11$, $0{\cdot}83$, $0{\cdot}48$, $0{\cdot}3$. The ineffectiveness of the tab balance when $\lambda_t = 1{\cdot}0$ and $N = 6$, and its effectiveness when $\lambda_t = 0{\cdot}3$, are illustrated by the relative positions of the points J_1, J_1' and J_2 in Fig. 17.

The following general conclusions are drawn regarding the absolute prevention of binary aileron–tab flutter with non-preloaded spring tab No. 2.

(*a*) The density ratio Δ, as defined by (16.2), should if possible exceed $0{\cdot}5$, and is preferably of the order unity.

(*b*) Any addition of mass to the main aileron only (*e.g.*, an aileron balancing or overbalancing mass) is advantageous.

(*c*) The tab-balancing mass, if present, must be placed behind the position which divides the distance between the aileron and tab hinge axes in the spring tab gear ratio N.

(*d*) If condition (*c*) cannot be satisfied, tab mass balance should not be attempted.

Condition (*d*), which requires the omission of tab mass balance in certain cases, may at first sight appear surprising. The ineffectiveness of the balancing in those cases is, of course, attributable to the presence of the elastic cross-stiffness due to the spring tab. The importance of this elastic coupling is strikingly illustrated by a comparison of the base curves already considered (*e.g.*, Fig. 13a) with those shown in Fig.19 for the same aileron–tab combination, but with the cross-stiffness removed. The new curves are appropriate to the *unbarred* dynamical coefficients, and are thus applicable for an aileron with the normal type of control, but carrying an elastically hinged tab. It is seen that as the product of inertia a_{34} reduces the oval base curves shrink continuously, and disappear when $a_{34} < 0{\cdot}44 \times 10^{-4}$ about. Hence mass balance in this case has its normal stabilising influence.

Another relevant illustration is provided by a simpler problem—the flexure–torsion flutter of a cantilever wing. If, in the analysis of this motion, the reference centre R is chosen *behind* the flexural centre F instead of at F as normally, a negative cross-stiffness is introduced, as with the spring tab. The flexural and torsional co-ordinates defined in relation to R here correspond

to the unbarred aileron and tab co-ordinates, and the conventional wing co-ordinates referred to F correspond to the barred aileron and tab co-ordinates. It is easy to see that in this case mass balance of the wing about R (corresponding to tab mass balance) is not necessarily always advantageous. For example, if the balancing mass is added behind F, the product of inertia *relative to* F *is increased,* and the critical speed is therefore likely to be reduced.

17. *Bearing of the Preceding Conclusions on Servo-rudder Flutter.*—In para. 10 a correspondence was established between binary tab–aileron flutter and binary servo-rudder flutter. It is therefore of some importance to consider the bearing of the conclusions drawn in para. 16 on servo-rudder flutter.

Numerical data appropriate to a particular full-scale aeroplane are given in para. 8 of R. & M. 1527[5]. Expressed in the notation of para. 10 the data are as follows.

TABLE A (para. 17)

Dynamical Coefficients for Servo-rudder System

(units: slug/ft/sec)

Servo-rudder	Value for full scale	Main rudder	Value for full scale
d_2	0·037 (standard)	p	0·22 (standard)
e_2	0·008	e_3	0·09
f_2	0·0038	f_3	0·088
p	0·22 (standard)	g_3	6·0
j_2	0·025	j_3	0·80
k_2	0·0013	k_3	+ 0·072
t_β	+126·3	h_β	−305·76
t_ξ	−305·76	h_ξ	+834·7

The standard values of d_2 and g_3 are stated to have been derived from experiments in air, and p was calculated. For the special servo-linkage considered $\sigma_\xi = 0$ and $\nu = 2{\cdot}73$: hence the transformation formulae in Table A of para. 10 are applicable with $n = 0$ and $N\ (= \nu) = 2{\cdot}73$. The barred elastic stiffnesses for rudder-bar locked work out as $\bar{t}_\beta = 106{\cdot}56$, $\bar{h}_\xi = 834{\cdot}7$, $\bar{t}_\xi = \bar{h}_\beta = 0$. With rudder-bar free $\bar{h}_\xi = 0$. The barred inertias corresponding to various inertial conditions of the system are as follows.

TABLE B (para. 17)

Values of Barred Inertias

(λ denotes length of balancing arm in inches)

Inertial condition of system	$\bar{d}_2$	$\bar{p}$	$\bar{g}_3$
Standard	7·477	6·601	6·0
Servo-rudder statically balanced* ($\lambda = 6$)	7·615	6·912	6·724
Servo-rudder dynamically balanced ($\lambda = 6$)	7·667	7·047	7·047
Servo-rudder dynamically balanced ($\lambda = 10{\cdot}2$)	7·488	6·525	6·525

* New inertias calculated from data given in Ref. 7.

It may be added that the values of e_2 and f_2 estimated by vortex strip-theory, and the use of approximate representations for the air-load coefficients, worked out as $0{\cdot}0065$ and $0{\cdot}00314$ (compared with the tabulated values $0{\cdot}008$ and $0{\cdot}0038$). In this calculation the triangular fin was replaced by a rectangular fin of approximately equal area, and a correction factor $1{\cdot}4/\pi$ was applied to the derivatives to allow for the small aspect ratio $1{\cdot}47$ of the fin–rudder–servo combination.

Figs. 20a and 20b show the base curves and the frequency-parameter curves corresponding to values of $\bar{p}$ ranging from $6{\cdot}601$ to $7{\cdot}2$. With the standard inertias (point I_1) the critical speeds for rudder-bar locked and rudder-bar free roughly estimated from the diagrams are respectively 285 ft/sec and 290 ft/sec. The corresponding speeds given in R. & M. 1527 are 292 and 286. When the tab is statically balanced (point I_2) or dynamically balanced by the short arm (point I_3) no flutter occurs. This is also shown by the points J_1, J_2, J_3 in Fig. 21, which corresponds to Fig. 17.

The values of the constants in (16.6) for the particular aeroplane considered are $D = 34{\cdot}55$ in., $c_t = 10{\cdot}2$ in., and $N = 2{\cdot}73$. The maximum advisable length of the servo-balancing arm is then given by $\lambda = D/(N+1) = 9{\cdot}26$ in. The point J_3' in Fig. 21, corresponding to $\lambda = 10{\cdot}2$, illustrates the case in which mass balance fails.

18. *Aileron–Tab Flutter with Spring Tab No.* 1.—With spring tabs No. 1 the gear ratio defined by n is not zero, and the ' barred ' inertial and aerodynamic coefficients for this case accordingly differ from those given for spring tabs No. 2. Formulae for the new inertial coefficients are given by (5.4) and the appropriate aerodynamic coefficients are defined similarly. The two gear ratios n and N are always subject to the restriction $N > n$. . The numerical values of the inertial coefficients for $N = 3$ and $n = 0{\cdot}5$, $1{\cdot}0$ and $2{\cdot}0$ are given in Table 10, and the corresponding elastic stiffnesses are obtained from (5.5) and Table 5.

19. *Flutter Prevention with Spring Tab No.* 1.—The inertia-stiffness diagrams for spring tabs No. 1 closely resemble those for spring tabs No. 2 which are shown in Figs. 15a and 15b. In view of this similarity, the actual diagrams for spring tabs No. 1 are omitted, but the maximum abscissa $W_{\max}$ for each curve is plotted against $\bar{p}$ in Fig. 22. The values of the gear ratios assumed in the calculations are $N = 3$ and $n = 0{\cdot}5$, $1{\cdot}0$ and $2{\cdot}0$. The case $n = 0$ corresponds to spring tabs of No. 2 type. For each value of n, $W_{\max}$ plots linearly against $\bar{p}$, so that $-W_{\max}/\bar{p}$ tends to a constant value M for large values of $\bar{p}$, where M is a function of N and n only. As for spring tabs No. 2, the stability condition $\bar{a}_{44} < -W_{\max}$ is then replaced by

$$\frac{\bar{a}_{44}}{\bar{p}} < M \qquad \ldots\ldots\ldots\ldots\ldots\ldots \quad (19.1)$$

where $M > 1$.

This inequality can be written alternatively

$$\bar{a}_{44} - \bar{p} < (M-1)\bar{p} \qquad \ldots\ldots\ldots\ldots \quad (19.2)$$

where $\bar{a}_{44} - \bar{p}$ is independent of a_{33} and therefore unaffected by addition to mass to the main aileron. It should be noted that in practice $\bar{a}_{44} > \bar{p}$ since by (5.4)

$$\bar{a}_{44} - \bar{p} = (N-n)(p + Na_{44}) .$$

The expression on the right is necessarily positive unless the tab is considerably over-mass-balanced.

It will now be shown that the conclusions drawn in para. 16 regarding the effects of mass-balancing apply to both types of spring tab. Firstly, if a mass m is added to the main aileron at a distance X from the aileron hinge axis, the resulting increments of the inertial constants are

$$\delta A_{33} = mX^2 , \qquad \delta P = 0 , \qquad \delta A_{44} = 0 ,$$
$$\delta \bar{A}_{33} = mX^2 , \qquad \delta \bar{P} = mX^2 , \qquad \delta \bar{A}_{44} = mX^2 .$$

In this case, the stability condition (19.2), for the modified system, can be written

$$\bar{A}_{44} - \bar{P} < (M - 1)(\bar{P} + mX^2) ,$$

and it is then clear that the addition of the mass m is beneficial.

Secondly, suppose a mass m to be added to the tab at a distance λ ($\equiv \lambda_t c_t$) forward of the tab hinge axis and at a distance Λ($\equiv D - \lambda$) behind the aileron hinge axis. Then the additions to the inertias are

$$\delta A_{33} = m\Lambda^2 , \qquad \delta P = - m\Lambda\lambda , \qquad \delta A_{44} = m\lambda^2$$

$$\delta \bar{A}_{33} = m\Lambda^2 , \qquad \delta \bar{P} = m(\Lambda - n\lambda)(\Lambda - N\lambda), \qquad \delta \bar{A}_{44} = m(\Lambda - N\lambda)^2.$$

The stability condition (19.2) for the modified system can here be expressed as

$$\bar{A}_{44} - \bar{P} = m\lambda(N - n)(\Lambda - N\lambda) < (M - 1)(\bar{P} + \delta\bar{P}) .$$

Now both $m\lambda(N - n)(\Lambda - N\lambda)$ and $\delta\bar{P}$ are positive provided $\Lambda > N\lambda$, and hence, in this case also, mass-balancing of the tab is beneficial.

It may be noted that since spring tab No. 2 can be regarded as a particular spring tab of No. 1 type for which $n = 0$, the stability conditions for both types may be expected to be similar as just shown.

Section III.—Numerical Applications to Ternary Flutter

20. *Preliminary Remarks.*—In this section flexure–aileron–tab (134) and torsion–aileron–tab (234) flutter are investigated for a wing fitted with spring tab No. 2. Inertial values corresponding to a fabric aileron and tab are used in the calculations, and a value $N = 2$ is taken for the spring tab gear ratio. A qualitative analysis of ternary flutter under the following inertial conditions is made :—

(i) flutter of (134) type with
  (*a*) aileron unbalanced
  (*b*) aileron statically balanced ($a_{13} = 0$),

(ii) flutter of (234) type with
  (*a*) aileron unbalanced
  (*b*) aileron statically balanced ($a_{13} = 0$)
  (*c*) aileron dynamically balanced ($a_{23} = 0$).

The corresponding inertia stiffness diagrams show that

(*a*) flutter of the (134) and (234) types is possible when the aileron is unbalanced although binary (34) flutter is absent

(*b*) flutter of (134) type is eliminated by static balancing ($a_{13} = 0$), but (234) type flutter is still possible

(*c*) flutter of (234) type is prevented by balancing the aileron dynamically ($a_{23} = 0$).

The ternary inertia-stiffness diagrams are usually complicated, and no simple criterion for ternary flutter prevention analogous to that given for binary (34) flutter in para. 16 and para. 19 can be deduced. However, the least favourable conditions for flutter can be recognised from an examination of the relatively simple binary curves from which the positions of the asymptotes for the ternary diagrams are determined. When the vertical asymptotes are far to the left and the horizontal asymptotes are well below the first inertia point I, the possibility of flutter is very remote. This condition implies that all types of binary flutter must be eliminated.

The notation used in the following analysis is listed in Section II except for some symbols which are introduced in para. 21 to simplify the computational work.

21. *Flexure–Aileron–Tab* (134) *Flutter.*—The equations of motion for (134) type flutter are given by (9.2) and (9.3) and they can be expressed in the binary form of para. 8 by writing

$$\left.\begin{aligned} z' &= z - \frac{E_{13}}{x}, \qquad w' = w - \frac{E_{14}}{x} \\ C_{33}' &= \bar{C}_{33} - \frac{E_{13}}{x}, \qquad C_{44} = \bar{C}_{44} - \frac{E_{14}}{x} \\ B_{33}' &= \bar{B}_{33} - \frac{F_{13}}{x} + \frac{\bar{B}_{11}E_{13}}{x^2} \\ B_{44}' &= \bar{B}_{44} - \frac{F_{14}}{x} + \frac{\bar{B}_{11}E_{14}}{x^2} \\ E_{34}' &= E_{34} - \frac{K_1}{x} + \frac{E_{13}E_{13}}{x^2} \\ F_{34}' &= F_{34} - \frac{H_0 + 2\bar{B}_{11}\bar{B}_{33}\bar{B}_{44}}{x} \\ &\quad + \frac{K_1\bar{B}_{11} + E_{13}F_{14} + E_{14}F_{13}}{x^2} - \frac{2\bar{B}_{11}E_{13}E_{14}}{x^3} \\ K_1 &= K_0 + \bar{B}_{11}F_{34} + \bar{B}_{33}F_{14} + \bar{B}_{44}F_{13} \end{aligned}\right\} \quad \ldots \quad (21.1)$$

On substitution, equations (9.2) and (9.3) reduce to

$$\left.\begin{aligned} z'w' &= E_{34}' \\ B_{44}'z' + B_{33}'w' &= F_{34}' \end{aligned}\right\} \quad \ldots \quad (21.2)$$

and give

$$\left.\begin{aligned} z' &= \omega^2 Z + C_{33}' = \frac{F_{34}' \pm \sqrt{G_{34}'}}{2B_{44}'} \\ w' &= \omega^2 W + C_{44}' = \frac{F_{34}' \pm \sqrt{G_{34}'}}{2B_{33}'} \end{aligned}\right\} \quad \ldots \quad (21.3)$$

where

$$G_{34}' = F_{34}'^2 - 4B_{33}'B_{44}'E_{34}' .$$

The method of calculation adopted is to regard the value of $X(= (x - C_{11})/\omega^2)$ as assigned and to derive by (21.3) pairs of values of Z and W corresponding to a range of values of ω for which G_{34}' is positive (*see* para. 9 and Fig. 5). The graph of Z against W is the required base curve appropriate to the given value of X.

The base curves are usually complicated by the presence of asymptotes. From (21.2) and (21.3) it is seen that when ω is such that B_{33}' is zero, w' becomes infinite and $z' = 0$. Accordingly, $W \to \infty$ at $Z = -C_{33}'/\omega^2$ (where ω has the appropriate value or values), and similarly $Z \to \infty$ at $W = -C_{44}'/\omega^2$ when $B_{44}' = 0$. Alternatively the positions of the asymptotes and the corresponding ω values can be deduced from the base curves and frequency parameter diagrams relevant to the various associated types of binary flutter. For instance, equations (9.2) and (9.3) reduce to

$$xz = E_{13}, \qquad B_{33}x + B_{11}z = F_{13}$$

which define flutter of the flexure–aileron (13) type. The values of Z and ω at which $W \to \infty$ for a particular value of X can therefore be read off the curves, in Figs. 9a and 9b corresponding to the appropriate value of a_{13}. For example, if $a_{13} = 0{\cdot}0836$, and $-7{\cdot}0 < X < -2{\cdot}0$, the values of Z are greater than $-a_{33}$ and therefore lead to asymptotes above the inertia point in the ternary diagram (*see* Fig. 23a, 23b).

Diagrams for (134) type flutter are given for the following conditions :—

(*a*) aileron unbalanced (Figs. 23a, 23b),

and

(*b*) aileron statically balanced (Fig. 24).

The diagrams show that flutter can occur in the first case but not in the second, as then the relevant curves have no branches to the right and above the inertia point $(-\bar{a}_{44}, -\bar{a}_{33})$. Tables 11, 12, 13 give the values of Z and W for a range of values of ω and X for each inertial condition, but some of the results are omitted in the diagrams.

22. *Torsion–Aileron–Tab* (234) *Flutter.*—The simplified equations of motion for this type of flutter are similarly obtained by writing y for x and replacing the suffix 1 by 2 wherever it occurs in para. 21. Inertia-stiffness diagrams of Z against W are plotted for assigned values of Y for the following cases :—

(*a*) aileron unbalanced (Figs. 25a, 25b, 25c)

(*b*) aileron statically balanced (Figs. 26a, 26b)

(*c*) aileron dynamically balanced (Fig. 27).

Flutter is possible under conditions (*a*) and (*b*) but not under (*c*).. The calculated values of Z and W are given for various values of ω and Y in Tables 14, 15, 16, 17, 18 and most of these results are included in the diagrams.

23. *Analysis of Diagrams.*—A graphical method of analysing the ternary inertia-stiffness diagrams is described in para. 9, but it is not always easy to apply. It is sometimes more convenient to find the values of l_ϕ which lead to flutter for various values of X. It is shown in para. 9 and Fig. 5 that flutter occurs when $X = k$, if l_ϕ is such that

$$\frac{X'}{W'} = \frac{(k + \bar{a}_{11})}{W_1 + \bar{a}_{41}} = \frac{l_\phi c_0^2}{\sigma r^2 N^2 l^2} \qquad .. \quad .. \quad .. \quad .. \quad .. \quad .. \quad (23.1)$$

where W_1 is the abscissa of the point of intersection P_1 of the Z'/W' stiffness line with the curve for $X = k$, and where Z', W' are assumed to be known. Values of l_ϕ can be calculated by (23.1) for various values of k for which curves have been drawn. The value of k corresponding to the flexural stiffness l_ϕ of the wing can then be deduced from a curve of l_ϕ against k. The corresponding frequency parameter can be obtained by a supplementary curve of ω_1 against k or l_ϕ, where ω_1 is the value of the frequency parameter at P_1. The critical flutter speed would then be given by $X' = \omega^2(k + \bar{a}_{11})$. However, critical speeds are not estimated in this section as the intervals between the values of X, Y and ω chosen in the calculations are not sufficiently small to allow a quantitative analysis of the diagrams.

Section IV.—Approximations to some Binary Inertia-Stiffness Diagrams

24. *Approximate Air-Load Coefficients.*—Good approximations to the inertia-stiffness diagrams for flexure–torsion, flexure–aileron, torsion–aileron and aileron–tab flutter are obtained by using approximate air-load coefficients of the form $C_{ij} = \hat{c}_{ij} - \hat{a}_{ij}\omega^2$, $B_{ij} = \hat{d}_{ij} + \hat{b}_{ij}\omega^2$ as listed in Table 19. The constants $\hat{a}_{ij}$ and $\hat{b}_{ij}$ represent the limiting values of $-c_{ij}/\omega^2$ and B_{ij}/ω as $\omega \to \infty$, and $\hat{c}_{ij}$, $\hat{d}_{ij}$ are chosen to yield the true values of the air-load coefficients at $\omega = 2$. The coefficients $\hat{a}_{ij}$ correspond to the aerodynamic inertias and their numerical values are given by formula (16) of Appendix III. Approximations were also tried on the basis of classical derivative theory in which $\hat{d}_{ij}$ is assumed to be zero, and in which allowance is made for the aerodynamic inertias. They were found to be unsatisfactory except in the case of aileron–tab flutter where ' barred ' air-load coefficients which depend on the gear ratio N are used (*see* para. 5).

25. *Binary Flutter.*—In the calculations the inertial values corresponding to a fabric aileron and a fabric tab are assumed (*see* Tables 7 and 8). Approximations to the curves for the following cases are considered :—

(i) flexure–torsion ($a_{12} = 2{\cdot}19$; $j = 0{\cdot}1$),

(ii) flexure–aileron ($a_{13} = 0{\cdot}0836$, unbalanced),

(iii) torsion–aileron ($a_{23} = 0{\cdot}0307$, unbalanced, $a_{23} = 0{\cdot}0107$, balanced)

(iv) aileron tab ($\bar{a}_{34} = 0{\cdot}0054$; $N = 2$; $\bar{a}_{34} = 0{\cdot}006$, $N = 6$).

Comparisons of the true curves and their approximations are made in Figs. 28 to 32. In all cases good approximations are obtained for values of $\omega > 1$. For lower values of ω, the approximate derivatives are less accurate, and lead to errors in the approximate forms of the various curves. For this reason, approximations were not made for the cases where the wing and the aileron are mass-balanced as the true maximum value of ω for both flexure–torsion ($a_{12} = 0$) and flexure–aileron ($a_{13} = 0$) flutter is about $0{\cdot}25$ (*see* Figs. 8b and 10b).

The approximate curves for aileron–tab flutter are shown in Figs. 31 and 32. They are in good agreement with the true curves for both values of N. Equally good agreement is obtained by the use of air-load coefficients of the classical type, namely, $C_{ij} = \hat{c}_{ij}$, and $B_{ij} = \hat{b}_{ij}\omega$, where allowance is made for the aerodynamic inertia a_{ij} by adding it to the true value of the product of inertia in vacuo. It may be recalled that the inertia-stiffness diagram depends only on the product of inertia and the aerodynamic coefficients. Since the values of $\hat{d}_{ij}$ required in the calculation of the aileron–tab inertia-stiffness diagrams are small compared with $\hat{b}_{33}$, they can be neglected without appreciable loss of accuracy when $\omega > 1$.

26. *Stability Condition.*—In para. 16, it is stated that (34) flutter is prevented when $\hat{a}_{44} < M\bar{p}$, where

$$M = -\frac{W_{\max}}{\bar{p}}.$$

It can be readily proved that $-W_{\max} \to M\bar{p}$ when $\bar{p}$ is large, if it is assumed that the air-load coefficients are of the classical type. For $N = 2$, the approximate values of the aileron–tab ' barred ' coefficients obtained by the use of (5.4) and Table 19 are

$$\bar{C} \equiv \bar{c} - \bar{a}\omega^{2*} = \begin{vmatrix} 0{\cdot}01431 - 0{\cdot}0_35383\omega^2, & 0{\cdot}02810 - 0{\cdot}0_35507\omega^2 \\ 0{\cdot}01449 - 0{\cdot}0_35507\omega^2, & 0{\cdot}02926 - 0{\cdot}0_35651\omega^2 \end{vmatrix}$$

and

$$\bar{B} = \bar{b}\omega = 10^{-2}\omega \begin{vmatrix} 0{\cdot}9079 & 1{\cdot}018 \\ 0{\cdot}9246 & 1{\cdot}049 \end{vmatrix} \quad .. \quad .. \quad .. \quad .. \quad .. \quad (26.1)$$

where the terms d_{ij} have been neglected.

The abscissa W is given by

$$W = \left[-\bar{C}_{44} + \frac{F \pm \sqrt{G}}{2\bar{B}_{33}} \right] \Big/ \omega^2 .$$

Let $\alpha = \bar{p}'\omega^2 = (\bar{p} + \bar{a}_{34})\omega^2$ where $\bar{p}'$ represents the effective ' barred ' inertia, then

$$\frac{\alpha W}{\bar{p}'} = -\bar{c}_{44} + \bar{a}_{44}\frac{\alpha}{\bar{p}'} + \frac{f \pm \sqrt{g}}{2\bar{b}_{33}} . \quad .. \quad .. \quad .. \quad .. \quad .. \quad (26.2)$$

* $\bar{a}$ here denotes a matrix of the aerodynamic inertias.

where

$$f = \frac{F}{\omega} = -\alpha(\bar{b}_{34} + \bar{b}_{43}) + \bar{c}_{34}\bar{b}_{43} + \bar{c}_{43}\bar{b}_{34}\,,$$

$$e = E = \alpha^2 - \alpha\left(\bar{c}_{34} + \bar{c}_{43} - \frac{\bar{b}_{33}\bar{b}_{44} - b_{34}b_{43}}{p'}\right) + \bar{c}_{34}\bar{c}_{43}\,,$$

$$g = \frac{G}{\omega} = f^2 - 4\bar{b}_{33}\bar{b}_{44}e \equiv g_0\alpha^2 + g_1\alpha + g_2\,.$$

For large values of p', the above expressions become functions of α only, since the term $\bar{b}_{33}\bar{b}_{44} - \bar{b}_{34}\bar{b}_{43}$ is then small compared with $p'(\bar{c}_{34} + \bar{c}_{43})$. When W is a maximum $\delta W/\delta\alpha = 0$, and then (26.2) gives

$$\left(1 - \alpha\frac{\delta}{\delta\alpha}\right)(f \pm \sqrt{g}) = 2\bar{b}_{33}\bar{c}_{44}\,, \qquad \ldots\ \ldots\ \ldots\ \ldots \quad (26.3)$$

which leads to the quadratic equation

$$g = \frac{(g_1\alpha + 2g_2)^2}{4D^2} = g_0\alpha^2 + g_1\alpha + g_2\,, \qquad \ldots\ \ldots\ \ldots\ \ldots \quad (26.4)$$

where $D = 2\bar{b}_{33}\bar{c}_{44} - \bar{c}_{34}\bar{b}_{43} - \bar{c}_{43}\bar{b}_{34}$. From equation (26.4) the values of $\alpha(= p'\omega^2)$ are then readily determined. When p' is large $\alpha \to 0{\cdot}0343$; for $p' = 0{\cdot}006$, $\alpha = 0{\cdot}0353$; hence, since $\pm 2D\sqrt{g} = g_1\alpha + 2g_2$ when W is a maximum equation (26·2) gives after some reduction

$$W_{\max} = -\frac{p'}{2\bar{b}_{33}}\left(\bar{b}_{34} + \bar{b}_{43} - \frac{g_1}{2D}\right) - \frac{(D^2 - g_2)p'}{2\bar{b}_{33}D\alpha} + \bar{a}_{44}$$

$$= -0{\cdot}981p' - \frac{0{\cdot}00203p'}{\alpha} + 0{\cdot}0_35651 \qquad \ldots\ \ldots\ \ldots\ \ldots \quad (26.5)$$

$$= -1{\cdot}04\bar{p} - 0{\cdot}0_58\,.$$

The slight variation in α with p' does not affect the slope of this line appreciably so that when $p' \geqslant 0{\cdot}006$, which represents roughly the lower limit of the ' barred ' effective product of inertia in practice, the value of the stability factor M is 1·04 as compared with a true value of 1·05 obtained graphically for N = 2. (*See* Table 3 and Figs. 13a, 13b).

REFERENCES

No.	*Author*	*Title, etc.*
1	S. B. Gates	Notes on the spring tab. R.A.E. Report B.A.1665. A.R.C. 5058. April, 1941.
2	W. S. Brown	Spring tab controls. R. & M. 1979. September, 1941.
3	R. A. Frazer, W. J. Duncan and A. R. Collar.	*Elementary Matrices.* Cambridge University Press. 1938
4	P. Cicala	The torsional-bending oscillations of a wing in a uniform current. *L'Aerotechnica.* Vol. 16, No. 11, p. 785. November, 1936. Translated as A.R.C. 3030.
5	W. J. Duncan and A. R. Collar	Binary servo-rudder flutter. R. & M. 1527. February, 1933.
6	W. J. Duncan and H. M. Lyon	Calculated flexural–torsional flutter characteristics of some typical cantilever wings. R. & M. 1782. April, 1937.
7	H. Boden	Moments of inertia of rudder surfaces and stiffnesses of fuselage and tail parts of Gloster C.16/28 Troop Carrier. R.A.E. Report M.T.5546A. A.R.C. 1667. March, 1935.
8	R. A. Frazer	Flexure–torsion flutter derivatives for semi-rigid wings. R. & M. 1952. May, 1941.
9	R. A. Frazer and S. W. Skan ..	A comparison of the observed and predicted flexure–torsion flutter characteristics of a tapered model wing. R. & M. 1943. August, 1941.
10	W. P. Jones	Aerodynamic forces on an oscillating aerofoil–aileron–tab combination. R. & M. 1948. September, 1941.

LIST OF SYMBOLS

Notes: For the significance of barred symbols *see* Introduction (*d*). Symbols with double suffices, unless specially defined, denote the elements of a corresponding square matrix. Numbers in round brackets indicate equations.

A		Matrix of inertial constants	para. 2
a		Matrix of non-dimensional inertial coefficients	(2.9)
a (as suffix)		Relating to the aileron	
$\hat{a}$			para. 3 (*a*)
$\mathscr{A}(\equiv C + iB)$		Matrix of air-load coefficients	(3.3)
B		*See* $\mathscr{A}$	(3.3)
B_a, B_t		Statically balanced aileron, statically balanced tab	Appendix II
$\hat{b}$		Matrix of damping derivatives	para. 3 (*a*)
β		Tab angle relative to aileron	Figs. 1a and 1b
C		*See* $\mathscr{A}$	(3.3)
c, c_0		Local chord of wing, root chord	
c_a, c_t		Aileron and tab chords	Appendix I
$\hat{c}$		Matrix of aerodynamic stiffness derivatives	para. 3 (*a*)
D		Square matrix $-a\omega^2 + C$; also denotes $\frac{d}{d\tau}$	para. 2 (5, 9)
d_a, d_t		Distances of aileron and tab hinge axes behind OY	(7.2), (7.3)
Δ		Aileron–tab density ratio σ_a/σ_t; discriminant	(16.2), (8.12)
E		Matrix of elastic stiffnesses	(1.6)
E_{ij}		Defined generally as in (8.2)	
e		Matrix of non-dimensional elastic coefficients	(2.10)
ε		Defined as e, but with $\sigma_0 = 0$	(4.3)
$\varepsilon_a, \varepsilon_t$		Aileron and tab density ratios ρ/σ_a, ρ/σ_t	(16.2)
η	$=$	y/l	
$F(\eta), f(\eta)$		Torsional and flexural distortion modes	(7.1)
F_{ij}		Defined generally as in (8.3)	
f		Frequency; critical frequency	
f_a, f_v		Natural frequency in still air and *in vacuo*	para. 6
G_{ij}		Defined generally as in (8.6)	
γ		Matrix of aerodynamic inertial coefficients	(6.2), Appendix III
H_1, H_2, H_3		Constants in calculation of inertias	Table 6
H		Aileron hinge moments	para. 2
H_0		Used in calculation of ternary diagrams	(9.4)

h_β, h_ξ		Elastic stiffnesses in simplified theory	para. 10
I		Inertia point in inertia-stiffness diagram	para. 8
J		Inertia point in stability diagram	para. 16
j		Distance of c.g. behind OY as function of chord	
K_0		Used in calculation of ternary diagrams	(9.4)
$k \equiv \{k_1, k_2, k_3, k_4\}$		Column of complex amplitudes of motion	(3.1)
L		Aerodynamic flexural moment on wing	para. 2
l		Distance reference section from wing root	
l_ϕ		Flexural stiffness of wing	
Λ		Distance of tab-balancing mass behind aileron hinge axis	(16.6)
λ		Distance of tab-balancing mass ahead of tab hinge axis	(16.6)
λ		Complex exponential time factor	para. 3
λ_a, λ_t		Distances of aileron and tab-balancing masses ahead of hinge axes, as fractions of aileron and tab chords	Appendix II
M		Aerodynamic torsional moment on wing	para. 2
M		Slope of lines in stability diagram	(16.3)
M_0		Equivalent mass of control column	(1.7)
m_0	$=$	$M_0/\rho c_0^2 l$	(2.8)
m_θ		Torsional stiffness of wing	
μ		Damping factor; matrix of transformation	para. 3 (*b*), (2.5)
N		Second spring-tab gear ratio R'/r'	para. 1 (*d*)
n		First spring-tab gear ratio R/r	para. 1 (*d*)
n_0	$=$	$2\sigma_0/\rho V^2 l c_0$	(2.6)
ν		A gearing constant of control circuit	para. 1 (*b*)
ξ, ξ_η		Aileron angle in reference section; local aileron angle	para. 7
P_0		Preloading force of spring tab	para. 1 (*a*)
p		Generic symbol for product of inertia: also used as suffix to denote port side	
p_0	$=$	$P_0/\rho V^2 l^2 c_0$	(2.6)
$\tilde{\omega}$		Column $\{0, 0, -R, r\}$	(1.6)
$Q \equiv \{Q_1, Q_2, Q_3, Q_4\}$		Column of aerodynamic moment coefficients	(2.6)
$q \equiv \{q_1, q_2, q_3, q_4\}$		Column $\{\phi, (c_0/l)\theta, (c_0/l)\xi, (c_0/l)\beta\}$	(2.4)
q_0		Angular co-ordinate of control column	(2.4)

LIST OF SYMBOLS—*continued*

R	=	$AF - AI$ in Figs. 1; for spring tab No. 2 $R = 0$	para. 1 (*a*)
R'		νAF in Figs. 1; νHQ in Fig. 2	para. 1 (*b*)
r		TM in Figs. 1; CK $\times$ TM/CS in Fig. 2	para. 1 (*a*)
r'		νTM in Figs. 1; νHC $\times$ TM/CS in Fig. 2	para. 1 (*b*)
ρ		Air density	
s		Wing span: also used as suffix to denote starboard	
s_a, s_t		Aileron and tab spans	
σ		Stiffness rate of spring tab	para. 1 (*a*)
σ_0		Stiffness rate of control cables	para. 1 (*b*)
σ_a, σ_t		Aileron and tab mass coefficients	(16.2)
T		Aerodynamic tab hinge moment	
t		Time variable	
t_β, t_ξ		Elastic stiffnesses	para. 10
τ		Non-dimensional time variable tV/c_0	(2.4)
θ		Torsional co-ordinate of wing	
θ_η		Local angle of twist at section η	Appendix III
ϑ		Column $\{0, 0, R', -r'\}$	(1.6)
ϑ'		Transposed of ϑ	(1.8)
U		Column of moments $\{L, M, H, T\}$	para. 2
U_a, U_t		Unbalanced aileron, unbalanced tab	Appendix II
V		Airspeed; critical speed	
X, Y, Z, W		Co-ordinates in inertia-stiffness diagrams	(5.8)
X_a, Y_a, Z_a, W_a		Values of X, Y, Z, W for oscillations in still air	(6.3)
X_v, Y_v, Z_v, W_v		Values of X, Y, Z, W for oscillations *in vacuo*	(6.1)
X', Y', Z', W'		Barred direct elastic stiffness coefficients	(5.7)
x, y, z, w		$X' + D_{11}$, etc.; also spatial co-ordinates	(5.10)
ϕ		Flexural co-ordinate of wing	
χ		Column of angles $\{\phi, \theta, \xi, \beta\}$	(1.6)
ω		Non-dimensional frequency parameter $2\pi fc_0/V$	(3.2)
∇		A modified discriminant	(8.17)

APPENDIX I

Dimensions, Distortion Modes, and Elastic Stiffnesses of Aeroplane S

The numerical constants adopted for the wing–aileron–tab combination were based—with drastic simplifications—on design data supplied for the *Spitfire*.

1. *Dimensions.*—The relevant data for the *Spitfire* are as follows.

Dimensions of Spitfire

(Areas in ft² and lengths in ft)

Gross wing area	242
Area of each aileron	9·45
Area of each tab	0·68
Overall span	37
Span of each aileron (s_a)	6·85
Span of each tab (s_t)	2·14
Root chord of wing	8·33
Tip chord	4·2
Aileron chord/wing chord (c_a/c)	0·235
Tab chord/aileron chord (c_t/c_a)	0·23

For aeroplane *S* the geometrical characteristics were modified in accordance with the following assumptions:

(*a*) The tapered *Spitfire* wing was replaced by a rectangular wing–aileron–tab combination of constant section

(*b*) The effective areas of each component and the values of s_a, s_t, c_a/c, c_t/c_a were left unaltered.

(*c*) The ratio of wing area outboard of aileron to aileron area was left unaltered.

(*d*) The wing dihedral was removed, and the flexural axis was assumed to lie as normally at $0{\cdot}3c$ from the leading edge.

(*e*) The aileron and the tab were assumed to be hinged continuously along their leading edges.

Thus, for aeroplane S

$$s_a = 6{\cdot}85; \qquad c_a = 9{\cdot}45/6{\cdot}85 = 1{\cdot}38$$

$$s_t = 2{\cdot}14; \qquad c_t = 0{\cdot}68/2{\cdot}14 = 0{\cdot}32 \text{ (rounded)}$$

$$c = 1{\cdot}38/0{\cdot}235 = 5{\cdot}87; \qquad s = 217/(2 \times 5{\cdot}87) = 18{\cdot}5^*.$$

For the *Spitfire* the ratio of wing area outboard of aileron to aileron area was estimated as 0·695. Hence for aeroplane S the wing span extending beyond the aileron was taken as $(0{\cdot}695 \times 9{\cdot}45)/5{\cdot}87 = 1{\cdot}12$ ft.

The finally accepted rounded dimensions are as shown in Fig. 6.

2. *Reference Section and Distortion Modes.*—The tab connection is for convenience assumed to be situated at the inner end of the tab, and the corresponding wing section is adopted as the reference section. The choice of this position for the tab connection simplifies the calculations, and it would also greatly simplify the construction of a model should wind-tunnel tests be required to check the theory.

---

* The effective wing area was taken to be 217 ft², 25 ft² being allowed for the centre section.

The simplified linear distortion modes adopted are (*see* (7.1) and para 11 (*b*))

$$f(\eta) = \frac{0{\cdot}57\eta - 0{\cdot}35}{0{\cdot}22} \text{ for } \eta > \frac{0{\cdot}35}{0{\cdot}57} \text{ and } f(\eta) = 0 \text{ for } \eta \leqslant \frac{0{\cdot}35}{0{\cdot}57},$$

$$F(\eta) = \frac{0{\cdot}57\eta - 0{\cdot}2}{0{\cdot}37} \text{ for } \eta > \frac{0{\cdot}2}{0{\cdot}57} \text{ and } F(\eta) = 0 \text{ for } \eta \leqslant \frac{0{\cdot}2}{0{\cdot}57}.$$

3. *Elastic Stiffnesses.*—(*a*) *Wing Stiffnesses.*—The figures supplied for the elastic stiffnesses of the *Spitfire* measured at mid-aileron span are as follows :—

Flexural stiffness	$3{\cdot}6 \times 10^6$ lb ft/radian
Torsional stiffness (symmetrical torques)	$0{\cdot}488 \times 10^6$ lb ft/radian
Torsional stiffness (antisymmetrical torques)	$0{\cdot}406 \times 10^6$ lb ft/radian.

The distance from the effective wing root to mid-aileron span is taken to be 11·42 ft.

The elastic stiffnesses for aeroplane S are chosen so that the values of the stiffness rates measured at mid-aileron span agree with those for the *Spitfire*. Now for aeroplane S the reference section and the mid-aileron span section lie at distances $0{\cdot}22s$ and $0{\cdot}405s$ respectively from the axis for linear flexure, and at distances $0{\cdot}37s$ and $0{\cdot}555s$ from the axis for linear twist. Moreover l (distance of reference section from wing root) = 10·54 ft. Hence, if l_ϕ, m_θ denote the elastic stiffnesses defined on the usual basis for aeroplane S

$$l_\phi = l^2\left(\frac{\text{load at reference section}}{\text{linear deflection at reference section}}\right)$$

$$= \left(\frac{0{\cdot}405l}{0{\cdot}22}\right)^2\left(\frac{\text{load at mid-aileron span}}{\text{linear deflection at mid-aileron span}}\right).$$

Or, on substitution of the value appropriate to the *Spitfire*

$$l_\phi = \left(\frac{0{\cdot}405 \times 10{\cdot}54}{0{\cdot}22 \times 11{\cdot}42}\right)^2 \times 3{\cdot}6 \times 10^6 = 10{\cdot}4 \times 10^6 \text{ lb ft/radian.}$$

Similarly, for symmetrical conditions of loading

$$m_\theta = \left(\frac{0{\cdot}555}{0{\cdot}37}\right)^2 \times 0{\cdot}488 \times 10^6 = 1{\cdot}1 \times 10^6,$$

while for antisymmetrical loading $m_\theta = 0{\cdot}915 \times 10^6$. The rounded values finally adopted are

$$l_\phi = 10{\cdot}4 \times 10^6;\ m_\theta = 1{\cdot}0 \times 10^6 \text{ (for both types of loading),}$$

giving

$$l_\phi/\rho l^3 = 3{\cdot}74 \times 10^6;\ m_\theta/\rho lc^2 = 1{\cdot}16 \times 10^6.$$

(*b*) *Control Stiffnesses.*—The following dimensions relate to the spring tab No. 2 which was tested on the *Spitfire*. Two alternative lengths for the tab lever TM were provided: these are denoted below by $(TM)_1$ and $(TM)_2$

$$CK = 2{\cdot}30 \text{ in.};\quad CS = 1{\cdot}7 \text{ in.};\quad HQ = 2{\cdot}85 \text{ in.};\quad HC = 1{\cdot}6 \text{ in.};$$

$$(TM)_1 = 0{\cdot}54 \text{ in.};\quad (TM)_2 = 1{\cdot}0 \text{ in.}$$

These yield the two sets of values

$$r = 0{\cdot}0609 \text{ (ft)};\qquad N\ (\equiv R'/r') = 5{\cdot}61 \text{ (short lever)}$$

$$r = 0{\cdot}113 \text{ (ft)};\qquad N\ (\equiv R'/r') = 3{\cdot}03 \text{ (long lever)},$$

Five different springs (Nos. 1 to 5) were provided for the spring tab, but it is understood that only spring No. 1 was tested in flight. The specified spring rates and preloadings are as below.

Spring No.	Stiffness rate (lb/in.)	Preloading P_0 (lb)
1	77*	23·8
2	40	21·8
3	23	18·6
4	11·5	13·7
5	6	9·0

In numerical applications it may be assumed that the practical values can range up to 100 (lb/in.) for the stiffness rate and up to 40 lb for P_0.

The value of the control circuit stiffness was obtained from a loading test carried out by the R.A.E. on the *Spitfire* aileron, under conditions appropriate to symmetrical flutter. This test gave $2R'^2\sigma_0 = 3650$. The numerical values of the elastic stiffnesses with σ taken as 89 lb/in. (1068 lb/ft) are as given in Tables 4 and 5.

APPENDIX II

Inertial Coefficients

1. *Main Wing Inertias.*—General expressions for the inertial coefficients are given in para. 7. The flexural and torsional natural frequencies given for the *Spitfire* are 10 and 28 c.p.s. respectively and the same frequencies are adopted for aeroplane S. Thus, since $l_\phi = 10{\cdot}4 \times 10^6$ and $m_\theta = 1{\cdot}0 \times 10^6$ (*see* para. 3, Appendix I),

$$A_{11} = 10{\cdot}4 \times 10^6/4\pi^2 10^2 = 2640 \text{ slug ft}^2, \text{ giving } a_{11} = 27{\cdot}5$$
$$A_{22} = 1{\cdot}0 \times 10^6/4\pi^2 28^2 = 32{\cdot}3 \text{ slug ft}^2, \text{ giving } a_{22} = 1{\cdot}09\,.$$

The value of A_{12} appropriate to the *Spitfire* was not specified, and this coefficient is—so far as possible—left general in the calculations. If $A_{11} = 2640$ as above, and if the wing masses for aeroplane S are assumed to be distributed uniformly along the span, then the total wing mass is about 12·5 slugs. In this case the estimated value of A_{12} is about $1170j$ (giving $a_{12} = 21{\cdot}9j$) where jc denotes the distance of the centre of mass in each section behind OY. The condition $A_{11}, A_{22} > A_{12}^2$ requires that $j < 0{\cdot}25$.

2. *Inertias of Control Surfaces.*—For the evaluation of the remaining inertial coefficients, the dimensions and distortion modes are assumed to be given as in Appendix I, and the masses of both the aileron and the tab (excluding any balancing masses) are taken to be distributed uniformly along the span and to be proportional to the distance from the trailing edge. Thus the mass per unit span (slug/ft) of an element of width dx situated at distance x from OY is taken to be $2\sigma_a(0{\cdot}7c - x)dx$ in the case of the aileron, and $2\sigma_t(0{\cdot}7c - x)dx$ in the case of the tab, where σ_a and σ_t are density constants. In order to define the aileron density in practical terms, it is convenient first to imagine the actual tab to be replaced by one constructed of the same material as the main aileron. Then, if μ_a (slugs) denotes the mass of the complete homogeneous aileron so obtained, and if μ_t denotes the mass of the actual tab

$$\sigma_a \equiv \mu_a/s_a c_a^2; \qquad \sigma_t \equiv \mu_t/s_t c_t^2\,.$$

Alternatively, σ_a may be defined as $\mu_a/(s_a c_a^2 - s_t c_t^2)$, where μ_a' is the mass of the aileron with its tab removed. For the purposes of these definitions balancing masses are to be excluded from μ_a and μ_t.

* Direct measurement of the stiffness rate of spring No. 1 at the N.P.L. gave 89 lb/in.

The following additional symbols are introduced

ε_a (aileron density ratio) $\equiv \rho/\sigma_a$

ε_t (tab density ratio) $\equiv \rho/\sigma_t$

Δ (aileron–tab density ratio) $\equiv \sigma_a/\sigma_t = \varepsilon_t/\varepsilon_a$.

The values $\sigma_a = \sigma_t = 0{\cdot}03837_5$ (slug/ft^3), giving $\varepsilon_a = \varepsilon_t = 0{\cdot}06197$ and $\Delta = 1$, correspond to a fabric covered combination. If the dimensions are as given for the *Spitfire*, the total weight of the combination (without balancing masses) is about 16 lb. The actual combination used for the *Spitfire* tests consisted of an aluminium tab and a fabric covered aileron, and the density constants corresponded more nearly to $\sigma_t = 3{\cdot}7\sigma_a = 0{\cdot}1151$ (slug/ft^3), giving $\varepsilon_a = 0{\cdot}06197$, $\varepsilon_t = 0{\cdot}01675$, $\Delta = 0{\cdot}2703$. When these values are adopted the estimated weights are 1·31 lb for the *balanced* tab and about 29 lb for the *balanced* aileron, as against 1·3 lb and 26·5 lb obtained from direct weighing of the components at the N.P.L. The density constants appropriate to a fabric–steel combination would be about $\varepsilon_a = 0{\cdot}06197$, $\varepsilon_t = 0{\cdot}006197$, $\Delta = 0{\cdot}1$.

In the theoretical investigation, any balancing masses present are (unless the contrary is stated) understood to be distributed along the span so as to render the relevant control surface *uniformly statically balanced* (*see* para. 7). The masses are assumed to lie at distances $\lambda_a c_a$ and $\lambda_t c_t$ ahead of the aileron and tab hinge axes, respectively. For brevity, the three cases considered are distinguished as follows

Case (U_a, U_t) unbalanced aileron, unbalanced tab,

Case (B_a, U_t) balanced aileron, unbalanced tab,

Case (B_a, B_t) balanced aileron, balanced tab.

Table 6 and Fig. 7 give the calculated inertial coefficients with ε_t, Δ, λ_a and λ_t left general, when the dimensions of the combination and the distortion modes are as specified in paras. 1 and 2 of Appendix I. For the practical ranges of λ_a and λ_t, the values of a_{33} appropriate to cases (B_a, U_t) and (B_a, B_t) differ only slightly. The contribution of the tab balancing mass to $a_{33}\varepsilon_t \times 10^3$ is given by $H_2 - H_1$ (in Table 6): the values of this correction are shown below.

Values of $H_2 - H_1$

λ_a	λ_t				
	0·1	0·3	0·5	1·0	1·5
0·25	0·08122	0·02423	0·01293	0·004652	0·002085
0·5	0·1016	0·03060	0·01650	0·006124	0·002859
0·75	0·1220	0·03697	0·02007	0·007597	0·003630

Table 7 summarises the estimated coefficients for the special cases of fabric covering ($\varepsilon = 0{\cdot}06197$) and metal covering ($\varepsilon = 0{\cdot}01675$). When balancing masses are fitted, their positions are standardised in this table as $\lambda_a = 0{\cdot}5$ and $\lambda_t = 1{\cdot}0$. The values of the corresponding barred coefficients $\bar{a}_{33}$, $\bar{a}_{34}$, $\bar{a}_{44}$, calculated for spring tab No. 2 with $N = 2, 3, 6$ are given in Table 8.

APPENDIX III

Air-Load Coefficients

The air-load coefficients for a semi-rigid wing–aileron–tab combination can be calculated by a method similar to that adopted for flexure torsion flutter in R. & M. 1952[8] and R. & M. 1943[9]. The basis of the method may be described as ' vortex strip theory '.

For the present application the necessary values of the two-dimensional coefficients were calculated by the formulae obtained in R. & M. 1948[10]. In that paper the reference point adopted lies at mid-chord, and the complex amplitudes of the air force and moments per unit span are given in terms of the air-load coefficients by the relation

$$\begin{bmatrix} cZ \\ M \\ H \\ T \end{bmatrix} = -\pi\rho c^2 V^2 \begin{bmatrix} Z_{12} & Z_{34} & Z_{56} & Z_{78} \\ M_{12} & M_{34} & M_{56} & M_{78} \\ H_{12} & H_{34} & H_{56} & H_{78} \\ T_{12} & T_{34} & T_{56} & T_{78} \end{bmatrix} \begin{bmatrix} z'/c \\ \theta' \\ \xi' \\ \beta' \end{bmatrix}, \quad \ldots \quad \ldots \quad \ldots \quad (1)$$

where z', θ', ξ', β' denote the complex amplitudes of the motion. The air-load coefficients Z_{ij}, M_{ij}, etc., are all functions of the frequency parameter* ω, the functional form being typified by

$$Z_{12} = d + e\omega^2 + if\omega + (p + iq\omega)C\,, \quad \ldots \quad \ldots \quad \ldots \quad \ldots \quad \ldots \quad (2)$$

in which d, e, f, p, q are constants depending only on the geometry of the aerofoil system, and C is a known function expressible in terms of Hankel functions of argument $\omega/2$. When ω is very great $C \to 0{\cdot}5$, and when ω is small $C \to 1 + \frac{1}{2}i\omega \log \omega$.

A relation similar to (1) applies when the reference point lies at distance $h'c$ forward of mid-chord, except that M_{12}, M_{34}, M_{56}, M_{78} must then be replaced respectively by

$$M_{12} + h'Z_{12}, \quad M_{34} + h'(Z_{34} + M_{12}) + h'^2 Z_{12}, \quad M_{56} + h'Z_{56}, \quad M_{78} + h'z_{78},$$

and Z_{34}, H_{34}, T_{34} by

$$Z_3 + h'Z_{12}, \quad H_{34} + h'H_{12}, \quad T_{34} + h'T_{12}\,.$$

Next consider a semi-rigid wing with aileron and tab. As in para. 7 the distortion modes are assumed to be

$$z_{w\text{-}a\text{-}t} = \phi l f(\eta) + \theta x F(\eta) \quad \ldots \quad \ldots \quad \ldots \quad \ldots \quad \ldots \quad \ldots \quad \ldots \quad (3)$$

for points of the main wing

$$z_{a\text{-}t} = \phi l f(\eta) + [x + d_a\{F(\eta) - 1\}]\theta + (x - d_a)\xi, \quad \ldots \quad \ldots \quad \ldots \quad (4)$$

for points of the main aileron, and

$$z_t = z_a + (x - d_t)\beta \quad \ldots \quad \ldots \quad \ldots \quad \ldots \quad \ldots \quad \ldots \quad \ldots \quad (5)$$

for points of the tab.

Let $P_{w\text{-}a\text{-}t}$, $P_{a\text{-}t}$, P_t denote typical forces applied at (x, η) to the main wing, the main aileron, and the tab, respectively. By the principle of virtual work, the first force is equivalent to a force P' applied at x' in the reference section $\eta = 1$, if

$$P'(\phi l + \theta x') = P_{w\text{-}a\text{-}t}\{\phi l f(\eta) + \theta x F(\eta)\}\,.$$

---

* In preceding reports the frequency parameter is usually denoted by λ.

Hence the flexural moment L and the torsional moment M equivalent to P_{w-a-t} are

$$L \equiv lP' = lf(\eta)P_{w-a-t}; \quad M = x'P' = F(\eta)xP_{w-a-t} . \quad .. \quad .. \quad .. \quad .. \quad (6)$$

Similarly the three moments equivalent to P_{a-t} can be written

$$L = lf(\eta)P_{a-t}; \quad M = F(\eta)xP_{a-t} + \{1 - F(\eta)\}(x - d_a)P_{a-t} ; \quad H = (x - d_a)P_{a-t} , \; .. \quad (7)$$

while the moments equivalent to P_t are similar to (7) with $T = (x - d_t)P_t$ in addition.

From the preceding relations it follows that if a complete distribution of loads represented by $lZ_\eta d\eta$, $lM_\eta d\eta$, $lH_\eta d\eta$, $lT_\eta d\eta$ is applied to a wing element of width $l\,d\eta$, then the total equivalent moments on the system are given by

$$L = l^2 f(\eta)Z_\eta d\eta , \quad .. \quad .. \quad .. \quad .. \quad .. \quad .. \quad .. \quad .. \quad (8)$$

$$M = lF(\eta)M_\eta d\eta + l\{1 - F(\eta)\}H_\eta d\eta , \quad .. \quad .. \quad .. \quad .. \quad .. \quad (9)$$

$$H = lH_\eta d\eta , \quad .. \quad .. \quad .. \quad .. \quad .. \quad .. \quad .. \quad .. \quad .. \quad (10)$$

$$T = lT_\eta d\eta . \quad .. \quad .. \quad .. \quad .. \quad .. \quad .. \quad .. \quad .. \quad .. \quad (11)$$

If the wing section considered does not contain the tab then (11) is to be ignored, and if it does not contain the aileron then (10) and (11) are to be ignored.

Now suppose the system of forces applied to the wing element to be the air-loads. Then the complex amplitudes of these loads per unit span are given by

$$\begin{bmatrix} cZ_\eta \\ M_\eta \\ H_\eta \\ T_\eta \end{bmatrix} = -\pi\rho c^2 V^2 \begin{bmatrix} Z_{12}' & Z_{34}' & Z_{56}' & Z_{78}' \\ M_{12}' & M_{34}' & M_{56}' & M_{78}' \\ H_{12}' & H_{34}' & H_{56}' & H_{78}' \\ T_{12}' & T_{34}' & T_{56}' & T'_{78} \end{bmatrix} \begin{bmatrix} z_\eta'/c \\ \theta_\eta' \\ \xi_\eta' \\ \beta_\eta' \end{bmatrix} , \quad .. \quad .. \quad (12)$$

where the accented symbols in the square matrix denote the two dimensional air-load coefficents appropriate to a reference centre at $h'c$ forward of mid-chord, and z_η', θ_η', ξ_η', β_η' denote the amplitudes of the local flexural displacement z_η, the local angle of twist θ_η', and the local aileron and tab angles ξ_η, β_η. From equations (2.4) and para. 7 of the main text it is readily shown that these local displacements are expressible in terms of the dynamical co-ordinates q by the relations

$$\begin{bmatrix} z_\eta/c \\ \theta_\eta \\ \xi_\eta \\ \beta_\eta \end{bmatrix} = \frac{l}{c} \left[\begin{array}{cccc|c} f(\eta) & 0 & 0 & 0 & 0 \\ 0 & F(\eta) & 0 & 0 & 0 \\ 0 & 1 - F(\eta) & 1 & 0 & 0 \\ 0 & 0 & 0 & 1 & 0 \end{array}\right] \begin{bmatrix} q_1 \\ q_2 \\ q_3 \\ q_4 \end{bmatrix} \quad .. \quad .. \quad .. \quad .. \quad .. \quad (13)$$

$$= (l/c)Wq \text{ say.}$$

Hence, in the notation (3.3) for complex amplitudes

$$\{z_\eta'/c, \; \theta_\eta', \; \xi_\eta', \; \beta_\eta'\} = (l/c)Wk . \quad .. \quad .. \quad .. \quad .. \quad .. \quad .. \quad .. \quad (14)$$

From (12) and (14) it follows that

$$\begin{bmatrix} cZ_\eta \\ M_\eta \\ H_\eta \\ T_\eta \end{bmatrix} = -\pi\rho clV^2 \begin{bmatrix} fZ_{12}' & FZ_{34}' + (1 - F)Z_{56}' & Z_{56}' & Z_{78}' \\ fM_{12}' & FM_{34}' + (1 - F)M_{56}' & M_{56}' & M_{78}' \\ fH_{12}' & FH_{34}' + (1 - F)H_{56}' & H_{56}' & H_{78}' \\ fT_{12}' & FT_{34}' + (1 - F)T_{56}' & T_{56}' & T_{78}' \end{bmatrix} \begin{bmatrix} k_1 \\ k_2 \\ k_3 \\ k_4 \end{bmatrix} . \quad .. \quad (15)$$

If the wing section considered does not contain the tab, the last row and last column in the square matrix in (15) will be null. If the section does not contain the aileron, the last two rows and columns will be null and also $Z_{56}' = M_{56}' = 0$.

Expressions for the total effective moments on the system can now be derived by integration of the air-loads. Let $\int_w d\eta$, $\int_a d\eta$, $\int_t d\eta$ denote integration with respect to η over the complete wing span, over the complete aileron span, and over the tab span only. Then the complex amplitude of the flexural moment is given by

$$
\begin{aligned}
-L/\rho V^2 l_3 &= -\int_w f(\eta)(Z_\eta/\rho V^2 l)\,d\eta \\
&= \pi k_1 \int_w f^2 Z_{12}'\,d\eta + \pi k_2 \Big[\int_w fFZ_{34}'\,d\eta + \int_a f(1-F)Z_{56}'\,d\eta\Big] \\
&\quad + \pi k_3 \int_a fZ_{56}'\,d\eta + \pi k_4 \int_t fZ_{78}'\,d\eta\,,
\end{aligned}
$$

and the remaining moments can be evaluated similarly. The elements of the final matrix $\mathscr{A}$ of the air-load coefficients are

$$
\begin{aligned}
\mathscr{A}_{11} &= \pi \int_w f^2 Z_{12}'\,d\eta \\
\mathscr{A}_{12} &= \pi \int_w fFZ_{34}'\,d\eta + \pi \int_a f(1-f)Z_{56}'\,d\eta \\
\mathscr{A}_{13} &= \pi \int_a fZ_{56}'\,d\eta \\
\mathscr{A}_{14} &= \pi \int_t fZ_{78}'\,d\eta \\
\mathscr{A}_{21} &= \pi \int_w FfM_{12}'\,d\eta + \pi \int_a f(1-F)H_{12}'\,d\eta \\
\mathscr{A}_{22} &= \pi \int_w F^2 M_{34}' + \pi \int_a F(1-F)(M_{56}' + H_{34}')\,d\eta + \pi \int (1-F)^2 H_{56}'\,d\eta \\
\mathscr{A}_{23} &= \pi \int_a FM_{56}'\,d\eta + \pi \int (1-F)H_{56}'\,d\eta \\
\mathscr{A}_{24} &= \pi \int_t FM_{78}'\,d\eta + \pi \int (1-F)H_{78}'\,d\eta \\
\mathscr{A}_{31} &= \pi \int_a fH_{12}'\,d\eta \\
\mathscr{A}_{32} &= \pi \int_a FH_{34}'\,d\eta + \pi \int_a (1-F)H_{56}'\,d\eta \\
\mathscr{A}_{33} &= \pi \int_a H_{56}'\,d\eta \\
\mathscr{A}_{34} &= \pi \int_t H_{78}'\,d\eta \\
\mathscr{A}_{41} &= \pi \int_t fT_{12}'\,d\eta \\
\mathscr{A}_{42} &= \pi \int_t FT_{34}'\,d\eta + \pi \int_t (1-F)T_{56}'\,d\eta \\
\mathscr{A}_{43} &= \pi \int_t T_{56}'\,d\eta \\
\mathscr{A}_{44} &= \pi \int_t T_{78}'\,d\eta\,,
\end{aligned}
$$

In the particular case of a rectangular wing–aileron–tab combination, the coefficients Z_{ij}', M_{ij}'. etc., are independent of η, and may be brought in front of the integrals. In this case the actual integrals required in the calculations of the air-load coefficients are

$$J_{11} = \pi \int_w f^2 \, d\eta \, ; \quad J_{22} = \pi \int_w F^2 \, d\eta \, ; \quad J_{33} = \pi \int_a d\eta \, ; \quad J_{44} = \pi \int_t d\eta \, ;$$

$$J_{12} = J_{21} = \pi \int_w fF \, d\eta \, ; \quad J_{13} = J_{31} = \pi \int_a f \, d\eta \, ; \quad J_{14} = J_{41} = \pi \int_t f \, d\eta \, ;$$

$$J_{23} = J_{32} = \pi \int_a F \, d\eta \, ; \quad J_{24} = J_{42} = \pi \int_t F \, d\eta \, ; \quad J_{34} = J_{43} = \pi \int_t d\eta \, ;$$

$$K_{12} = \pi \int_a f(1 - F) d\eta \, ; \quad K_{22} = \pi \int_a F(1 - F) d\eta \, ;$$

$$K_{32} = \pi \int_a (1 - F) d\eta \, ; \quad K_{42} = \pi \int_t (1 - F) d\eta \, .$$

The numerical values of these integrals for aeroplane S are given by

$$J = \begin{bmatrix} 10{\cdot}425 & 8{\cdot}3441 & 3{-}7540 & 0{\cdot}79684 \\ 8{\cdot}3441 & 6{\cdot}8713 & 3{\cdot}0588 & 0{\cdot}73005 \\ 3{\cdot}7540 & 3{\cdot}0588 & 2{\cdot}0392 & 0{\cdot}63209 \\ 0{\cdot}79684 & 0{\cdot}73005 & 0{\cdot}63209 & 0{\cdot}63209 \end{bmatrix}$$

and $K_{12} = -2{\cdot}1627$; $K_{22} = -1{\cdot}6992$; $K_{32} = -1{\cdot}0196$; $K_{42} = -0{\cdot}09796$.

Tables 9 give the air-load coefficients calculated for aeroplane S on the foregoing basis. The asymptotic values for $\omega \to \infty$ are as follows.

$$\gamma \equiv -C/\omega^2 = \begin{bmatrix} 2{\cdot}606 & 0{\cdot}4079 & 0{\cdot}01617 & 0{\cdot}00009084 \\ 0{\cdot}4079 & 0{\cdot}1167 & 0{\cdot}005009 & 0{\cdot}00003554 \\ 0{\cdot}01617 & 0{\cdot}005009 & 0{\cdot}0005383 & 0{\cdot}0_5 6194 \\ 0{\cdot}00009084 & 0{\cdot}00003554 & 0{\cdot}0_5 6194 & 0{\cdot}0_6 5057 \end{bmatrix} \quad .. \quad (16)$$

$$B/\omega = \begin{bmatrix} +5{\cdot}213 & 3{\cdot}765 & 0{\cdot}3452 & 0{\cdot}008407 \\ -0{\cdot}2138 & 0{\cdot}6266 & 0{\cdot}09936 & 0{\cdot}003236 \\ +0{\cdot}009010 & 0{\cdot}02145 & 0{\cdot}009079 & 0{\cdot}0005493 \\ 0{\cdot}00004654 & 0{\cdot}0001511 & 0{\cdot}00008344 & 0{\cdot}00003559 \end{bmatrix} \quad .. \quad (17)$$

TABLE 1

Flexure–Torsion Flutter Characteristics of Aeroplane S

		Upper Critical			Lower Critical			Natural Frequencies (c.p.s.)			
j	p	V_1(m.p.h.)	f_1	ω_1	V_2(m.p.h.)	f_2	ω_2	f_{1v}	f_{2v}	f_{1a}	f_{2a}
0·2	4·39	?	?	?	649	21·7	0·84	9·60	48·7	9·17	42·0
0·1	2·19	1868	6·69	0·09	665	17·9	0·675	9·89	30·9	9·43	29·9
0·05	1·10	1453	8·67	0·15	778	16·6	0·535	9·97	28·6	9·52	27·6
0	0	None	—	—	None	—	—	10·0	28·0	9·56	26·7

TABLE 2

Aileron–Tab Natural Frequencies with Spring Tab No. 2

($N = 3$)

f_v, f_a denote frequencies (c.p.s.) corresponding to oscillations *in vacuo* and in still air

Description of system*		Control column locked (symmetrical oscillations)				Column free (antisymmetrical)		Column locked and tab locked to aileron (f_v)	Column locked and aileron locked to wing (f_v)	Column free and aileron locked to wing (f_v)
Aileron	Tab	f_{1v}	f_{2v}	f_{1a}	f_{2a}	f_{1v}	f_{2v}			
F U	F U	4·25	288·0	4·05	270·0	51·2	∞	24·2	277·0	50·1
F B	F U	3·04	285·0	2·96	267·0	51·4		17·1	277·0	50·1
F B	F B	3·03	134·0	2·95	132·0	24·2		17·0	159·0	28·7
F U	A U	3·72	166·0	3·58	162·0	28·4		22·1	144·0	26·0
F B	A U	2·76	157·0	2·70	154·0	27·6		15·9	144·0	26·0
F B	A B	2·77	92·3	2·71	91·7	16·4		15·8	82·7	15·0
A U	A U	2·21	159·0	2·18	156·0	28·3		12·6	144·0	26·0
A B	A U	1·58	154·0	1·57	151·0	27·7		8·87	144·0	26·0
A B	A B	1·57	71·7	1·57	71·4	12·9		8·86	82·7	15·0

* F denotes fabric covering; A aluminium covering; U not mass-balanced; B uniformly statically balanced.

TABLE 3

Values of W_{max} for Aileron–Tab Flutter

$N = 2$			$N = 3$			$N = 6$			$N = 10$		
$\bar{p}$	$-W_{max}$	$1{\cdot}05\bar{p}$	$\bar{p}$	$-W_{max}$	$1{\cdot}07\bar{p}$	$\bar{p}$	$-W_{max}$	$1{\cdot}18\bar{p}$	$\bar{p}$	$-W_{max}$	$1{\cdot}31\bar{p}$
0	0·00014	0	0·00544	0·00587	0·00582	0·006	0·00733	0·00708	0·01	0·0134	0·0131
0·002	0·00218	0·00210	0·006758	$0{\cdot}00741_5$	0·00723	0·007155	0·00869	0·00844	0·04	0·0524	0·0524
0·0054	0·00574	0·00567	0·01	0·0108	0·0107	0·008	0·00970	0·00944			
0·010	0·0105	0·0105	0·0125	0·0135	0·0134	0·01	0·0122	0·0118			
0·0125	0·0131	0·0131	0·015	$0{\cdot}0162_5$	0·0161	0·04	0·0473	0·0472			
			0·02	0·0215	0·0214						
			0·04	0·0429	0·0428						
		$M = 1{\cdot}05$		$M = 1{\cdot}07$		$M = 1{\cdot}18$		$M = 1{\cdot}31$			

TABLE 4

Spring–Tab Constants (units : feet and pounds)

(See Appendix I, para. 3 (b))

	R	r	n $(= R/r)$	N $(= R'/r')$	σ	P_0	$2\sigma_0 R'^2$	$2\sigma_0 R'r'$	$2\sigma_0 r'^2$	σr^2
Short lever	0	0·0609	0	5·61	1068	24	3650	651	116	3·96
Long lever	0	0·113	0	3·03	1068	24	3650	1205	398	13·6

TABLE 5

Constants for Elastic Matrices e and ε

(See Appendix I, para. 3 (b), and equations (2.10), (4.3))

	$\frac{l_\phi}{\rho l^3}$	$\frac{m_\theta}{\rho l c_0^2}$	$\frac{2\sigma_0 R'^2}{\rho l c_0^2}$	$\frac{2\sigma_0 r'^2}{\rho l c_0^2}$	$\frac{2\sigma_0 r'^2}{\rho l c_0^2}$	$\frac{\sigma r^2}{\rho l c_0^2}$	$\frac{\sigma R^2}{\rho l c_0^2}$	$\frac{\sigma R r}{\rho l c_0^2}$
Short lever ($N = 5{\cdot}61$)	$3{\cdot}74 \times 10^6$	$1{\cdot}16 \times 10^6$	4227	754	134	4·59	0	0
Long lever ($N = 3{\cdot}03$)	$3{\cdot}74 \times 10^6$	$1{\cdot}16 \times 10^6$	4227	1395	461	15·75	0	0

$1/\rho l c_0^2 = 1{\cdot}158.$

TABLE 6

*Inertial Coefficients of Aileron and Tab**

Coefficient	Case (U_a, U_t)	Case (B_a, U_t)	Case (B_a, B_t)
$a_{13}\varepsilon_t \times 10^3$	$0{\cdot}1488 + 5{\cdot}020\Delta$	0	0
$a_{23}\varepsilon_t \times 10^3$	$0{\cdot}08692 + 2{\cdot}2017\Delta$	$H + \lambda_a(0{\cdot}02770 + 0{\cdot}6322\Delta) = H_1$	H_2*
$a_{33}\varepsilon_t \times 10^3$	$0{\cdot}02355 + 0{\cdot}3064\Delta = H$	H_1	H_2
$a_{14}\varepsilon_t \times 10^3$	0·01348	0·01348	0
$a_{24}\varepsilon_t \times 10^3$	0·007958	0·007958	$0{\cdot}0002884(1+2\lambda_t)$
$a_{34}\varepsilon_t \times 10^3$	0·002220	0·002220	$0{\cdot}0002884(1+2\lambda_t)$
$a_{44}\varepsilon_t \times 10^3$	0·0002884	0·0002884	$0{\cdot}0002884(1+2\lambda_t)$

$$* H_2 = H + \lambda_a\left(0{\cdot}02519 + 0{\cdot}6322\Delta + \frac{0{\cdot}008397}{\lambda_t}\right) + \frac{0{\cdot}01091}{\lambda_t}(0{\cdot}77 - 0{\cdot}23\lambda_t)^2$$

Note.—U denotes not mass balanced; B denotes uniformly statically balanced; $\Delta = \sigma_a/\sigma_t$ and $\varepsilon_t = \rho/\sigma_t$ (*see* Appendix II).

TABLE 7

Inertial Coefficients for Fabric or Metal Components (see *Appendix II*)

(*U denotes inertial un-balance : B denotes uniform static balance*)

Description of System	$10a_{13}$	$10a_{23}$	$10a_{33}$	10^3a_{14}	10^4a_{24}	10^4a_{34}	10^5a_{44}
Fabric aileron (U); fabric tab (U)	0·836	0·370	0·0533	0·218	1·29	0·358	0·0463
,, ,, (B); ,, ,, (U)	0	0·107	0·107	0·218	1·29	0·358	0·0463
,, ,, (B); ,, ,, (B)	0	0·108	0·108	0	0·140	0·140	0·140
Fabric aileron (U); Al. tab (U)	0·901	0·408	0·0636	0·806	4·76	1·33	0·171
,, ,, (B); ,, ,, (U)	0	0·123	0·123	0·806	4·76	1·33	0·171
,, ,, (B); ,, ,, (B)	0	0·127	0·127	0	0·518	0·518	0·518
Al. aileron (U); Al. tab (U)	3·09	1·37	0·197	0·807	4·76	1·33	0·171
,, ,, (B); ,, ,, (U)	0	0·395	0·395	0·807	4·76	1·33	0·171
,, ,, (B); ,, ,, (B)	0	0·399	0·399	0	0·518	0·518	0·518

Notes : (i) In all cases it is assumed that $a_{11} = 27{\cdot}5$, $a_{22} = 1{\cdot}09$, $a_{12} = 21{\cdot}9j$ where jc denotes the distance of the inertia axis behind the flexural axis.

(ii) The density constants for fabric-covered and aluminium-covered components are taken respectively as $\sigma = 0{\cdot}03837(\varepsilon = 0{\cdot}06197)$ and $\sigma = 0{\cdot}1151(\varepsilon = 0{\cdot}01675)$.

(iii) Factors used in conversion to non-dimensional coefficients are $1/\rho l^3c^2 = 0{\cdot}01043$; $1/\rho l^2c^3 = 0{\cdot}01873$; $1/\rho lc^4 = 0{\cdot}03364$.

TABLE 8

Barred Inertial Co-efficients of Aileron and Tab with Spring Tab No. 2 ($n = 0$)

Description of System	$N = 2$			$N = 3$			$N = 6$		
	$10^3\bar{a}_{33}$	$10^3\bar{a}_{34}$	$10^3\bar{a}_{44}$	$10^3\bar{a}_{33}$	$10^3\bar{a}_{34}$	$10^3\bar{a}_{44}$	$10^3\bar{a}_{33}$	$10^3\bar{a}_{24}$	$10^3\bar{a}_{44}$
Fabric aileron (U); fabric tab (U)	5·33	5·403	5·49	5·33	5·439	5·59	5·33	5·547	5·93
,, ,, (B); ,, ,, (U)	10·7	10·74	10·8	10·7	10·78	10·9	10·7	10·88	11·3
,, ,, (B); ,, ,, (B)	10·8	10·84	11·0	10·8	10·86	11·1	10·8	10·9	11·6
Fabric aileron (U); Al. tab (U)	6·36	6·624	6·96	6·36	6·757	7·31	6·36	7·155	8·57
,, ,, (B); ,, ,, (U)	12·3	12·57	12·9	12·3	12·70	$13{\cdot}2_5$	12·3	13·10	14·5
,, ,, (B) ,, ,, (B)	12·7	12·80	13·1	12·7	12·85	13·48	12·7	13·01	15·2
Al. aileron (U) Al. tab (U)	19·7	19·99	20·3	19·7	20·13	20·7	19·7	20·52	21·9
,, ,, (B); ,, ,, (U)	39·5	39·75	40·1	39·5	39·88	40·4	39·5	40·28	41·7
,, ,, (B); ,, ,, (B)	39·9	40·00	40·3	39·9	40·06	40·7	39·9	40·21	42·4

TABLE 9A

Air-Load Coefficients C_{1j} and B_{1j} (see *Appendix III*)

ω	C_{11}	B_{11}	C_{12}	B_{12}	C_{13}	B_{13}	C_{14}	B_{14}
0	0	0	7·064	0	2·223	0	0·2337	0
0·02	+ 0·008476	0·2048	6·942	− 0·2129	2·184	−0·09115	0·2296	−0·01042
0·04	0·02719	0·4019	6·817	− 0·3148	−2·143	−0·1468	0·2253	−0·01708
0·06	0·05186	0·5911	6·695	− 0·3709	2·103	−0·1875	0·2209	−0·02216
0·08	0·08006	0·7729	6·576	− 0·3970	2·063	−0·2181	0·2167	−0·02615
0·10	0·1101	0·9476	6·463	− 0·4011	2·025	−0·2414	0·2126	−0·02935
0·12	0·1408	1·115	6·356	− 0·3885	1·989	−0·2589	0·2086	−0·03192
0·16	0·2008	1·435	6·158	− 0·3259	1·921	−0·2809	0·2013	−0·03566
0·2	0·2550	1·735	5·982	− 0·2284	1·861	−0·2904	0·1947	−0·03803
0·4	0·3690	3·034	5·342	+ 0·4967	1·641	−0·2489	0·1684	−0·03995
0·6	+ 0·1834	4·159	4·932	1·343	1·510	−0·1564	0·1563	−0·03603
0·8	− 0·2919	5·212	4·622	2·201	1·426	−0·0551	0·1471	−0·03099
1·0	− 1·035	6·233	4·350	3·048	1·366	+0·0449	0·1410	−0·02599
1·2	− 2·029	7·240	4·088	3·880	1·322	0·1415	0·1366	−0·02132
1·4	− 3·263	8·241	3·818	4·699	1·286	0·2344	0·1333	−0·01701
1·6	− 4·729	9·242	3·532	5·508	1·256	0·3241	0·1308	−0·01304
1·8	− 6·422	10·24	3·224	6·308	1·230	0·4111	0·1289	−0·009379
2·0	− 8·334	11·25	2·891	7·101	1·205	0·4955	0·1274	−0·005957
2·2	−10·47	12·25	2·531	7·888	1·182	0·5781	0·1261	−0·002748
2·4	−12·81	13·26	2·143	8·674	1·159	0·6592	0·1251	+0·0002837
2·6	−15·38	14·27	1·722	9·450	1·137	0·7386	0·1242	0·003164
2·8	−18·16	15·28	1·273	10·22	1·114	0·8171	0·1235	0·005916
3·0	−21·15	16·29	0·7934	11·00	1·091	0·8946	0·1228	0·008558
3·2	−24·36	17·31	0·2815	11·77	1·067	0·9711	0·1222	0·01111
3·4	−27·78	18·33	−0·2622	12·54	1·042	1·047	0·1217	0·01357
3·6	−31·41	19·35	−0·8373	13·30	1·017	1·122	0·1212	0·01597
3·8	−35·24	20·37	−1·444	14·07	0·9905	1·197	0·1208	0·01830
4·0	−39·29	21·39	−2·084	14·83	0·9633	1·271	0·1204	0·02058
4·2	−43·55	22·41	−2·755	15·60	0·9348	1·345	0·1200	0·02281
4·4	−48·02	23·44	−3·459	16·36	0·9054	1·418	0·1196	0·02500
4·6	−52·70	24·46	−4·195	17·12	0·8748	1·491	0·1193	0·02715
4·8	−57·59	25·49	−4·963	17·88	0·8431	1·564	0·1190	0·02926
5·0	−62·69	26·52	−5·764	+18·65	0·8105	+1·636	0·1186	+0·03135

TABLE 9B

Air-Load Coefficients C_{2j} and B_{2j} (see *Appendix III*)

ω	C_{21}	B_{21}	C_{22}	B_{22}	C_{23}	B_{23}	C_{24}	B_{24}
0	0	0	−0·4713	0	0·2169	0	0·03787	0
0·02	−0·0005536	−0·008401	−0·4662	0·02476	0·2185	0·006110	0·03806	0·0005560
0·04	−0·001940	−0·01648	−0·4610	0·04481	0·2202	0·01072	0·03826	0·0009377
0·06	−0·003980	−0·02424	−0·4561	0·06231	0·2219	0·01471	0·03846	0·001246
0·08	−0·006578	−0·03169	−0·4515	0·07976	0·2235	0·01828	0·03866	0·001503
0·10	−0·009665	−0·03887	−0·4471	0·09565	0·2251	0·02154	0·03885	0·001724
0·12	−0·01319	−0·04584	−0·4432	0·1108	0·2266	0·02455	0·03903	0·001916
0·16	−0·02142	−0·05881	−0·4363	0·1397	0·2294	0·03003	0·03937	0·002235
0·2	−0·03105	−0·07115	−0·4309	0·1670	0·2319	0·03498	0·03968	0·002489
0·4	−0·09759	−0·1243	−0·4196	0·2935	0·2404	0·05601	0·04037	0·003304
0·6	−0·1928	−0·1706	−0·4291	0·4148	0·2447	0·07489	0·04146	0·003847
0·8	−0·3175	−0·2138	−0·4534	0·5357	0·2468	0·09343	0·04185	0·004339
1·0	−0·4724	−0·2557	−0·4902	0·6571	0·2472	0·1120	0·04214	0·004832
1·2	−0·6579	−0·2971	−0·5379	0·7792	0·2465	0·1307	0·04232	0·005341
1·4	−0·8747	−0·3383	−0·5962	0·9013	0·2451	0·1496	0·04245	0·005866
1·6	−1·124	−0·3793	−0·6645	1·025	0·2429	0·1686	0·04254	0·006408
1·8	−1·405	−0·4205	−0·7425	1·148	0·2402	0·1877	0·04260	0·006962
2·0	−1·717	−0·4611	−0·8300	1·271	0·2369	0·2069	0·04264	0·007530
2·2	−2·062	−0·5030	−0·9278	1·395	0·2331	0·2262	0·04266	0·008104
2–4	−2·438	−0·5436	−1·034	1·520	0·2288	0·2456	0·04268	0·008692
2·6	−2·849	−0·5853	−1·151	1·644	0·2241	0·2650	0·04268	0·009281
2·8	−3·291	−0·6268	−1·276	1·768	0·2189	0·2845	0·04267	0·009878
3·0	−3·765	−0·6684	−1·411	1·892	0·2133	0·3041	0·04265	0·01048
3·2	−4·272	−0·7100	−1·556	2·017	0·2072	0·3236	0·04263	0·01109
3·4	−4·812	−0·7517	−1·710	2·142	0·2007	0·3432	0·04261	0·01170
3·6	−5·383	−0·7935	−1·873	2·266	0·1938	0·3628	0·04257	0·01231
3·8	−5·988	−0·8354	−2·045	2·391	0·1865	0·3824	0·04253	0·01293
4·0	−6·625	−0·8774	−2·227	2·516	0·1788	0·4020	0·04249	0·01355
4·2	−7·294	−0·9193	−2·419	2·641	0·1707	0·4217	0·04244	0·01417
4·4	−7·997	−0·9613	−2·619	2·766	0·1621	0·4414	0·04239	0·01479
4·6	−8·731	−1·003	−2·829	2·891	0·1532	0·4611	0·04234	0·01542
4·8	−9·498	−1·046	−3·049	3·016	0·1438	0·4809	0·04228	0·01605
5·0	−10·30	−1·088	−3·278	3·140	0·1341	0·5005	0·04222	0·01668

TABLE 9c

Air-Load Coefficients C_{3j} and B_{3j} (see *Appendix* III)

ω	$10C_{31}$	$10B_{31}$	$10C_{32}$	$10B_{32}$	$10C_{33}$	$10B_{33}$	10^2C_{34}	10^2B_{34}
0	0	0	+0·06283	0	0·1680	0	0·7294	0
0·02	+0·00009983	0·003540	0·06080	−0·0004975	0·1670	−0·0007407	0·7281	−0·002933
0·04	0·000283	0·006945	0·05867	+0·0008560	0·1659	−0·000556	0·7265	−0·004435
0·06	0·0004764	0·01022	0·05655	0·002971	0·1648	+0·00001977	0·7248	−0·005331
0·08	0·000637	0·01336	0·05444	0·005586	0·1638	0·000856	0·7232	−0·005818
0·10	0·0007369	0·01638	0·05240	0·008567	0·1628	0·001886	0·7216	−0·006000
0·12	0·000755	0·01929	0·05044	0·01183	0·1618	0·003066	0·7201	−0·005945
0·16	+0·000484	0·02481	0·04667	0·01896	0·1600	0·005763	0·7174	−0·005297
0·2	−0·0002628	0·0300	0·04315	0·02668	0·1583	0·008789	0·7149	−0·004109
0·4	−0·01228	0·05244	0·02737	0·06914	0·1520	0·02622	0·7054	+0·005499
0·6	−0·03885	0·07189	+0·01192	0·1136	0·1476	0·04501	0·6997	0·01732
0·8	−0·07973	0·09009	−0·005302	0·1583	0·1440	0·06399	0·6966	0·02958
1·0	−0·1346	0·1077	−0·02539	0·2027	0·1407	0·08295	0·6940	0·04184
1·2	−0·2031	0·1252	−0·04877	0·2469	0·1374	0·1018	0·6921	0·05398
1·4	−0·2851	0·1425	−0·07577	0·2908	0·1339	0·1206	0·6902	0·06599
1·6	−0·3803	0·1598	−0·1065	0·3347	0·1301	0·1393	0·6890	0·07781
1·8	−0·4891	0·1771	−0·1410	0·3783	0·1260	0·1579	0·6877	0·08957
2·0	−0·6108	0·1944	−0·1795	0·4220	0·1216	0·1765	0·6871	0·1013
2·2	−0·7455	0·2118	−0·2218	0·4653	0·1169	0·1950	0·6858	0·1128
2·4	−0·8934	0·2292	−0·2681	0·5087	0·1117	0·2134	0·6852	0·1243
2·6	−1·055	0·2466	−0·3184	0·5521	0·1062	0·2319	0·6840	0·1358
2·8	−1·229	0·2641	−0·3725	0·5954	0·1002	0·2503	0·6831	0·1472
3·0	−1·416	0·2817	−0·4308	0·6386	0·09380	0·2687	0·6820	0·1585
3·2	−1·616	0·2992	−0·4929	0·6817	0·08708	0·2871	0·6812	0·1698
3·4	−1·829	0·3168	−0·5593	0·7248	0·07990	0·3054	0·6803	0·1811
3·6	−2·055	0·3344	−0·6292	0·7681	0·07230	0·3237	0·6793	0·1924
3·8	−2·294	0·3521	−0·7035	0·8112	0·06427	0·3420	0·6782	0·2036
4·0	−2·546	0·3697	−0·7819	0·8543	0·05583	0·3603	0·6770	0·2148
4·2	−2·811	0·3874	−0·8640	0·8975	0·04695	0·3786	0·6761	0·2261
4·4	−3·089	0·4051	−0·9502	0·9404	0·03766	0·3969	0·6749	0·2372
4·6	−3·380	0·4228	−1·040	0·9835	0·02794	0·4151	0·6737	0·2484
4·8	−3·684	0·4406	−1·135	1·026	0·01779	0·4334	0·6725	0·2596
5·0	−4·002	0·4584	−1·233	+1·070	0·007220	+0·4516	0·6713	+0·2707

TABLE 9D

Air-Load Coefficients C_{4j} and B_{4j} (see *Appendix III*)

ω	10^3C_{41}	10^3B_{41}	10^3C_{42}	10^3B_{42}	10^3C_{43}	10^3B_{43}	10^3C_{44}	10^3B_{44}
0	0	0	+0·06827	0	+0·1106	0	0·2547	0
0·02	0·00004857	0·001827	0·06668	−0·0001945	0·1100	−0·0002582	0·2545	−0·0002678
0·04	0·0001344	0·003585	0·06520	+0·0008457	0·1092	+0·0001815	0·2541	−0·0001880
0·06	0·0002193	0·005273	0·06380	0·002395	0·1084	0·0009152	0·2537	+0·00003881
0·08	0·0002816	0·006894	0·06238	0·004279	0·1076	0·001846	0·2533	0·0003652
0·10	0·0003065	0·008453	0·06104	0·006410	0·1069	0·002922	0·2529	0·0007655
0·12	0·0002831	0·009954	0·05970	0·008729	0·1061	0·004111	0·2525	0·001224
0·16	0·0000610	0·01280	0·05714	0·01378	0·1047	0·006745	0·2518	0·002270
0·2	−0·0004781	0·01546	0·05468	0·01888	0·1037	0·009610	0·2513	0·003413
0·4	−0·007570	0·02701	0·04371	0·04915	0·09861	0·02579	0·2490	0·01024
0·6	−0·02271	0·03705	0·03298	0·08044	0·09481	0·04292	0·2478	0·01757
0·8	−0·04590	0·04646	0·02047	0·1116	0·09165	0·06024	0·2465	0·02497
1·0	−0·07690	0·05562	+0·006606	0·1435	0·08786	0·07775	0·2459	0·03224
1·2	−0·1155	0·06462	−0·01021	0·1745	0·08470	0·09481	0·2453	0·03982
1·4	−0·1618	0·07355	−0·02904	0·2050	0·08091	0·1119	0·2446	0·04715
1·6	−0·2151	0·08207	−0·05091	0·2360	0·07648	0·1289	0·2440	0·05449
1·8	−0·2765	0·09164	−0·07570	0·2672	0·07206	0·1460	0·2434	0·06194
2·0	−0·3450	0·1004	−0·1028	0·2976	0·06700	0·1631	0·2427	0·06890
2·2	−0·4207	0·1092	−0·1327	0·3286	0·06194	0·1801	0·2427	0·07648
2·4	−0·5036	0·1179	−0·1660	0·3590	0·05626	0·1972	0·2421	0·08344
2·6	−0·5941	0·1273	−0·2014	0·3895	0·04970	0·2138	0·2414	0·09080
2·8	−0·6919	0·1363	−0·2399	0·4200	0·04290	0·2306	0·2408	0·09800
3·0	−0·7968	0·1450	−0·2815	0·4503	0·03565	0·2478	0·2402	0·1049
3·2	−0·9094	0·1544	−0·3253	0·4810	0·02790	0·2643	0·2394	0·1124
3·4	−1·029	0·1635	−0·3723	0·5114	0·01970	0·2812	0·2387	0·1196
3·6	−1·156	0·1726	−0·4221	0·5418	0·01090	0·2980	0·2380	0·1268
3·8	−1·290	0·1817	−0·4748	0·5723	+0·001700	0·3148	0·2372	0·1339
4·0	−1·432	0·1904	−0·5305	0·6025	−0·008028	0·3318	0·2364	0·1410
4·2	−1·581	0·1999	−0·5886	0·6331	−0·01810	0·3483	0·2356	0·1483
4·4	−1·737	0·2091	−0·6497	0·6634	−0·02890	0·3652	0·2347	0·1555
4·6	−1·900	0·2183	−0·7138	0·6938	−0·04000	0·3819	0·2337	0·1626
4·8	−2·071	0·2273	−0·7806	0·7241	−0·05170	0·3987	0·2328	0·1698
5·0	−2·249	0·2367	−0·8479	+0·7540	−0·06380	+0·4153	0·2320	+0·1770

TABLE 10

Barred Inertial Coefficients for Aileron–Tab with Spring Tab No. 1

Description of System	$N = 3$; $n = 0{\cdot}5$		$N = 3$; $n = 1{\cdot}0$		$N = 3$; $n = 2{\cdot}0$		$N = 3$
	$10^3\bar{a}_{33}$	$10^3\bar{p}$	$10^3\bar{a}_{33}$	$10^3\bar{p}$	$10^3\bar{a}_{33}$	$10^3\bar{p}$	$10^3\bar{a}_{44}$
Fabric aileron (U); Fabric tab (U)	5·37	5·462	5·41	5·487	5·49	5·537	5·59
,, ,, (B); ,, ,, (U)	10·7	10·83	10·8	10·86	10·9	10·91	10·90
,, ,, (B); ,, ,, (B)	10·8	10·87	10·8	10·90	10·9	10·95	11·10
Fabric aileron (U); Al.tab (U) ..	6·50	6·851	6·64	6·943	6·96	7·128	7·31
,, ,, (B); ,, ,, (U) ..	12·4	12·79	12·6	12·88	12·9	13·07	13·25
,, ,, (B); ,, ,, (B) ..	12·8	12·96	12·9	13·06	13·1	13·27	13·48
Al. aileron (U); Al. tab (U) ..	19·8	20·19	20·0	20·28	20·3	20·47	20·70
,, ,, (B); ,, ,, (U) ..	39·6	39·99	39·8	40·08	41·0	40·27	40·40
,, ,, (B); ,, ,, (B) ..	40·0	40·16	40·1	40·26	40·3	40·47	40·70

Al. denotes aluminium, U unbalanced, B uniform static balance.

TABLE 11A

Flexure–Aileron–Tab Flutter (Aileron unbalanced)

ω	$X = 0$				$X = 5$				$X = 10$			
	Z_1	W_1	Z_2	W_2	Z_1	W_1	Z_2	W_2	Z_1	W_1	Z_2	W_2
0·2	−0·002360	−0·03184	+0·1884	−0·27899	—	—	—	—	—	—	—	—
0·6	−0·005161	−0·008203	0·01744	−0·03703	+0·01590	−0·03549	−0·005301	−0·007895	−0·005578	−0·007346	+0·01248	−0·03217
0·8	—	—	—	—	—	—	—	—	−0·006793	−0·003923	$-0\cdot0_35739$	−0·01439
1·0	−0·005329	−0·006419	0·003195	−0·01727	$+0\cdot0_39515$	−0·01504	−0·005488	−0·006050	−0·005000	−0·006912	+0·3092	−0·03789
1·2	−0·005397	−0·006080	$+0\cdot0_37486$	−0·01390	−0·002338	−0·01063	−0·00554	−0·005702	−0·005190	−0·006311	0·008449	−0·01836
1·4	−0·005431	−0·005886	$-0\cdot0_37491$	−0·01186	−0·004714	−0·007021	−0·006728	−0·002812	−0·005260	−0·006018	0·002899	−0·01411
1·6	−0·005464	−0·005756	−0·001705	−0·01055	−0·005105	−0·006216	−0·01980	−0·03156	−0·005288	−0·005851	$+0\cdot0_35848$	−0·01193
1·8	−0·005500	−0·005652	−0·002353	−0·09676	−0·005298	−0·005797	+0·008725	−0·01336	−0·005289	−0·005764	$-0\cdot0_37427$	−0·01057
2·0	−0·005537	−0·005569	−0·002805	−0·00901	−0·005317	−0·005693	+0·001135	−0·01081	−0·005283	−0·005703	−0·001605	−0·009645
2·4	−0·005649	−0·005412	−0·003394	−0·008379	−0·005297	−0·005633	−0·001878	−0·008844	−0·005248	−0·005667	−0·002681	−0·008457
2·6	—	—	—	—	−0·005282	−0·005620	−0·002503	−0·008315	—	—	—	—
3·0	−0·005963	−0·005136	−0·003645	−0·008219	−0·005241	−0·005626	−0·003269	−0·007605	−0·005183	−0·005677	−0·003540	−0·007480
3·4	−0·006633	−0·005758	−0·003460	−0·009373	−0·005191	−0·005654	−0·003740	−0·007137	—	—	—	—
3·6	−0·008236	−0·004236	−0·002932	−0·01468	—	—	—	—	—	—	—	—
3·8	—	—	—	—	−0·005135	−0·005697	−0·004072	−0·006796	—	—	—	—
4·0	—	—	—	—	—	—	—	—	−0·005024	−0·005805	−0·004286	−0·006619
4·2	—	—	—	—	−0·005062	−0·005763	−0·004333	−0·006522	—	—	—	—
4·6	—	—	—	—	−0·004698	−0·005854	−0·004561	−0·006279	—	—	—	—

TABLE 11B

Flexure–Aileron–Tab Flutter (Aileron unbalanced)

ω	$X = -3{\cdot}0$				$X = -2{\cdot}5$				$X = -1{\cdot}0$			
	Z_1	W_1	Z_2	W_2	Z_1	W_1	Z_2	W_2	Z_1	W_1	Z_2	W_2
0·6	−0·005085	−0·008399	+0·01769	−0·03745	−0·005102	−0·008359	+0·01770	−0·03741	—	—	—	—
0·8	—	—	—	—	−0·005255	−0·007121	0·008051	−0·02400	−0·005282	−0·007020	+0·007935	−0·02378
1·0	−0·005441	−0·006489	+0·003574	−0·01796	−0·005347	−0·006553	0·003493	−0·01776	−0·005342	−0·006456	0·003375	−0·01749
1·2	—	—	—	—	−0·005476	−0·006216	+0·001034	−0·01446	−0·005409	−0·006127	$+0{\cdot}0_3 9130$	−0·01411
1·4	−0·006026	−0·006014	$-0{\cdot}0_3 4285$	−0·01331	−0·005702	−0·005963	$-0{\cdot}0_3 4255$	−0·01267	−0·005476	−0·005913	$-0{\cdot}0_3 5801$	−0·01209
1·6	—	—	—	—	−0·006460	−0·005629	−0·001224	−0·01234	−0·005566	−0·005750	−0·001519	−0·01083
1·8	−0·002619	−0·008457	−0·004046	−0·006721	—	—	—	—	−0·005666	−0·005600	−0·002143	−0·01001
2·0	−0·002930	−0·008157	−0·004554	−0·006157	—	—	—	—	—	—	—	—
2·2	−0·003278	−0·007831	−0·004661	−0·006116	−0·003699	−0·007165	−0·004124	−0·006632	−0·006143	−0·005218	−0·002793	−0·009336
2·6	−0·003782	−0·007277	−0·004741	−0·006084	−0·003987	−0·006976	−0·004502	−0·006330	−0·01191	−0·003722	−0·002420	−0·01255
3·0	−0·004170	−0·006806	−0·004668	−0·006146	—	—	—	—	—	—	—	—

TABLE 11C

Flexure–Aileron–Tab Flutter (Aileron unbalanced)

ω	$X = -10$				$X = -5$				$X = -4$			
	Z_1	W_1	Z_2	W_2	Z_1	W_1	Z_2	W_2	Z_1	W_1	Z_2	W_2
0·4	−0·004268	−0·01293	+0·04180	−0·07394	—	—	—	—	—	—	—	—
0·6	−0·003854	−0·01221	+0·008017	−0·03148	−0·005021	−0·008560	+0·01745	−0·03750	−0·005056	−0·008484	+0·01763	−0·03751
0·8	+0·01262	−0·02532	−0·005327	−0·006156	−0·005203	−0·007437	0·007695	−0·02419	—	—	—	—
1·0	0·005126	−0·01807	−0·005229	−0·006154	−0·005495	−0·007275	+0·002582	−0·01850	−0·005381	−0·006765	0·003332	−0·01805
1·2	—	—	—	—	−0·003066	−0·01285	−0·004551	−0·005088	−0·005968	−0·006647	$+0{\cdot}0_3 6371$	−0·01574
1·4	$+0{\cdot}0_3 1722$	−0·01223	−0·005264	−0·005832	$-0{\cdot}0_4 5265$	−0·01155	−0·004943	−0·005835	$+0{\cdot}0_3 1796$	−0·01014	−0·004040	−0·005572
1·8	−0·001840	−0·009744	−0·005173	−0·005796	−0·002044	−0·009441	−0·005018	−0·005860	−0·002154	−0·009210	−0·004863	−0·005930
2·2	−0·002835	−0·008494	−0·005132	−0·005766	−0·002999	−0·008287	−0·005008	−0·005851	−0·003084	−0·008158	−0·004915	−0·005917
2·6	−0·003428	−0·007749	−0·005089	−0·005775	—	—	—	—	$-0{\cdot}00363_5$	−0·007491	−0·004908	−0·005929
3·0	−0·003828	−0·007251	−0·005034	−0·005851	−0·003951	−0·007101	−0·004928	−0·005912	−0·004019	−0·007011	−0·004860	−0·005979

TABLE 12

Binary Flutter (Aileron unbalanced)

ω	$Z = \infty$ ($\bar{a}_{14} = 0{\cdot}0840$)				$W = \infty$ ($\bar{a}_{13} = 0{\cdot}0836$)				$X = \infty$ ($\bar{a}_{34} = 0{\cdot}00540$)			
	X_1	W_1	X_2	W_2	X_1	Z_1	X_2	Z_2	Z_1	W_1	Z_2	W_2
0·2	—	—	—	—	202·9	−0·4068	−29·61	−0·2893	—	—	—	—
0·4	—	—	—	—	41·44	−0·1078	−17·06	−0·05719	−0·00444	−0·01222	+0·07061	$-0{\cdot}0930_5$
0·6	22·544	−0·096959	−11·9983	−0·0554072	—	—	—	—	—	—	—	—
0·8	—	—	—	—	12·61	−0·0327	− 7·844	−0·007563	−0·00516	−0·00735	0·01201	−0·02658
1·0	9·91504	−0·0396836	− 5·96431	−0·0156952	—	—	—	—	−0·00523	−0·00643	0·00591	−0·01908
1·2	—	—	—	—	6·996	−0·01786	− 4·516	−0·001646	—	—	—	—
1·4	6·28488	−0·0233476	− 3·65010	−0·0067231	—	—	—	—	−0·005265	−0·00594	$+0{\cdot}0_36142$	−0·01266
1·6	—	—	—	—	4·817	−0·01229	− 2·946	$-0{\cdot}0_36093$	—	—	—	—
1·8	4·59006	−0·0162405	− 2·40448	−0·0038635	—	—	—	—	—	—	—	—
2·0	—	—	—	—	3·617	−0·009475	− 1·982	$-0{\cdot}0_36250$	−0·005225	−0·00574	−0·002155	−0·009265
2·4	—	—	—	—	2·850	−0·007658	− 1·346	$-0{\cdot}0_39375$	—	—	—	—
2·6	2·93724	−0·0099887	− 1·05762	−0·0025141	—	—	—	—	—	—	—	—
3·0	—	—	—	—	2·077	−0·005974	− 0·6330	−0·001502	−0·005053	−0·00582	−0·00376	−0·00729
3·4	2·04236	−0·0070727	− 0·262334	−0·0026469	—	—	—	—	—	—	—	—
4·0	—	—	—	—	0·9332	−0·003734	− 0·4438	−0·002911	−0·00494	−0·00590	−0·00437	−0·00655
4·2	1·24974	−0·0049490	+ 0·485629	−0·0034600	—	—	—	—	−0·00488	−0·00595	−0·00449	−0·00641
4·4	—	—	—	—	—	—	—	—	−0·00476	−0·00610	−0·00466	−0·00622

TABLE 13

Flexural–Aileron–Tab Flutter (Aileron statically balanced)

ω	$X = \infty$ ($\bar{a}_{34} = 0{\cdot}01074$)		$X = 10$		$X = 0$		$X = -5{\cdot}0$		$Z = \infty$ ($\bar{a}_{14} = 0{\cdot}0_3436$) $W = \infty$			
	Z	W	Z	W	Z	W	Z	W	X	W	X	Z
0·4	0·06577	−0·09888	+0·09266	−0·10990	0·06672	−0·09801	+0·06742	−0·09838				
1·0	+0·001254	−0·02511	+0·001734	−0·02524	+0·001234	−0·02480	+0·0$_3$9559	−0·02485				
1·6	−0·005399	−0·01705	−0·005360	−0·01701	−0·005589	−0·01674	−0·005588	−0·01698				
2·0	−0·006978	−0·01512	−0·006983	−0·01507	−0·007177	−0·01484	−0·007022	−0·01506				
2·6	−0·008253	−0·01356	−0·008271	−0·01353	−0·008484	−0·01327	−0·008285	−0·01353				
3·0	−0·008841	−0·01285	−0·008852	−0·01283	—	—	−0·008893	−0·01279	No real values for $\omega \geqslant 0{\cdot}4$			
3·0	−0·009879	−0·01166	−0·009911	−0·01162	—	—	−0·009805	−0·01174				
2·6	−0·01009	−0·01145	−0·01011	−0·01143	−0·009925	−0·01161	−0·01005	−0·01149				
2·0	−0·01032	−0·01127	−0·01033	−0·01127	−0·01029	−0·01130	−0·01031	−0·01129				
1·6	−0·01044	−0·01127	−0·01044	−0·01127	−0·01046	−0·01126	−0·01044	−0·01126				
1·0	−0·01054	−0·01171	−0·01050	−0·01181	−0·01056	−0·01183	−0·01058	−0·01172				
0·4	−0·009848	−0·01741	−0·008222	−0·02087	−0·008984	−0·01947	−0·008969	−0·01950				

TABLE 14A

Torsion–Aileron–Tab. Flutter (Aileron unbalanced)

ω	$Y = 0$				$Y = 0{\cdot}5$				$Y = 100$			
	Z_1	W_1	Z_2	W_2	Z_1	W_1	Z_2	W_2	Z_1	W_1	Z_2	W_2
0·2	+0·2249	−0·3081	−0·004955	−0·02604	—	—	—	—	—	—	—	—
0·6	+0·02280	−0·03885	−0·005465	−0·007197	—	—	—	—	—	—	—	—
0·8	−0·01563	−0·05072	−0·006385	$-0{\cdot}0_39292$	—	—	—	—	—	—	—	—
1·0	−0·005284	−0·006807	$-0{\cdot}0_44055$	−0·01552	−0·006089	−0·005094	$-0{\cdot}0_32250$	−0·01430	+0·005961	−0·01911	−0·005230	−0·006429
1·4	−0·005393	$-0{\cdot}005928_5$	−0·002276	−0·01083	−0·009422	−0·009117	−0·005132	−0·006282	$+0{\cdot}0_36465$	−0·01267	−0·005261	−0·005916
1·8	−0·005395	−0·005709	−0·003705	−0·008580	−0·007675	−0·01336	−0·005277	−0·005799	−0·001511	−0·01005	−0·005254	−0·005758
2·2	−0·005370	−0·005634	−0·004643	−0·007165	$-0{\cdot}0_35849$	−0·009831	−0·005264	−0·005694	−0·002618	−0·008712	−0·005224	−0·005715
2·6	−0·005569	−0·004399	−0·005378	−0·005457	−0·002310	−0·008492	−0·005230	−0·005669	−0·003274	−0·007920	−0·005185	−0·005719
3·0	−0·008741	−0·007957	−0·005313	−0·005561	−0·003136	−0·007737	−0·005183	−0·005681	−0·003711	−0·007393	−0·005135	−0·005751
3·4	−0·001373	−0·006939	−0·005265	−0·005590	−0·003640	−0·007241	−0·005127	−0·005717	−0·004027	−0·007013	−0·005077	−0·005803
3·8	−0·003758	−0·006519	−0·005208	−0·005629	−0·003989	−0·006884	−0·005067	−0·005765	−0·004273	−0·006719	−0·005012	−0·005867
4·2	−0·004413	−0·006219	−0·005123	−0·005697	−0·004273	−0·006586	−0·004982	−0·005844	−0·004507	−0·006442	−0·004908	−0·005979
4·6	—	—	—	—	−0·004563	−0·006278	−0·004837	−0·005990	—	—	—	—

TABLE 14B

Torsion–Aileron–Tab Flutter (Aileron unbalanced)

ω	$Y = -0{\cdot}05$				$Y = -0{\cdot}1$				$Y = -0{\cdot}15$			
	Z_1	W_1	Z_2	W_2	Z_1	W_1	Z_2	W_2	Z_1	W_1	Z_2	W_2
0·2	+0·2251	−0·3083	−0·004943	−0·02608	—	—	—	—	—	—	—	—
0·6	0·02230	−0·03869	−0·005440	−0·007269	+0·02192	−0·03857	−0·005418	−0·007332	+0·02163	−0·03849	−0·005398	−0·007385
0·8	+0·08353	−0·02775	−0·005717	−0·004853	0·02186	−0·02561	−0·005714	−0·005495	+0·01527	−0·02468	−0·005487	−0·005942
1·0	−0·05254	−0·007098	$-0{\cdot}0_36166$	−0·01547	+0·005168	−0·007948	−0·001971	−0·01504	—	—	—	—
1·2	−0·005378	−0·006261	−0·001205	−0·01298	−0·005395	−0·006375	−0·001347	−0·01327	−0·005624	−0·006257	−0·001572	−0·01412
1·4	−0·005406	−0·005967	−0·002167	−0·01112	−0·005430	−0·006014	−0·002114	−0·01146	−0·005482	−0·006090	−0·002152	−0·01198
1·8	−0·005415	−0·005722	−0·003468	−0·008996	−0·005452	−0·005731	−0·003276	−0·009438	−0·005523	−0·005736	−0·003118	−0·01007
2·2	−0·005402	−0·005630	−0·004248	−0·007902	−0·005456	−0·005613	−0·003943	−0·008572	−0·005560	−0·005578	−0·003667	−0·009599
2·6	−0·005379	−0·005626	−0·004851	−0·007347	−0·005458	−0·005561	−0·004354	−0·008871	−0·005613	−0·005482	−0·003897	$-0{\cdot}0127_5$
2·8	−0·005373	−0·005734	−0·005184	−0·007774	—	—	—	—	—	—	—	—
3·0	−0·005729	−0·006489	−0·005338	−0·005414	−0·005494	−0·005539	−0·004631	−0·001672	−0·005774	−0·005378	−0·003532	−0·003972
3·4	−0·003205	−0·006362	−0·005305	−0·005538	−0·002091	−0·005545	−0·004877	−0·005458	—	—	—	—
3·8	−0·004132	−0·006159	−0·005257	−0·005580	−0·004959	−0·005686	−0·005231	−0·005547	—	—	—	—
4·2	−0·004715	−0·005960	−0·005176	−0·004645	−0·005156	−0·005631	−0·005177	−0·005616	—	—	—	—

TABLE 14c

Torsion–Aileron–Tab Flutter (Aileron unbalanced)

ω	$Y = -0{\cdot}2$				$Y = -0{\cdot}3$				$Y = -0{\cdot}5$			
	Z_1	W_1	Z_2	W_2	Z_1	W_1	Z_2	W_2	Z_1	W_1	Z_2	W_2
0·2	—	—	—	—	+0·2262	−0·3091	−0·00491	−0·0262	—	—	—	—
0·6	+0·02140	−0·03843	−0·005381	−0·007433	0·02108	−0·03837	−0·00535	−0·00751	—	—	—	—
0·8	0·01287	−0·02429	−0·005443	−0·006134	—	—	—	—	+0·009790	−0·02385	$-0{\cdot}00534_5$	−0·006542
1·0	+0·1550	−0·01738	−0·005429	−0·004426	0·00673	−0·01688	−0·00535	−0·00570	−0·004457	−0·001699	−0·05311	−0·006054
1·2	−0·005828	−0·007000	−0·002843	−0·01668	0·005072	−0·01189	−0·005373	−0·00516	—	—	—	—
1·4	−0·005626	−0·006260	−0·002401	−0·01333	+0·00332	−0·00945	−0·00487	−0·005102	$-0{\cdot}0_34969$	−0·01105	−0·005209	−0·005776
1·8	−0·005693	−0·005739	−0·002984	−0·01166	−0·00283	−0·00644	−0·00391	−0·005770	−0·002509	−0·008742	−0·005111	−0·005755
2·2	−0·005834	−0·005497	−0·003309	−0·01427	—	—	—	—	−0·003474	−0·007627	−0·005033	−0·005796
2·6	−0·006234	−0·005258	−0·002798	$-0{\cdot}0_35621$	—	—	—	—	−0·004024	−0·006981	−0·004966	−0·005858
2·8	−0·008546	−0·004860	−0·05285	−0·004484	—	—	—	—	—	—	—	—
3·0	—	—	—	—	—	—	—	—	−0·004410	−0·006516	−0·004866	−0·005967

TABLE 15

Binary Flutter (Aileron unbalanced)

ω	$Y = \infty$ $(\bar{a}_{34} = 0{\cdot}0054)$				$Z = \infty$ $(\bar{a}_{24} = 0{\cdot}0373)$				$W = \infty$ $(\bar{a}_{23} = 0{\cdot}0370)$			
	Z_1	W_1	Z_2	W_2	Y_1	W_1	Y_2	W_2	Y_1	Z_1	Y_2	Z_2
0·4	−0·00444	−0·01222	+0·07061	$-0{\cdot}0930_5$	7·5686	−0·19537	+2·1296	−0·14302	—	—	—	—
0·2	—	—	—	—	3·4189	−0·092492	+0·41645	−0·056279	2·96957	0·0487691	+0·47594	−0·021711
0·8	−0·00516	−0·00735	0·01201	−0·02658	1·98256	−0·056145	−0·038268	−0·028943	1·71775	−0·0308518	+0·009234	−0·0104437
1·0	−0·00523	−0·00643	0·00591	−0·01908	1·30540	−0·0389624	−0·197355	−0·0174284	1·11770	−0·0222463	−0·157503	−0·0061487
1·2	—	—	—	—	0·92469	−0·029359	−0·257846	−0·011739	—	—	—	—
1·4	$-0{\cdot}00526_5$	−0·005940	$+0{\cdot}0_36142$	−0·01266	0·68561	−0·023374	−0·27881	−0·008618	0·561585	−0·0142179	−0·247829	−0·0033874
1·8	—	—	—	—	0·40341	−0·016442	−0·27536	−0·005728	0·303193	−0·0104444	−0·247449	−0·0028707
2·0	$-0{\cdot}00522_5$	−0·00574	−0·002155	−0·009265	—	—	—	—	—	—	—	—
2·2	—	—	—	—	—	—	—	—	0·148744	−0·0081852	−0·221083	−0·0030156
2·6	—	—	—	—	—	—	—	—	0·0330638	−0·0064882	−0·17833	−0·0035063
3·0	−0·005053	−0·00582	−0·00376	−0·00729	0·040583	−0·008116	−0·17824	−0·0045736	—	—	—	—

See results for $X = \infty$ in Table 11

TABLE 16

Torsion–Aileron–Tab Flutter (Aileron statically balanced)

ω	$Y = 1{\cdot}0$		$Y = 0{\cdot}5$		$Y = 0{\cdot}2$		$Y = 0$		$Y = -0{\cdot}2$	
	Z	W	Z	W	Z	W	Z	W	Z	W
0·6	+0·02014	−0·04543	+0·01510	−0·04414	+0·01503	−0·04439	+0·01518	−0·04461	+0·01538	−0·04483
0·8	−0·01077	−0·01152	+0·007878	−0·03005	—	—	+0·004648	−0·03036	—	—
1·0	−0·03276	−0·03374	−0·01093	−0·01353	$+0{\cdot}0_3 1012$	−0·02293	$-0{\cdot}0_3 3445$	−0·02355	$-0{\cdot}0_3 2911$	−0·02388
1·2	0·002867	−0·02152	−0·01074	−0·01186	−0·002615	−0·01768	−0·003234	−0·01963	—	—
1·4	−0·002912	−0·01849	−0·01386	−0·01344	—	—	−0·005195	−0·01701	−0·004856	−0·01789
1·6	—	—	−0·003401	−0·01462	−0·01208	−0·01075	—	—	—	—
1·8	−0·006200	−0·01567	—	—	−0·01161	−0·01069	−0·008623	−0·01281	−0·006907	−0·01525
2·0	—	—	−0·007344	−0·01389	−0·01156	−0·01058	—	—	−0·007552	−0·01444
2·2	—	—	—	—	−0·01182	−0·01036	—	—	—	—
2·4	−0·007990	−0·01377	−0·008392	−0·01311	—	—	—	—	—	—
3·0	−0·008921	−0·01272	−0·009300	−0·01224	—	—	—	—	—	—
3·0	−0·009951	−0·01157	−0·009849	−0·01165	—	—	—	—	—	—
2·4	−0·01021	−0·01132	−0·01013	−0·01136	—	—	—	—	—	—
2·2	—	—	—	—	−1·3440	−0·006488	—	—	—	—
2·0	—	—	−0·01030	−0·01122	+0·002639	−0·002670	—	—	−0·009998	−0·01156
1·8	−0·01042	−0·01121	—	—	−0·001197	$+0{\cdot}0_3 8964$	−0·008986	−0·01243	−0·01013	−0·01146
1·6	—	—	−0·01033	−0·01110	−0·001101	−0·003216	—	—	—	—
1·4	−0·01053	−0·01127	−0·01003	−0·01030	—	—	−0·01026	−0·01141	−0·01038	−0·01137
1·2	−0·01057	−0·01140	−0·007605	−0·03191	−0·01025	−0·01132	−0·01043	−0·01143	—	—
1·0	−0·01056	−0·01178	−0·009169	+1·0194	−0·01052	−0·01157	−0·01053	−0·01163	−0·01053	−0·01166
0·8	−0·007117	−0·02105	−0·01061	−0·01199	—	—	−0·01057	−0·01212	—	—
0·6	−0·01063	−0·01300	−0·01057	−0·01313	−0·01054	−0·01319	−0·01053	−0·01322	−0·01051	−0·01325

TABLE 17

Binary Flutter (Aileron statically balanced)

ω	X or $Y = \infty$ ($\bar{a}_{34} = 0{\cdot}01074$)				$W = \infty$ ($\bar{a}_{23} = 0{\cdot}0107$)				$Z = \infty$ ($\bar{a}_{24} = 0{\cdot}01096$)			
	Z_1	W_1	Z_2	W_2	Z_1	Y_1	Z_2	Y_2	Y_1	W_1	Y_2	W_2
0·4	+0·06577	−0·09888	−0·009848	−0·01741	−0·08739	5·8415	−0·06624	3·4741	—	—	—	—
0·6	—	—	—	—	−0·03889	2·5623	−0·02613	1·3868	3·051	−0·08208	1·105	−0·06071
0·8	—	—	—	—	−0·02188	1·4160	−0·01405	0·7600	—	—	—	—
1·0	+0·001254	−0·02511	−0·01054	−0·01171	−0·01394	0·8793	−0·009158	0·5003	1·090	−0·03017	0·4160	−0·02052
1·2	—	—	—	—	−0·009500	0·5787	−0·006861	0·3767	—	—	—	—
1·4	—	—	—	—	—	—	—	—	0·5557	−0·01581	0·2145	−0·01061
1·6	−0·005399	−0·01705	−0·01044	−0·01127	—	—	—	—	—	—	—	—
1·8	—	—	—	—	—	—	—	—	0·3294	−0·009768	0·1475	−0·006986
2·0	−0·006978	−0·01512	−0·01032	−0·01127	—	—	—	—	0·2592	−0·00794	0·1330	−0·00592
2·4	—	—	—	—	—	—	—	—	0·1996	−0·00646	0·1306	−0·00535
2·6	−0·008253	−0·01356	−0·01009	−0·01145	—	—	—	—	—	—	—	—
3·0	−0·008841	−0·01285	−0·009879	−0·00166	—	—	—	—	—	—	—	—

TABLE 18

Torsion–Aileron–Tab Flutter (Aileron dynamically balanced)

ω	$Y = 0$		$Y = 0{\cdot}2$		$Y = 0{\cdot}5$		$Y = \infty$ ($\bar{a}_{34} = 0{\cdot}01291$)		$Z = \infty$ ($\bar{a}_{24} = 0{\cdot}0_3258$)		$W = \infty$ ($\bar{a}_{23} = 0$)	
	Z	W	Z	W	Z	W	Z	W	Y	W	Y	Z
0·4	—	—	—	—	—	—	+0·06381	−0·1013	6·716	−0·1784	5·151	−0·07893
0·6	+0·01333	−0·04752	+0·01307	−0·04722	+0·01274	−0·04688	+0·01967	−0·05133	2·703	−0·07545		
1·0	−0·002067	−0·02676	−0·002218	−0·02644	−0·001980	−0·02540	$-0{\cdot}0_36566$	−0·02754				
1·4	−0·006559	−0·02073	−0·006924	−0·01994	−0·007147	−0·01935	−0·006036	−0·02104				
1·8	−0·008534	−0·01816	—	—	−0·009541	−0·01626	−0·008299	−0·01828				
2·2	−0·009717	−0·01663	—	—	−0·01073	−0·01515	−0·009537	−0·01677				
3·0	—	—	—	—	—	—	−0·01117	−0·01481	No values for $\omega > 0{\cdot}8$		No values for $\omega > 0{\cdot}6$	
3·0	—	—	—	—	—	—	−0·01157	−0·01434				
2·2	−0·01211	−0·01381	—	—	−0·01165	−0·01418	−0·01223	−0·01367				
1·8	−0·01237	−0·01362	—	—	−0·01199	−0·01383	−0·01243	−0·01354				
1·4	−0·01250	−0·01363	−0·01239	−0·01369	−0·01216	−0·01367	−0·01259	−0·01354				
1·0	−0·01268	−0·01391	−0·01268	−0·01391	−0·01259	−0·01401	−0·01269	−0·01388				
0·6	−0·01264	−0·01552	−0·01265	−0·01551	−0·01266	−0·01550	−0·01255	−0·01571	1·830	−0·06492		
0·4	—	—	—	—	—	—	−0·01204	−0·01951	3·895	−0·1512	4·422	−0·07242

TABLE 19

*Approximate Air-Load Coefficients**

C_{11}	$2\cdot090$	$-2\cdot606\omega^2$	B_{11}	$+0\cdot8240$	$+5\cdot213\omega$
C_{12}	$4\cdot523$	$-0\cdot4079\omega^2$	B_{12}	$-0\cdot4290$	$+3\cdot765\omega$
C_{13}	$1\cdot270$	$-0\cdot01617\omega^2$	B_{13}	$-0\cdot1949$	$+0\cdot3452\omega$
C_{14}	$0\cdot1278$	$-0\cdot0_49084\omega^2$	B_{14}	$-0\cdot02277$	$+0\cdot008407\omega$
C_{21}	$-0\cdot08540$	$-0\cdot4079\omega^2$	B_{21}	$-0\cdot03350$	$+0\cdot2138\omega$
C_{22}	$-0\cdot3632$	$-0\cdot1167\omega^2$	B_{22}	$+0\cdot01780$	$+0\cdot6266\omega$
C_{23}	$+0\cdot2569$	$-0\cdot005009\omega^2$	B_{23}	$0\cdot008180$	$+0\cdot09936\omega$
C_{24}	$0\cdot04278$	$-0\cdot0_43554\omega^2$	B_{24}	$0\cdot001058$	$+0\cdot003236\omega$
C_{31}	$0\cdot003600$	$-0\cdot01617\omega^2$	B_{31}	$+0\cdot001420$	$+0\cdot009010\omega$
C_{32}	$0\cdot002086$	$-0\cdot005009\omega^2$	B_{32}	$-0\cdot0_37000$	$+0\cdot02145\omega$
C_{33}	$0\cdot01431$	$-0\cdot0_35383\omega^2$	B_{33}	$-0\cdot0_35080$	$+0\cdot009079\omega$
C_{34}	$0\cdot006896$	$-0\cdot0_56194\omega^2$	B_{34}	$-0\cdot0_48560$	$+0\cdot0_35493\omega$
C_{41}	$0\cdot0_41836$	$-0\cdot0_49084\omega^2$	B_{41}	$+0\cdot0_57320$	$+0\cdot0_44654\omega$
C_{42}	$0\cdot0_43936$	$-0\cdot0_43554\omega^2$	B_{42}	$-0\cdot0_54600$	$+0\cdot0_31511\omega$
C_{43}	$0\cdot0_49178$	$-0\cdot0_56194\omega^2$	B_{43}	$-0\cdot0_53780$	$+0\cdot0_48344\omega$
C_{44}	$0\cdot0_32447$	$-0\cdot0_650577\omega^2$	B_{44}	$-0\cdot0_52280$	$+0\cdot0_43559\omega$

* ' Barred ' coefficients are obtained by use of formula (5.4).

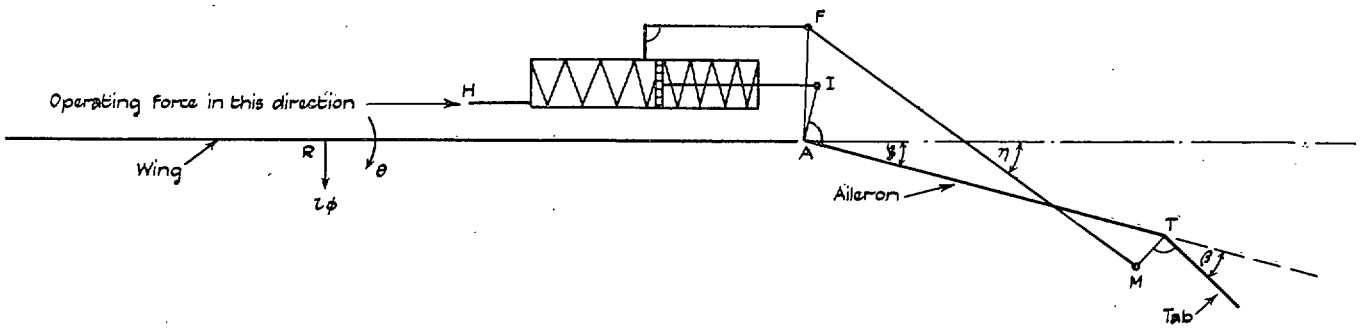

FIG. 1a. Diagram of non-preloaded spring tab No. 1.

(*Note.* Both the aileron and the tab are shown displaced from central position in the positive senses which are standard in flutter theory.)

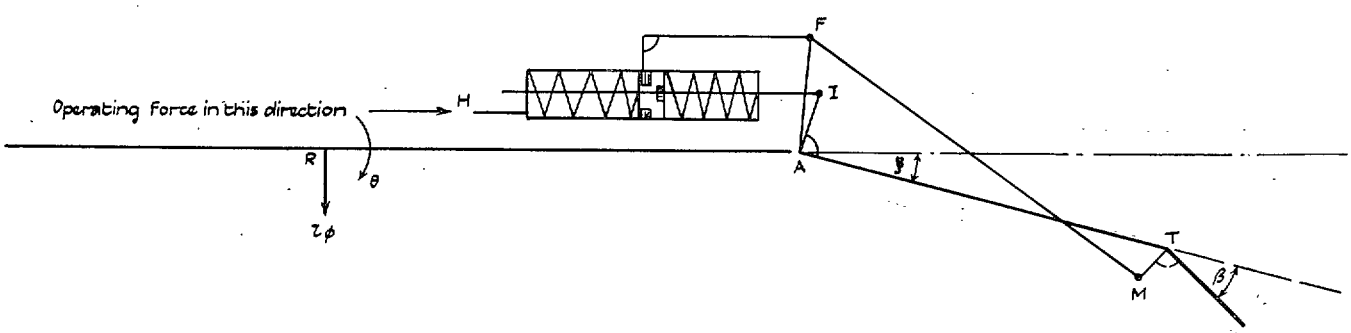

FIG. 1b. Diagram of preloaded spring tab No. 1.

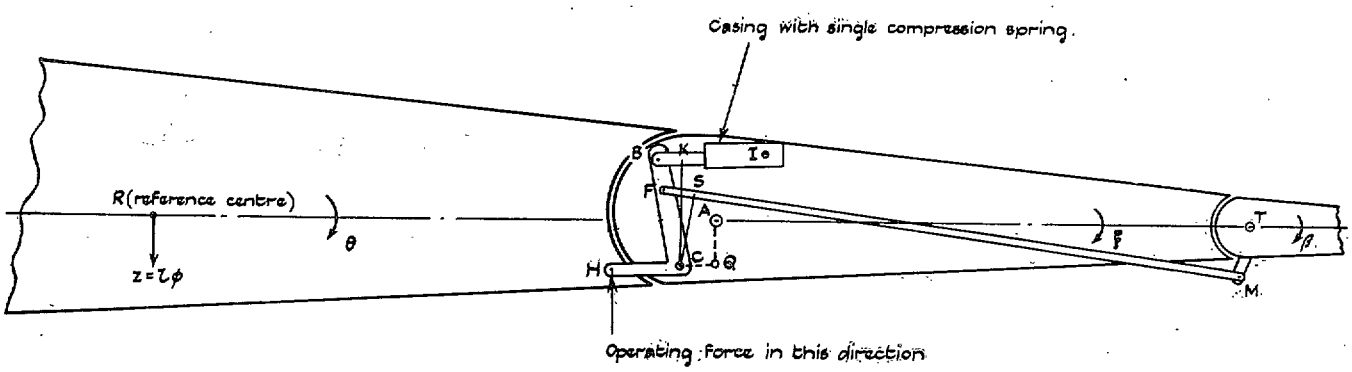

FIG. 2. Diagram of spring tab No. 2.

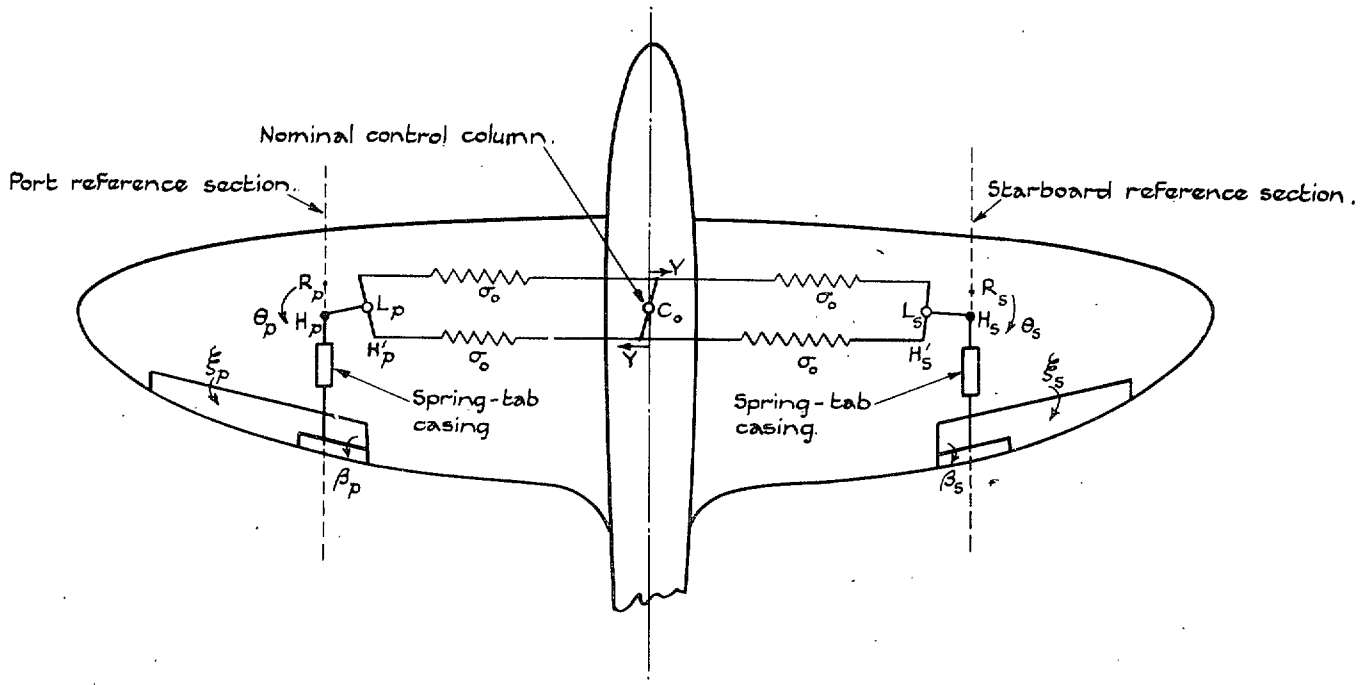

FIG. 3. Diagram of control circuit connections with spring tab No. 1.
(System is shown with small general displacements. For convenience the levers L_p, L_s, and the control column C_o are drawn in the plane of the wings.)

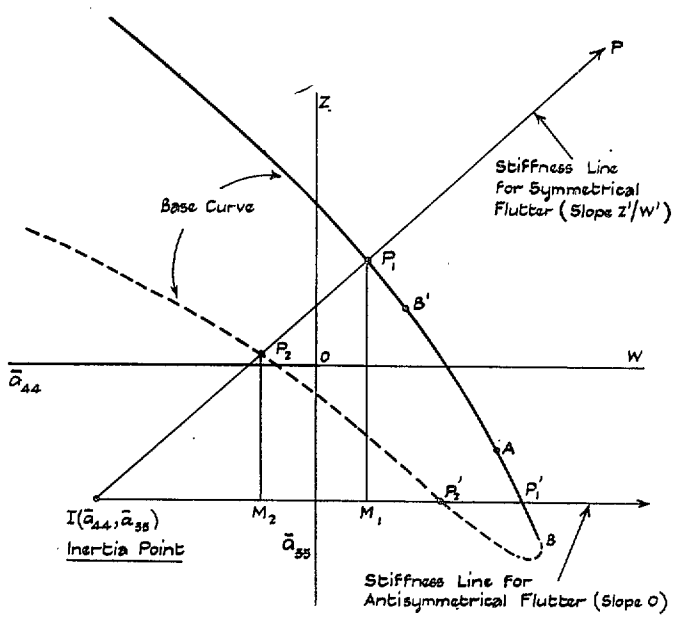

FIG. 4a. Inertia-stiffness diagram (para. 8).

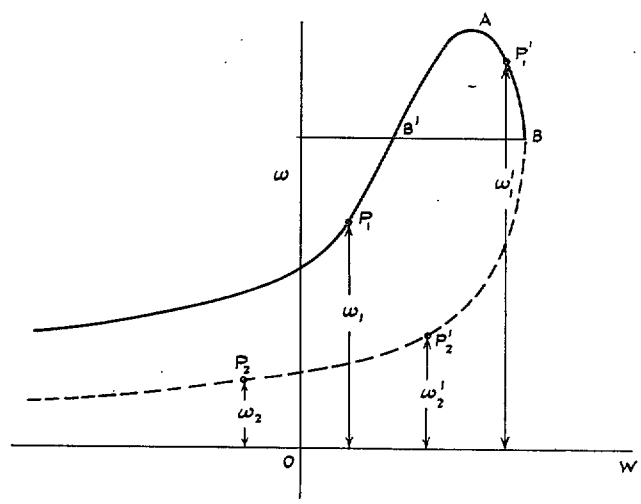

FIG. 4b. Frequency parameter diagram (para. 8).

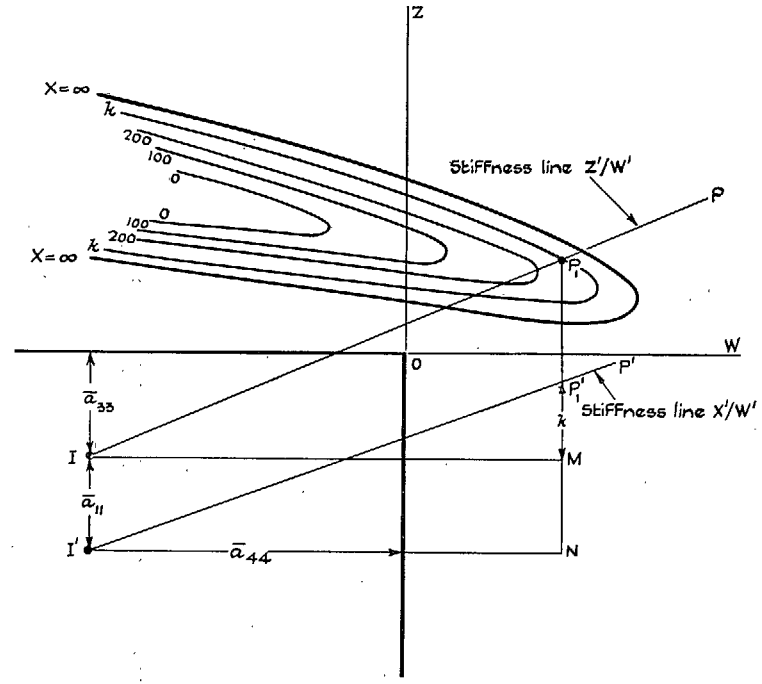

FIG. 5. Ternary inertia–stiffness diagram (para. 9).

Explanation : P_1 lies on that base curve $X = k$ for which $P_1'M = k$. The critical speed is then given by any of the relations

$$X' = \omega^2 P_1'N = \omega^2(k + a_{11}),\ Z' = \omega^2 P_1 M,\ W' = \omega^2 IM.$$

The appropriate value of ω^2 can be found from a supplementary frequency parameter diagram.

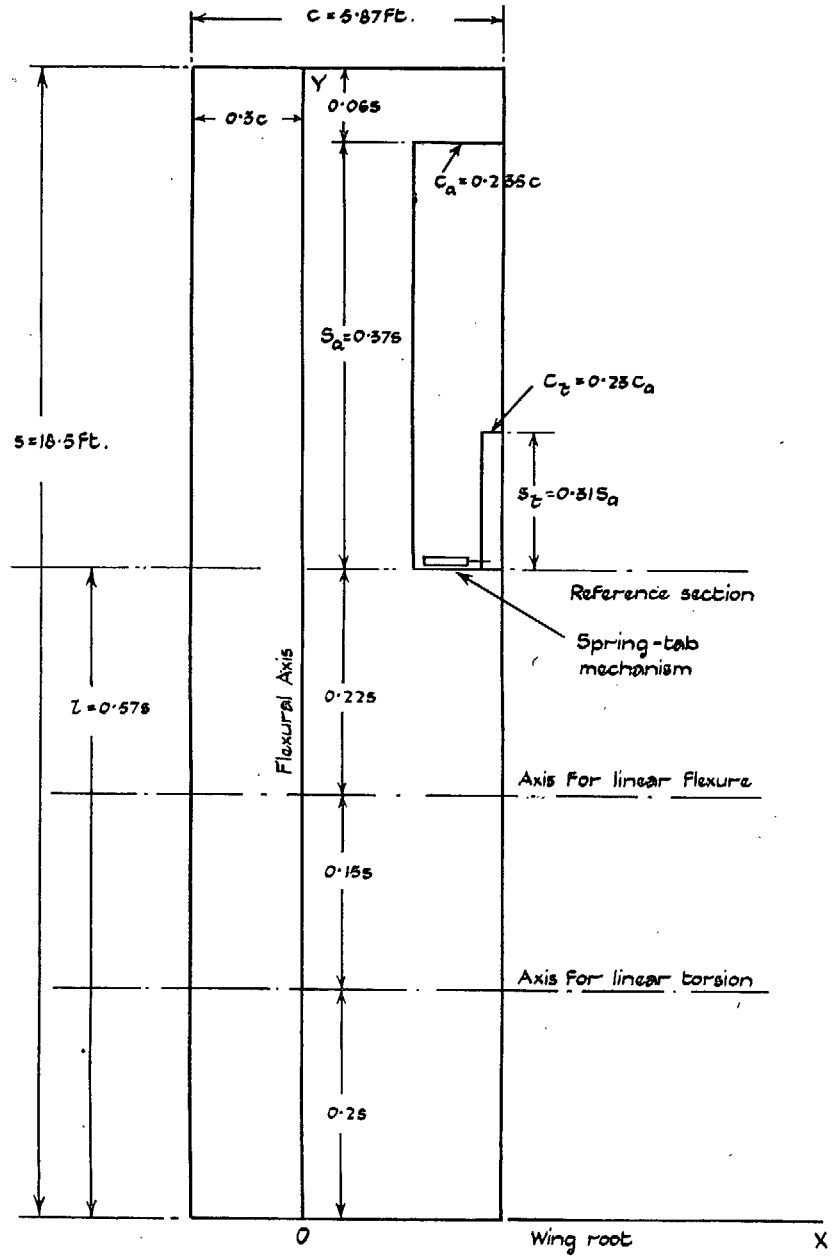

FIG. 6. Diagram of wing–aileron–tab combination.

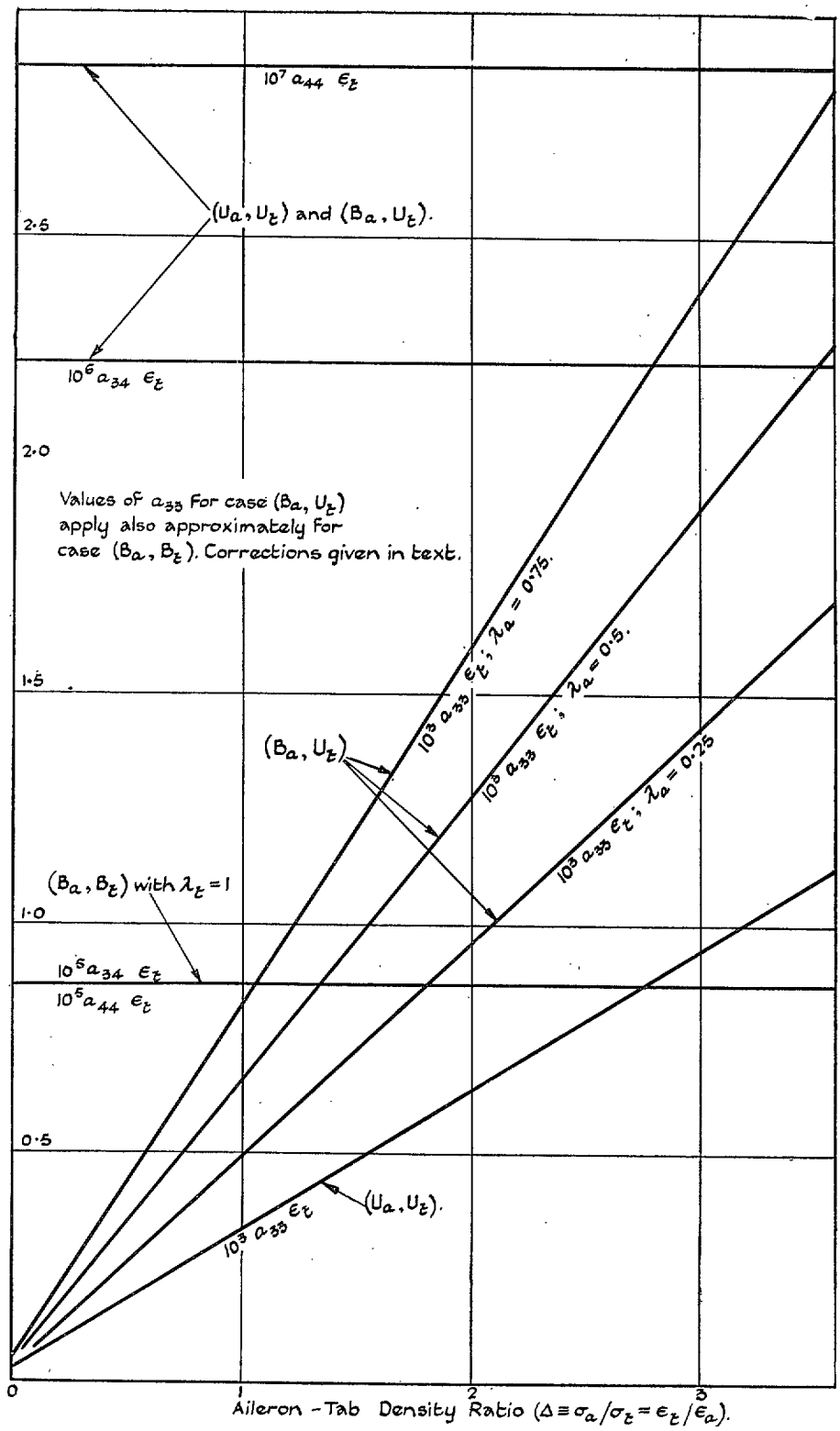

FIG. 7. Aileron–tab inertial coefficients.

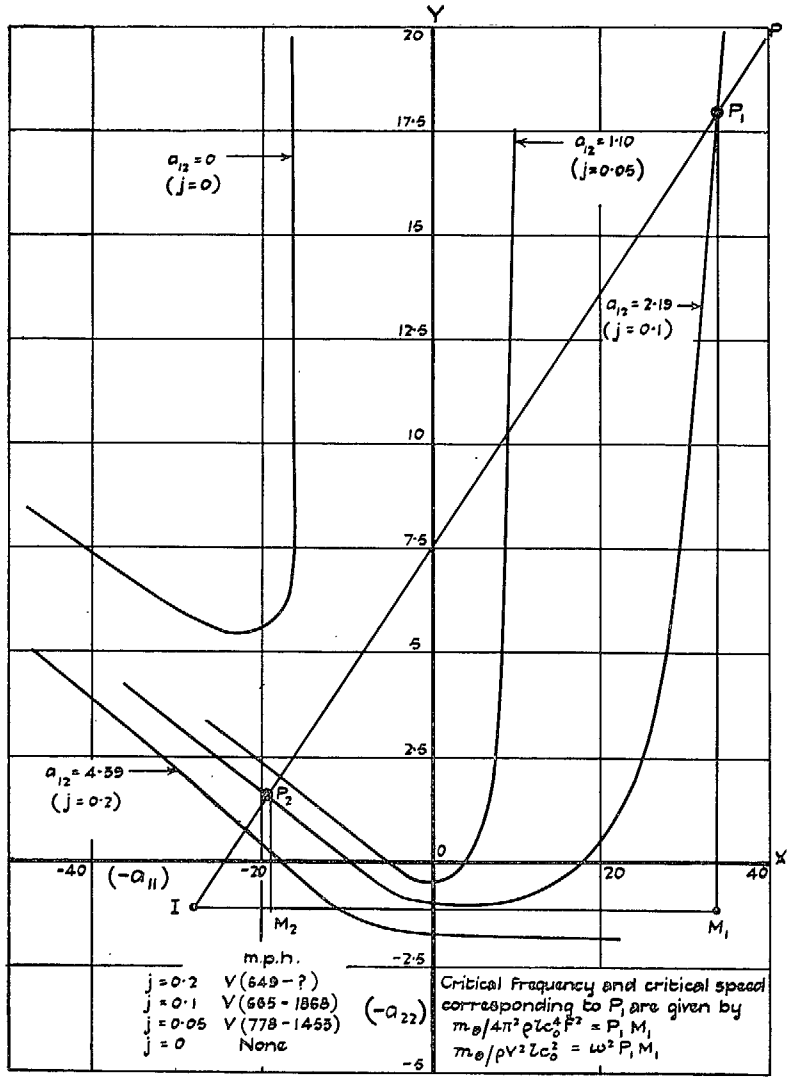

FIG. 8a. Flexure–torsion inertia-stiffness diagram (para. 2). Base curves.

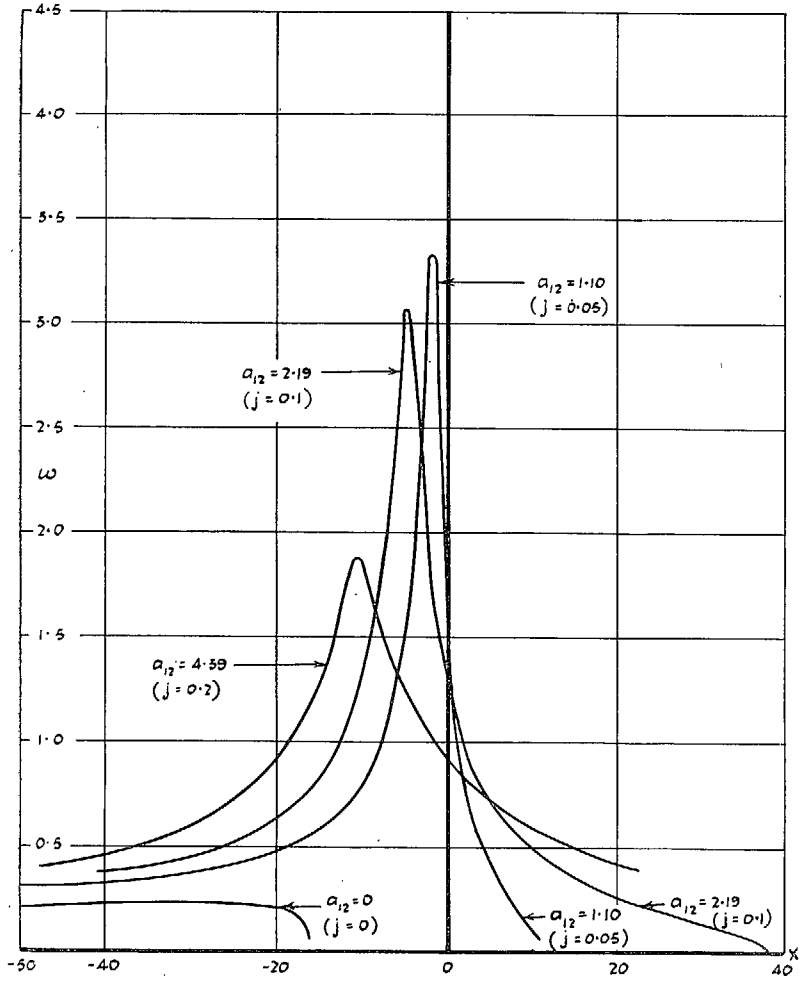

FIG. 8b. Flexure–torsion inertia-stiffness diagram (para. 12). Frequency parameter curves.

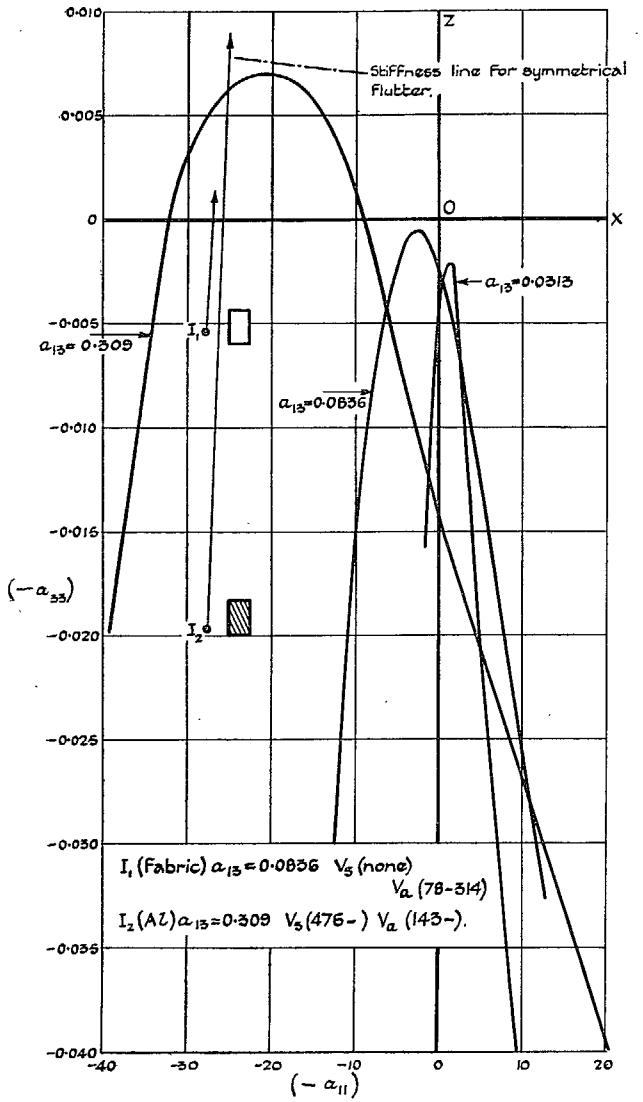

FIG. 9a. Flexure–aileron inertia-stiffness diagram (para. 13). Base curves.

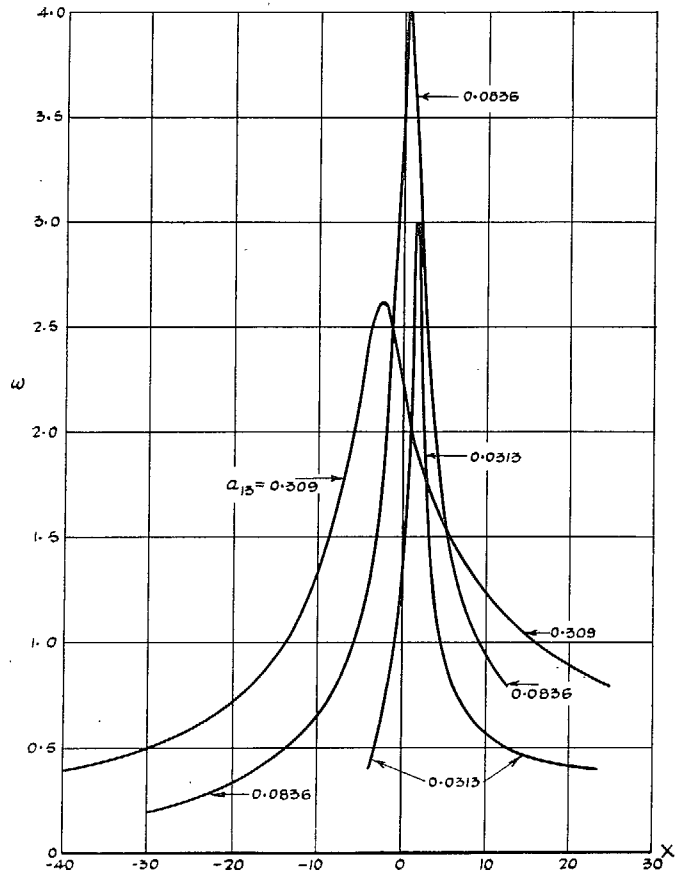

FIG. 9b. Flexure–aileron inertia-stiffness diagram (para. 13). Frequency parameter curves.

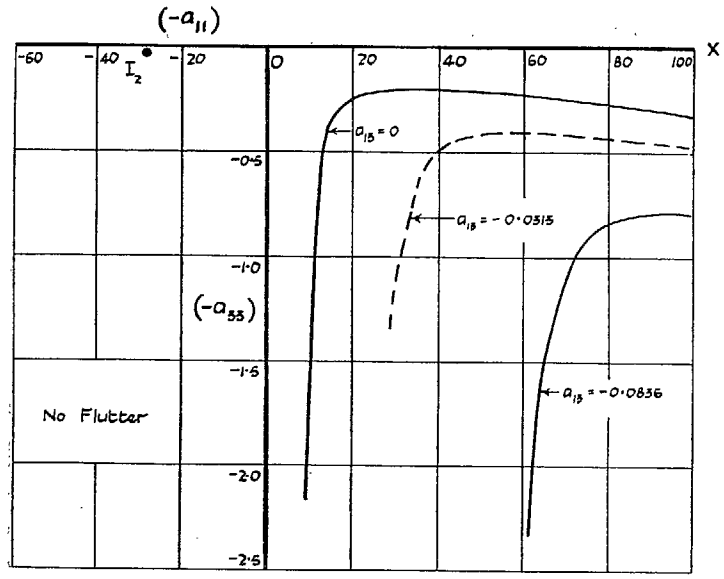

FIG. 10a. Base curves.

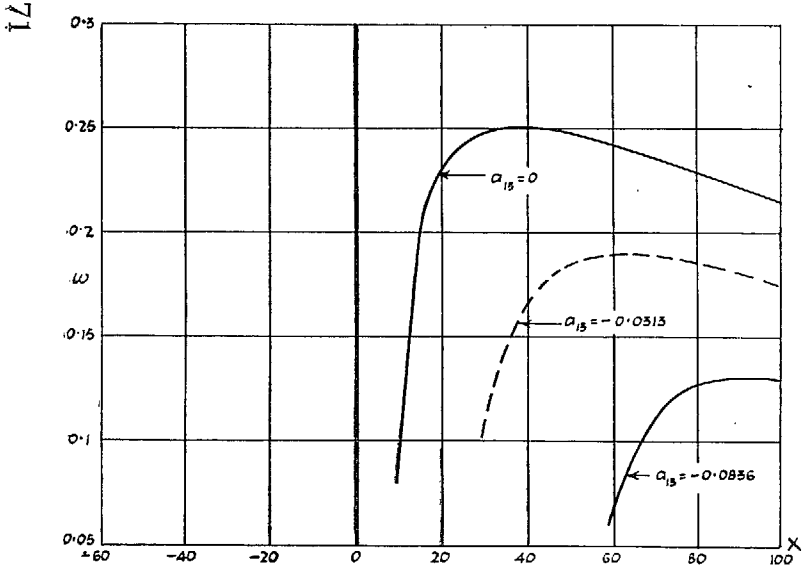

FIG. 10b. Frequency Parameter curves.

FIGS. 10a and 10b. Flexure–aileron inertia-stiffness diagram (para. 13). Effect of static overbalance.

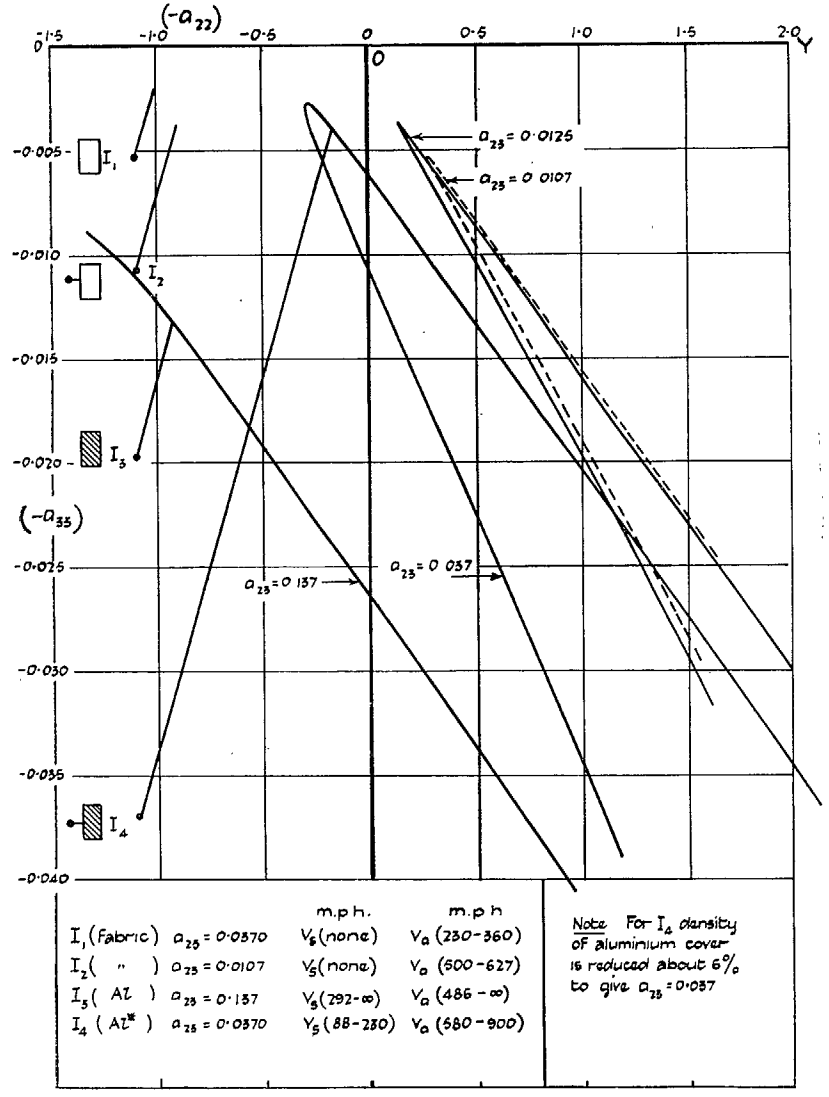

FIG. 11a. Torsion–aileron inertia-stiffness diagram (para. 14). Base curves.

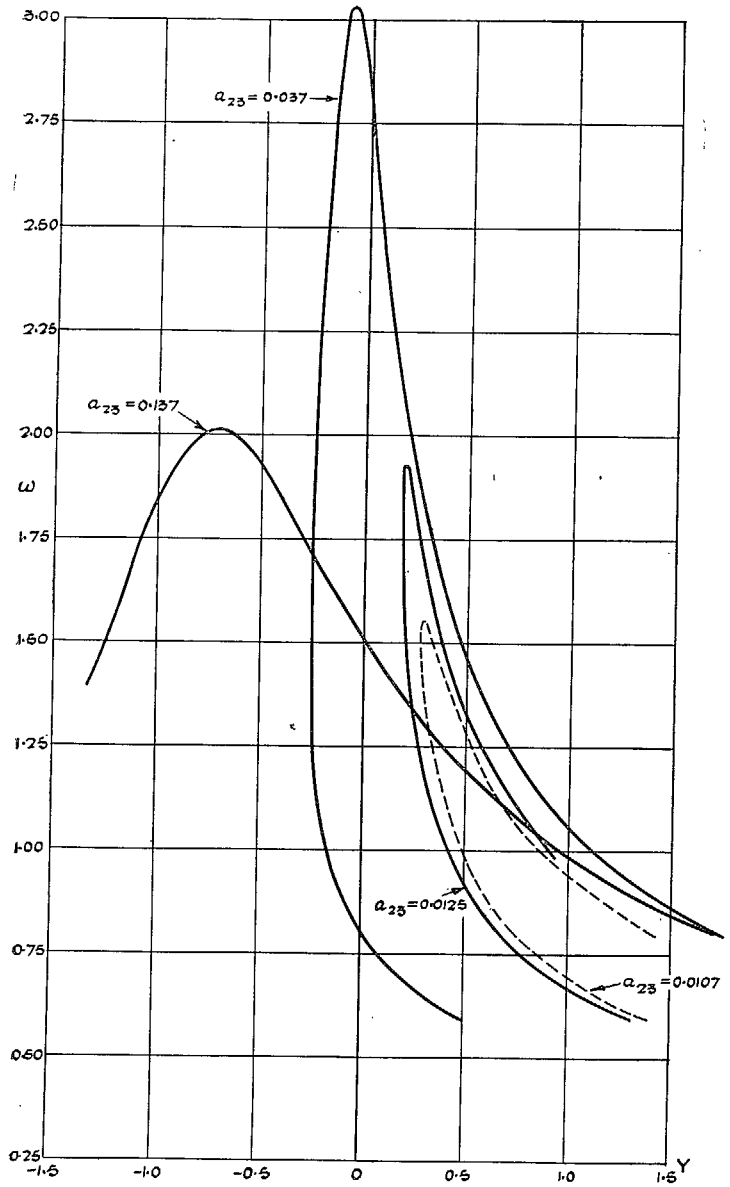

FIG. 11b. Torsion–aileron inertia-stiffness diagram (para. 14). Frequency parameter curves.

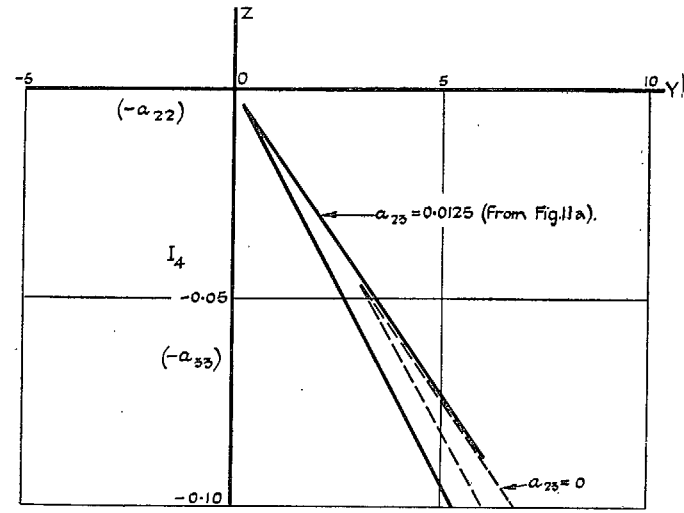

FIG. 12a. Base curves.

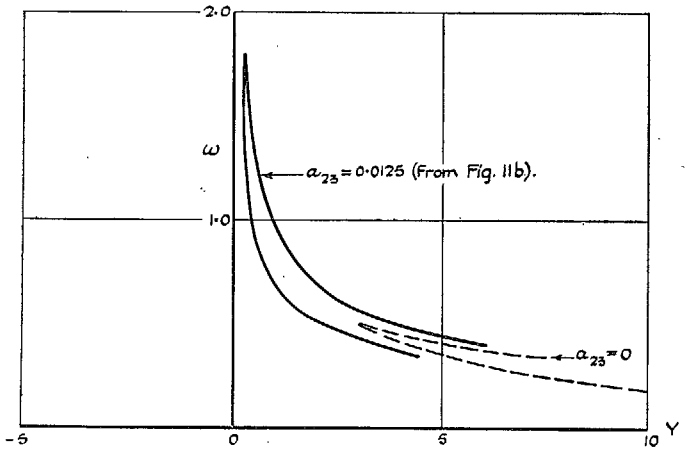

FIG. 12b. Frequency parameter curves.

FIGS. 12a and 12b. Torsion–aileron inertia-stiffness diagram (para. 14). Case $a_{23} = 0$.

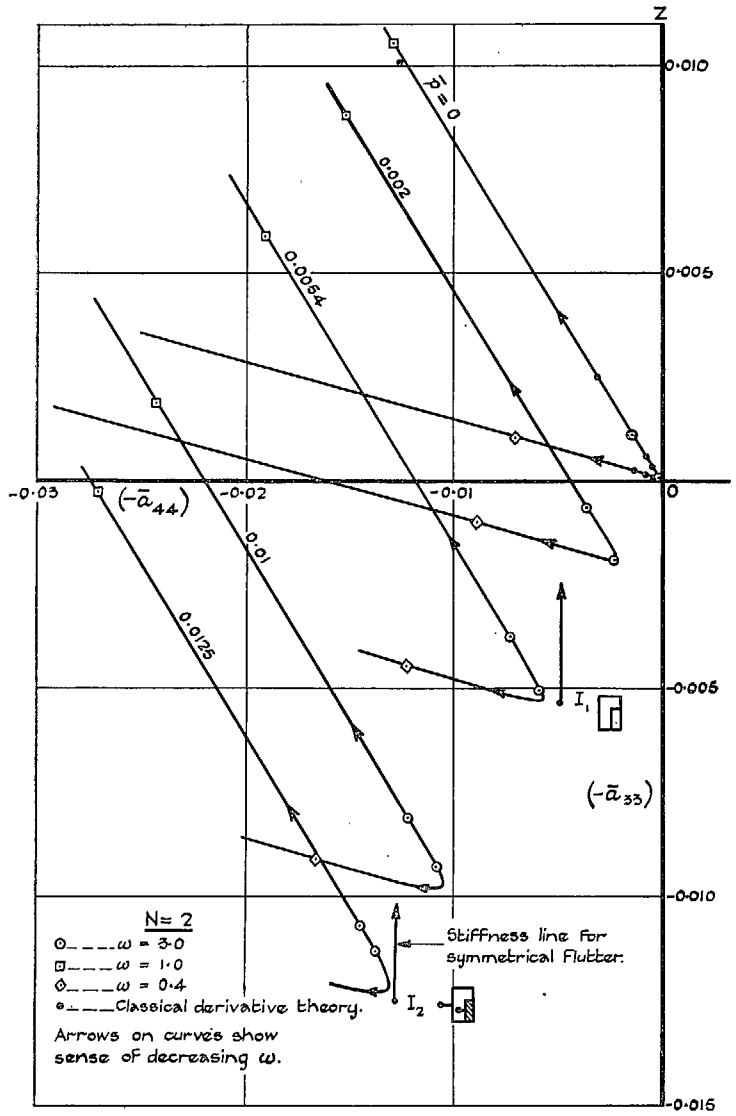

FIG. 13a. Aileron–tab inertia-stiffness diagram (para. 15). Base curves for $N = 2$ and $\bar{p} = 0$ to $0{\cdot}0125$.

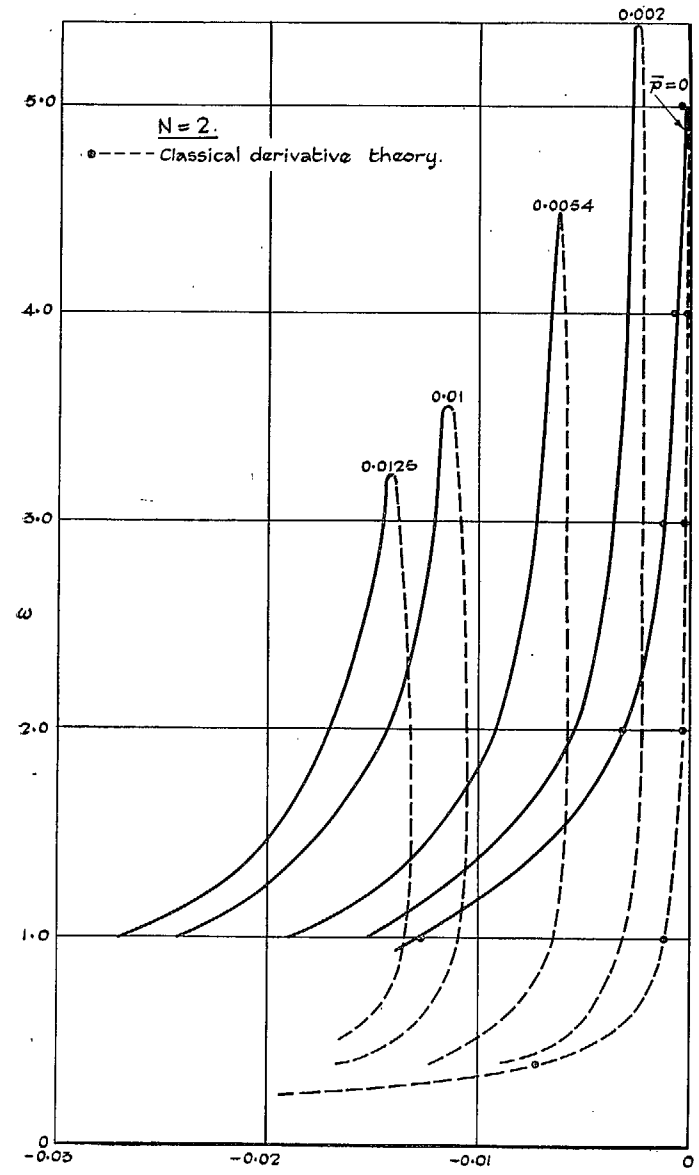

FIG. 13b. Aileron–tab inertia-stiffness diagram (para. 15). Frequency parameter curves for $N = 2$ and $\bar{p} = 0$ to $0{\cdot}0125$.

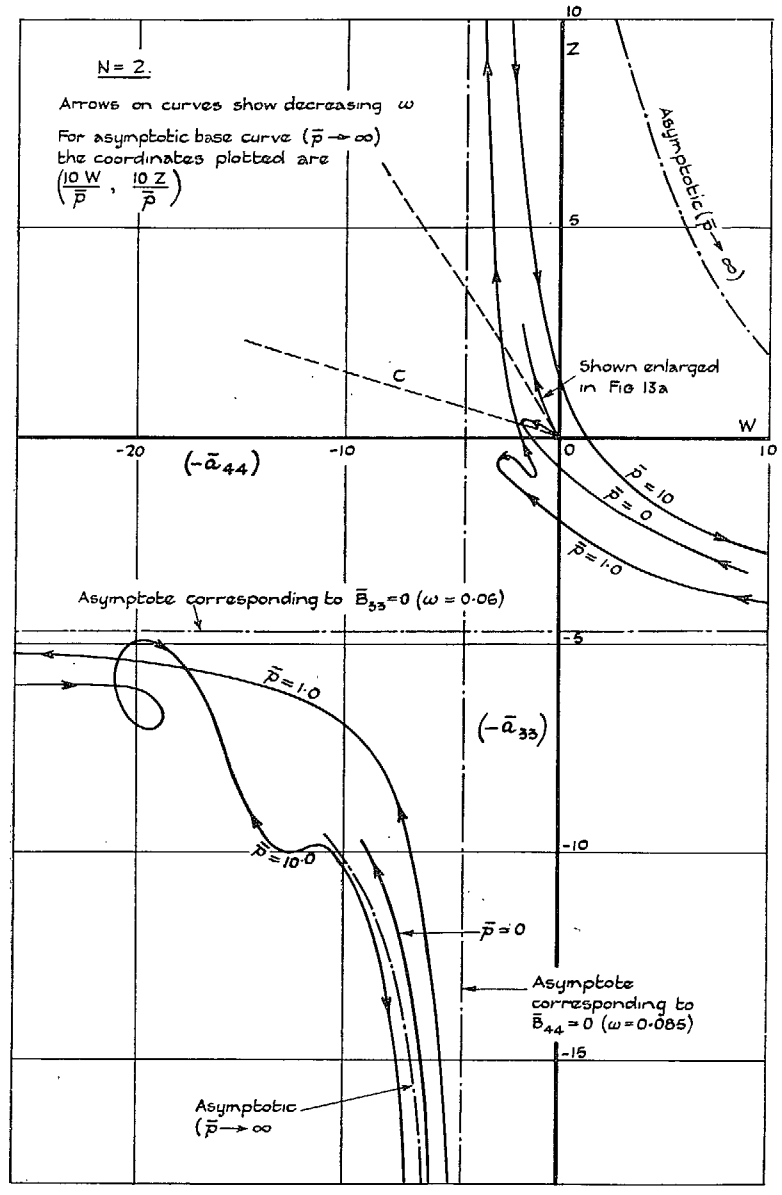

FIG. 14a. Aileron–tab inertia-stiffness diagram (para. 15).
Base curves for $N = 2$ and $\bar{p} = 0$ to ∞.

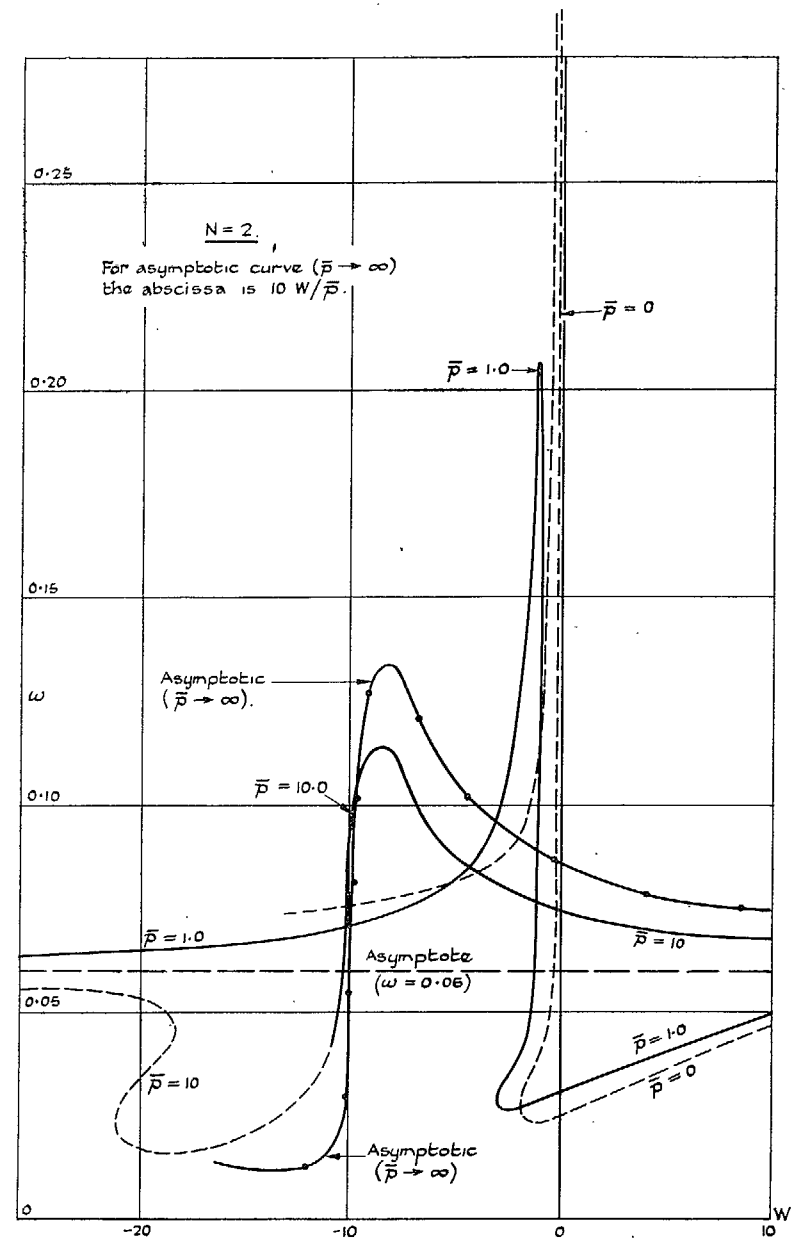

Fig. 14b. Aileron–tab inertia-stiffness diagram (para. 15).
Frequency parameter curves for $N = 2$ and $\bar{p} = 0$ to ∞.

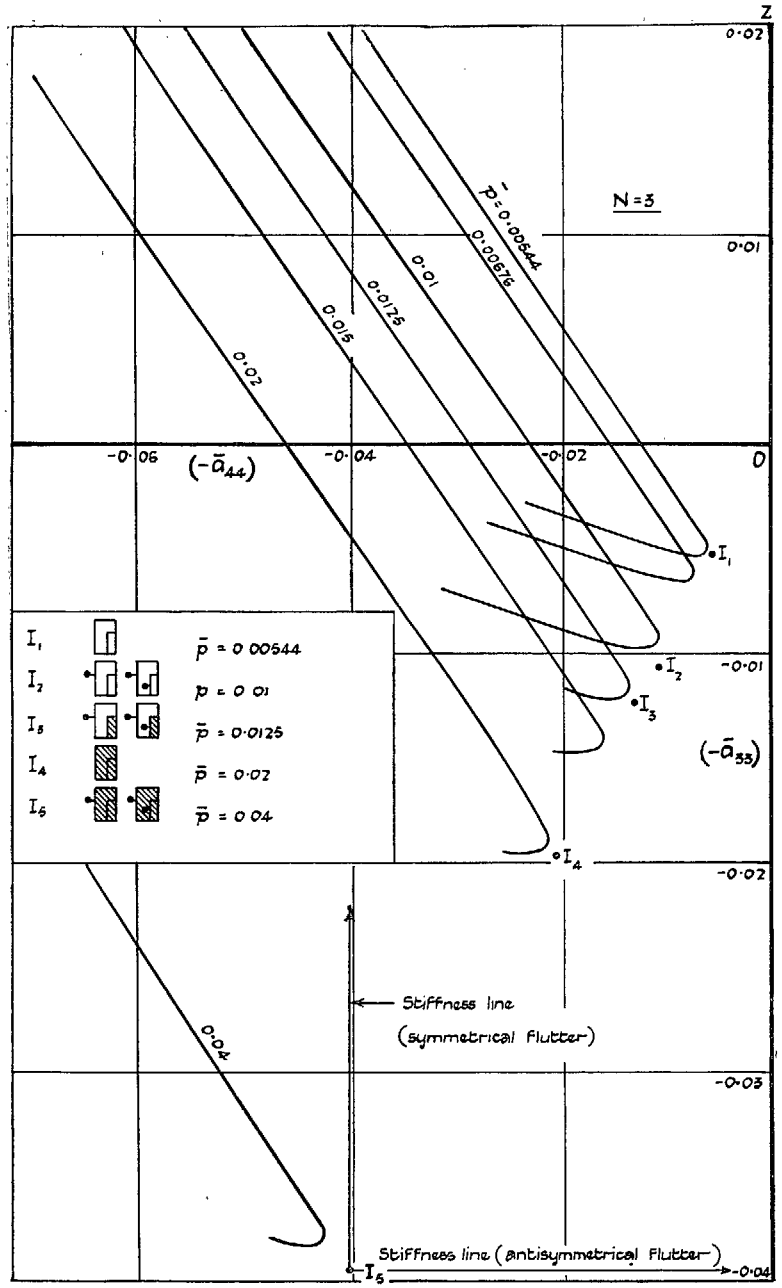

FIG. 15a. Aileron–tab inertia-stiffness diagram (para. 15). Base curves for $N = 3$.

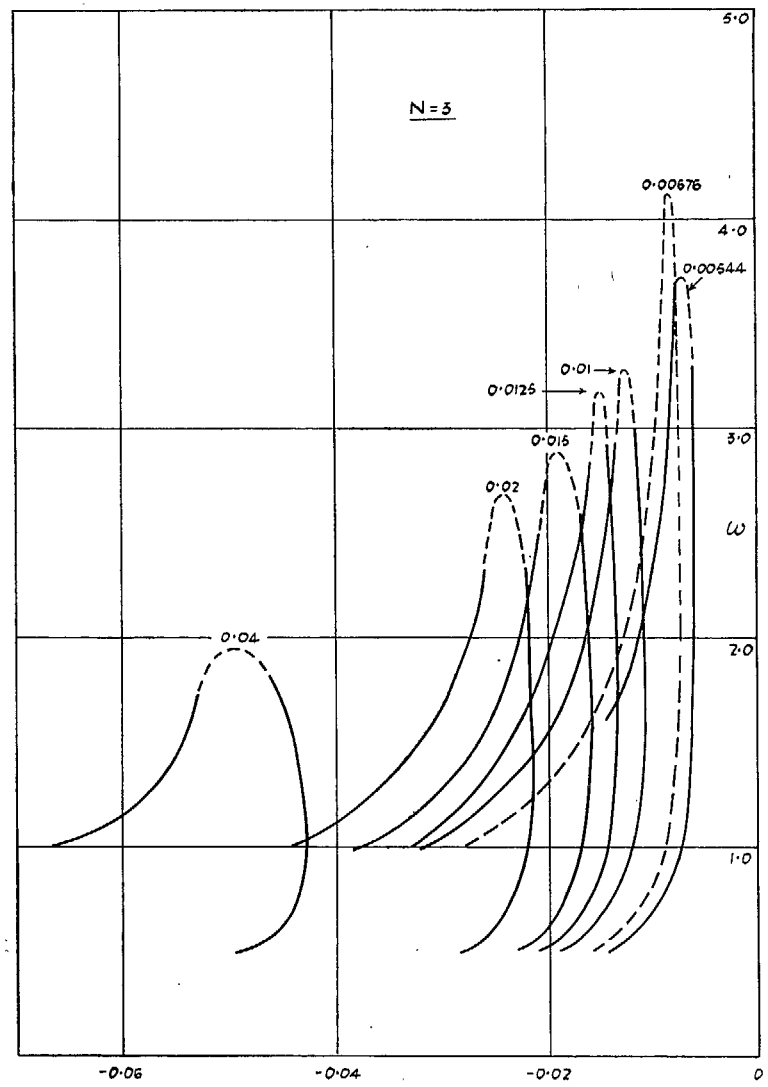

FIG. 15b. Aileron–tab inertia-stiffness diagram (para. 15). Frequency parameter curves for $N = 3$.

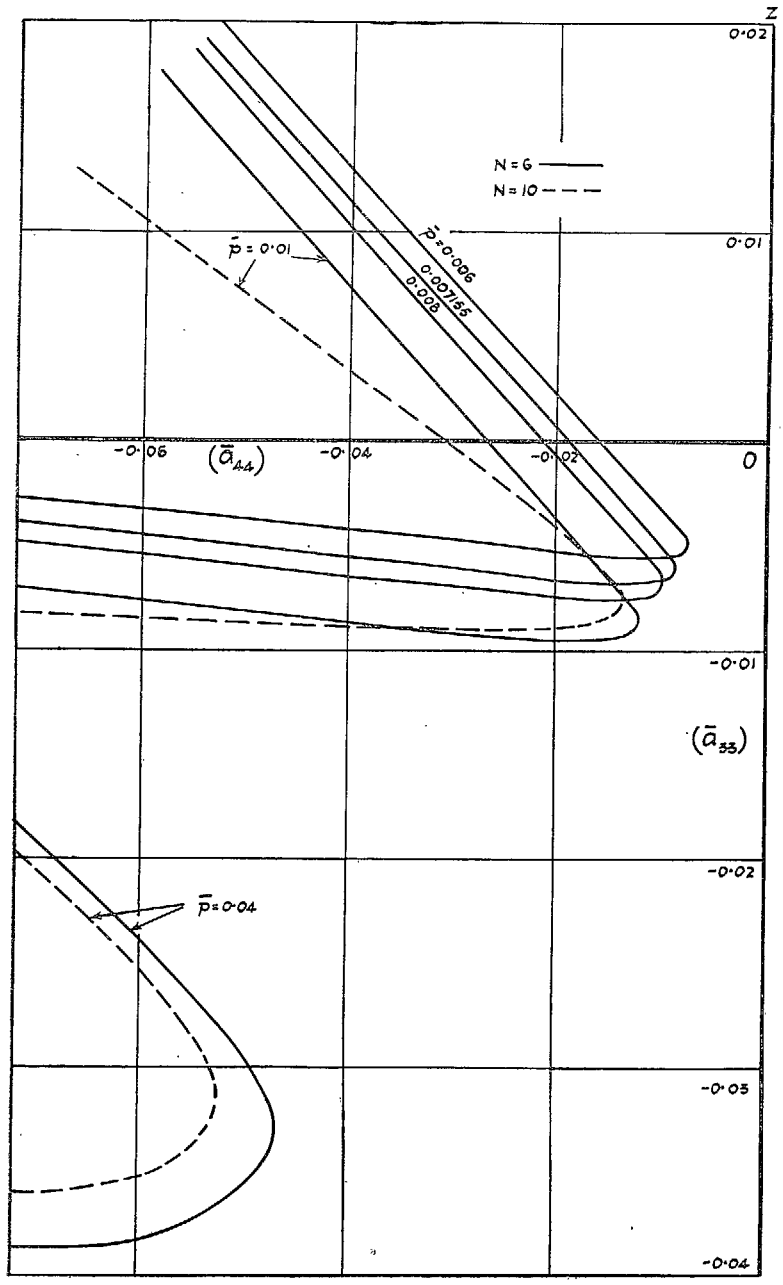

FIG. 16a. Aileron–tab inertia-stiffness diagram (para. 15). Base curves for N = 6 and $N = 10$.

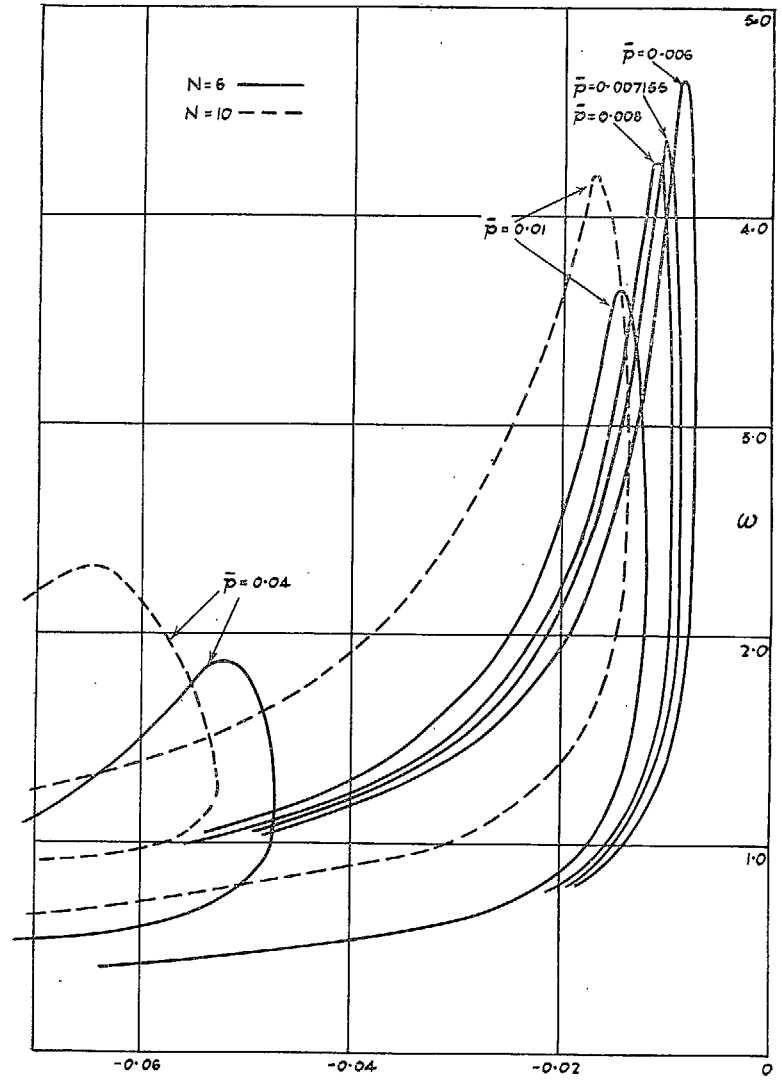

FIG. 16b. Aileron–tab inertia-stiffness diagram (para. 15). Frequency parameter curves for $N = 6$ and $N = 90$.

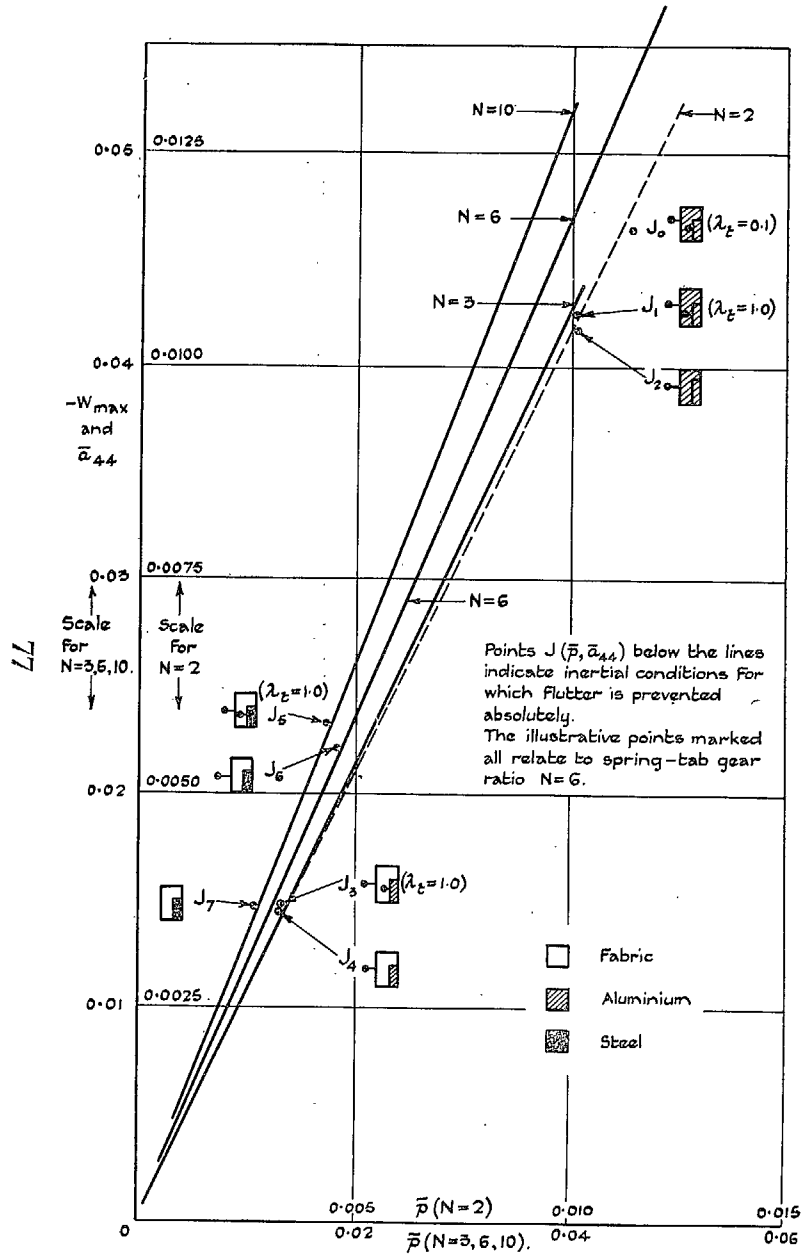

FIG. 17. Stability diagram for binary aileron–tab flutter (para. 16).
Spring tab No. 2.

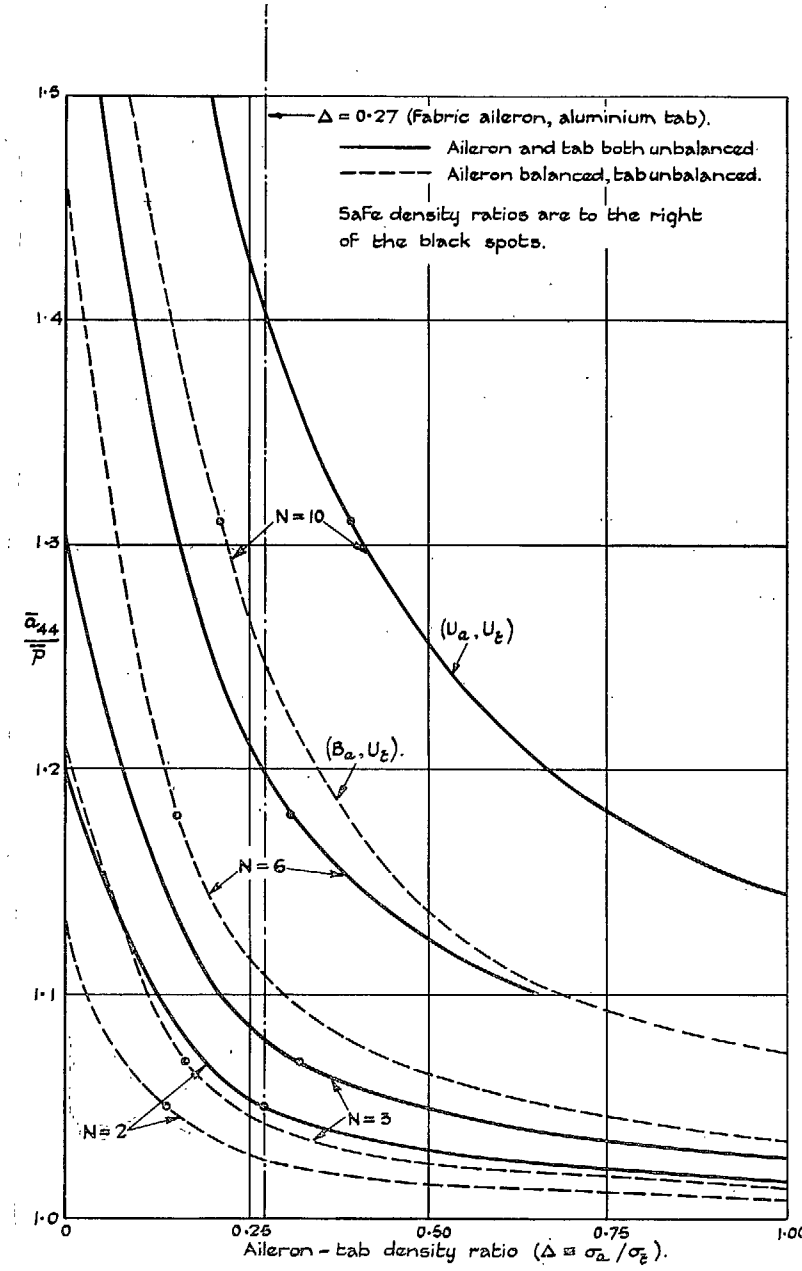

FIG. 18. Influence of density ratio on stability (para. 16).

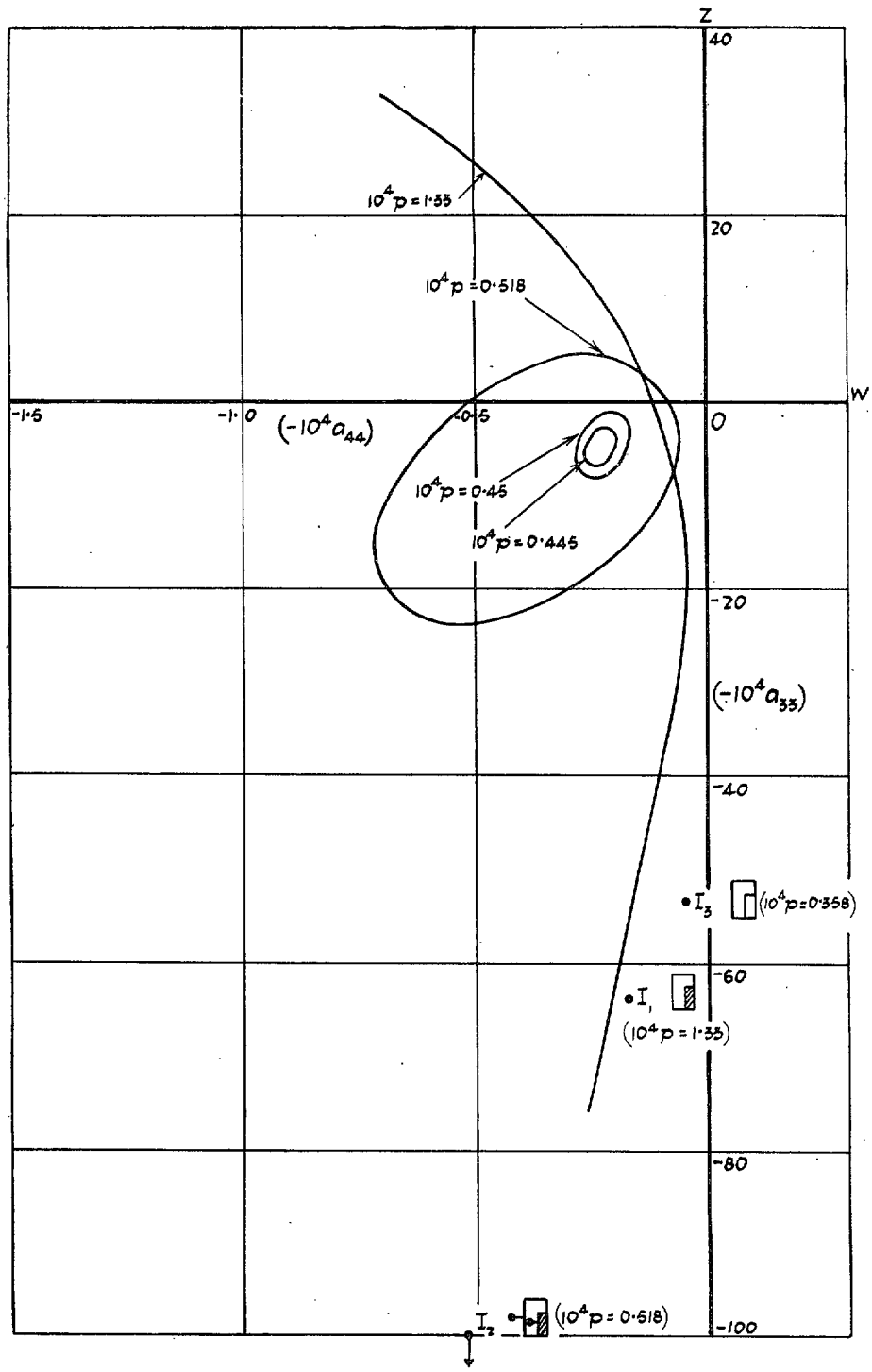

FIG. 19. Base curves for normal aileron with elastically hinged tab (*see* end of para. 16).

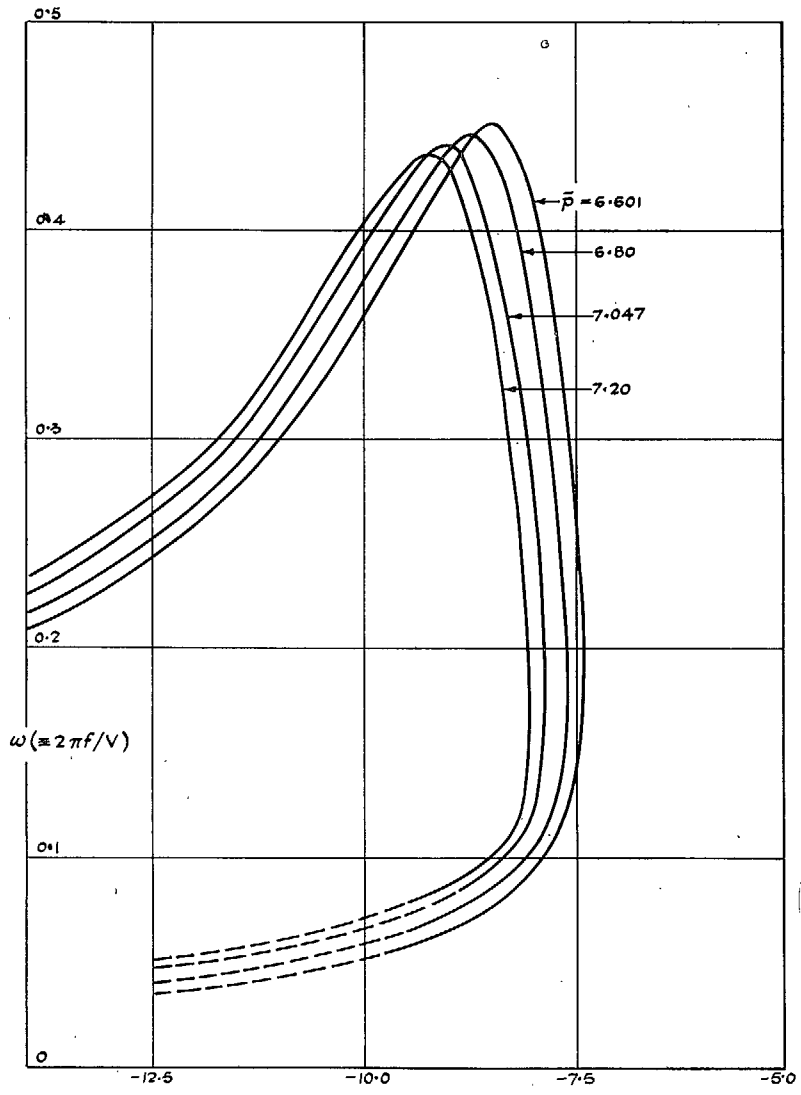

FIG. 20b. Binary servo-rudder flutter (para. 17). Frequency parameter diagram.

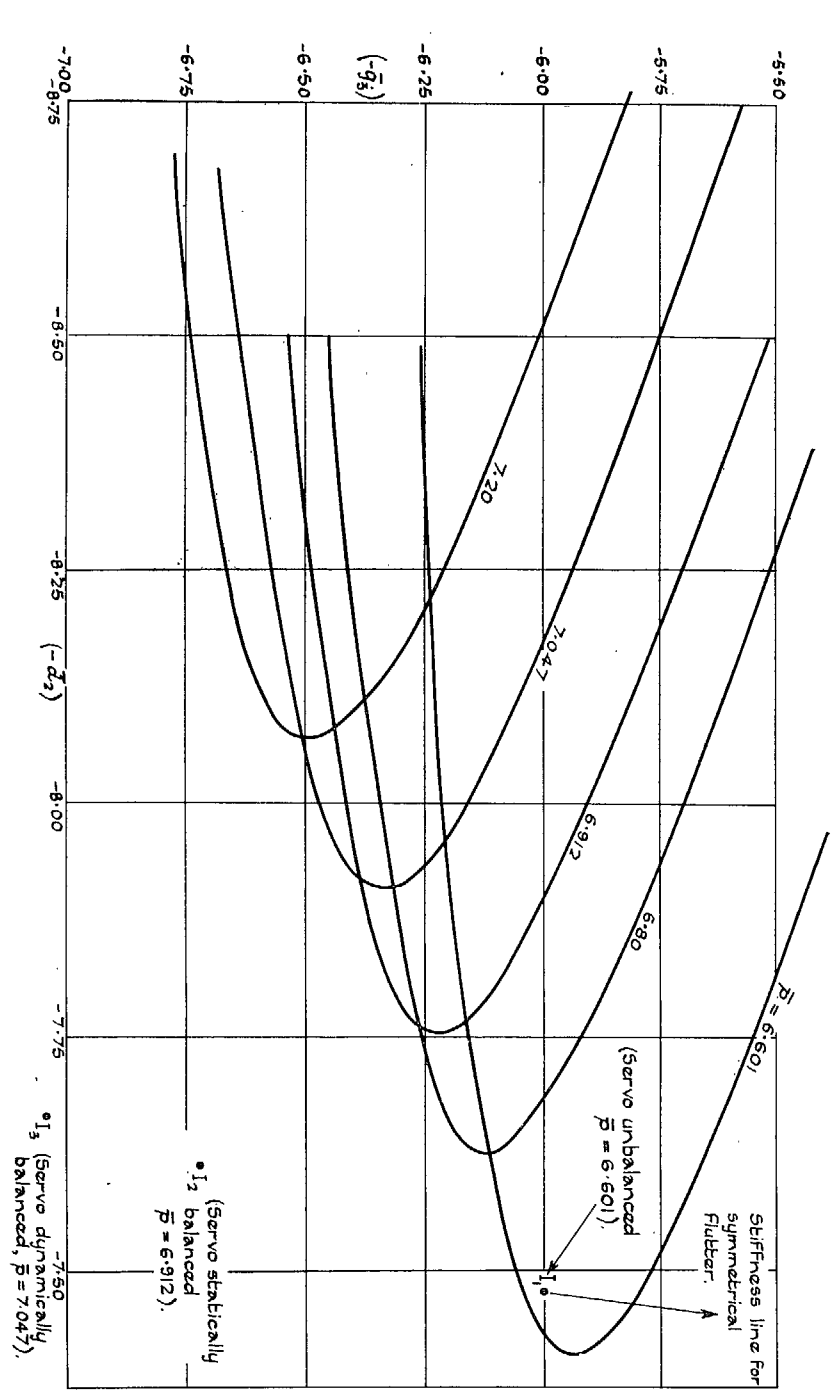

FIG. 20a. Base curves for servo-rudder flutter of a particular aeroplane (para. 17).

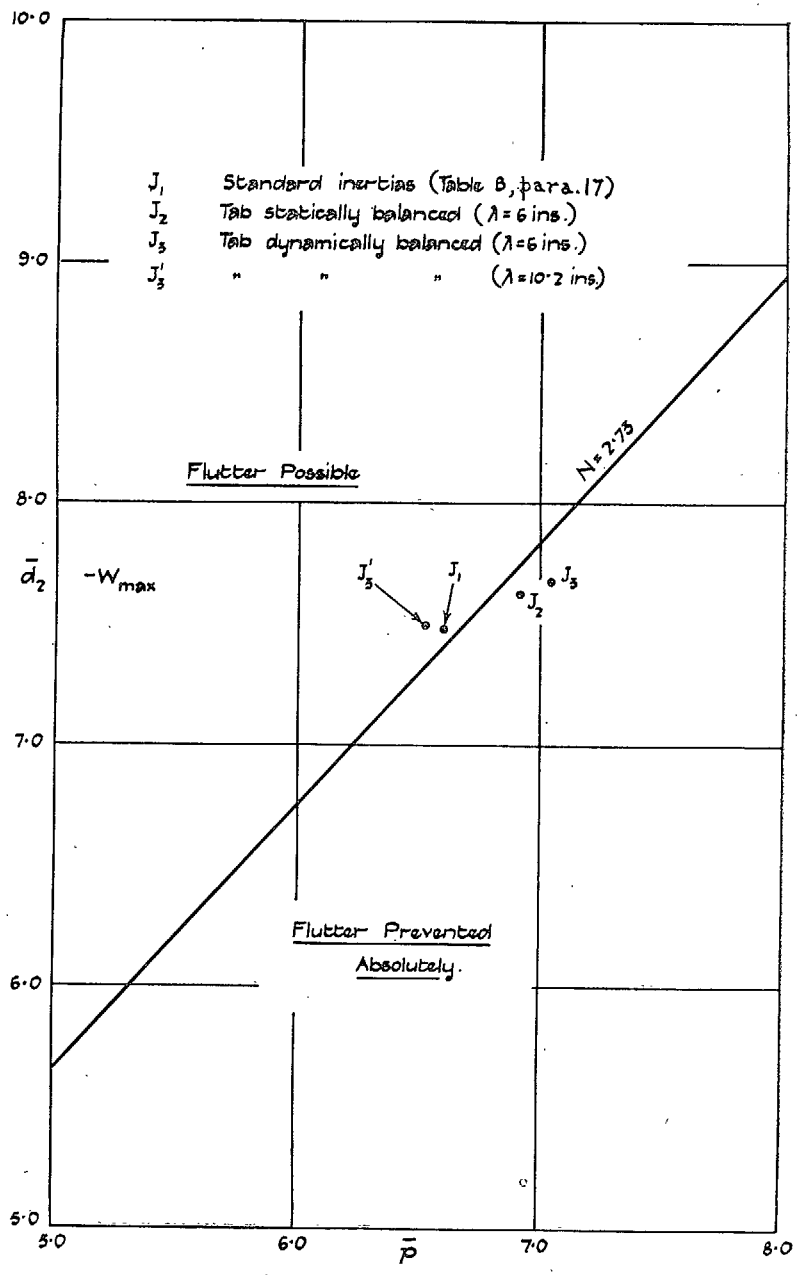

FIG. 21. Stability diagram for servo-rudder flutter (para. 17).

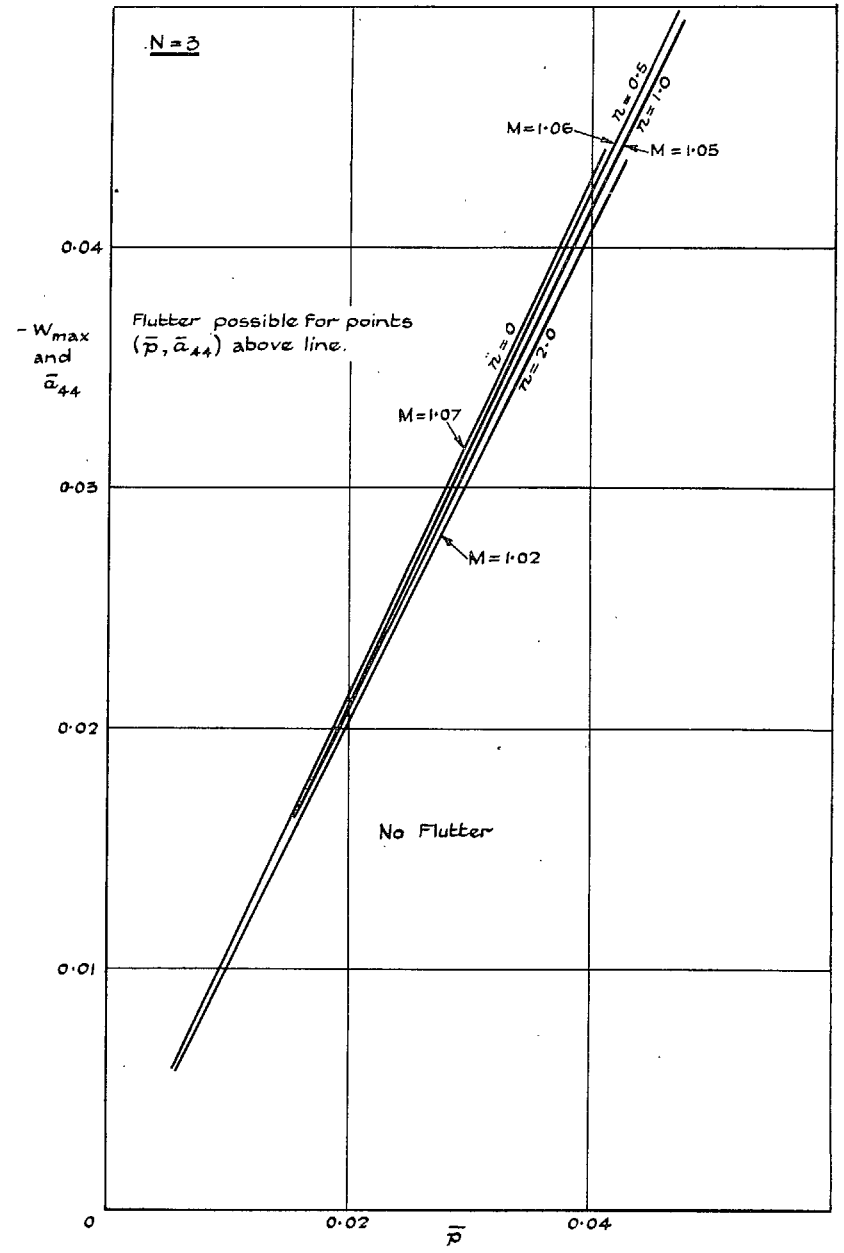

FIG. 22. Stability diagram for binary aileron–tab flutter (para. 19). Spring tab No. 1.

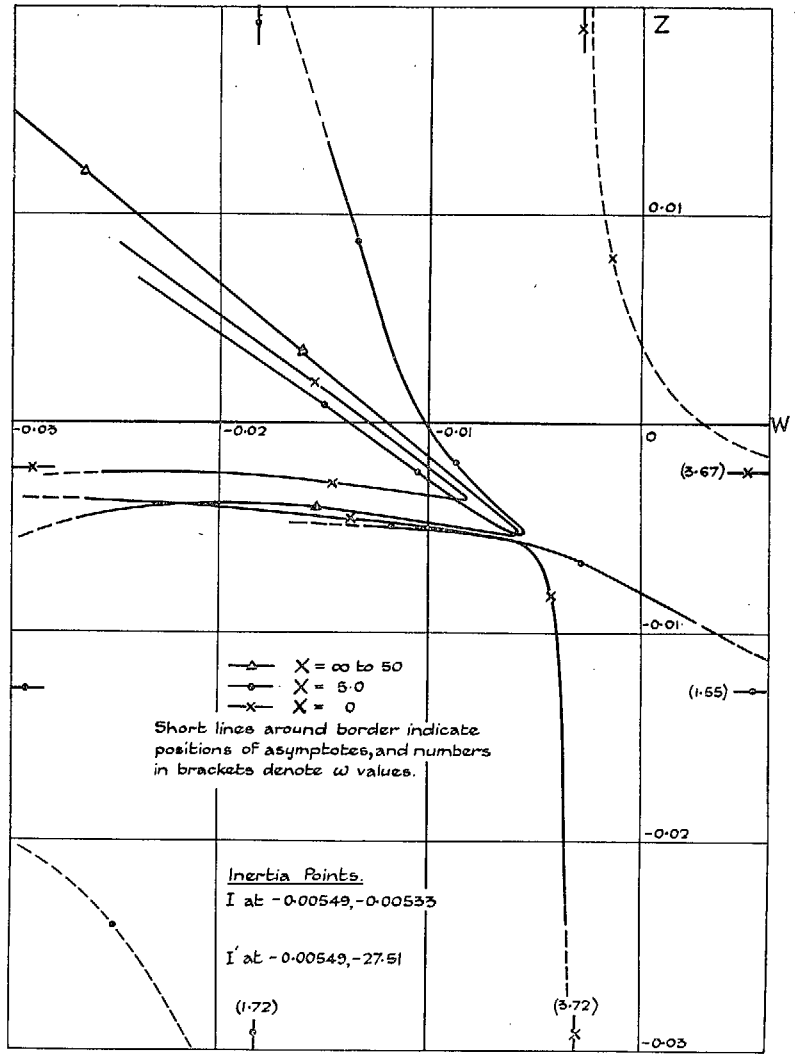

FIG. 23a. Flexure-aileron–tab inertia-stiffness diagram (aileron unbalanced).

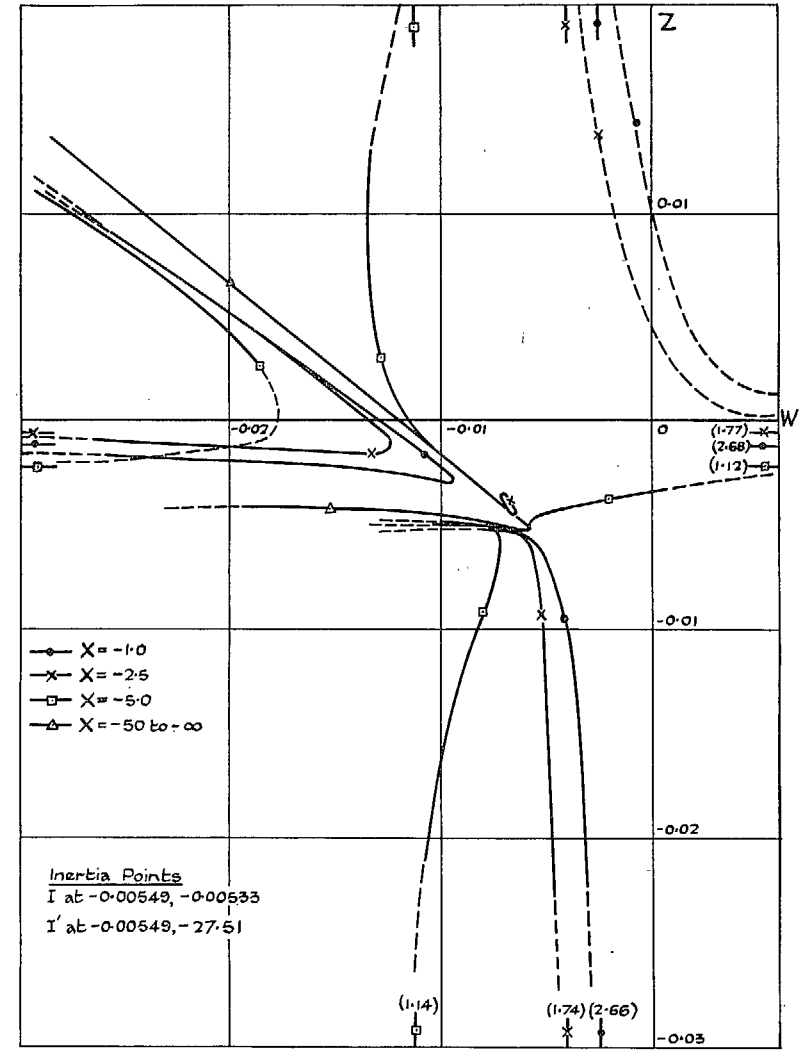

FIG. 23b. Flexure–aileron–tab inertia-stiffness diagram (aileron unbalanced).

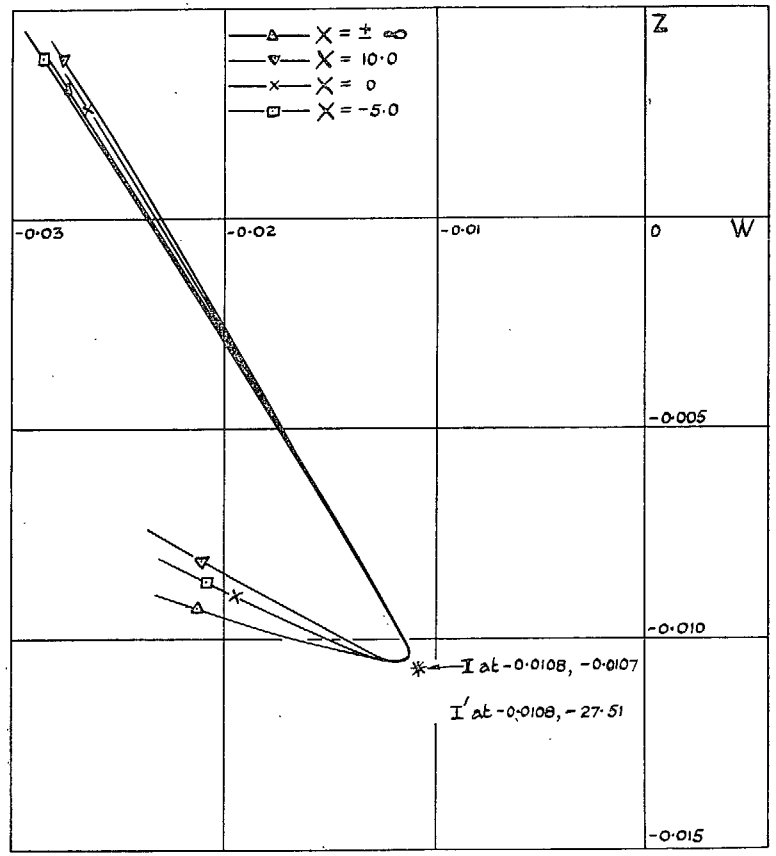

FIG. 24. Flexure–aileron–tab inertia-stiffness diagram (aileron statically balanced).

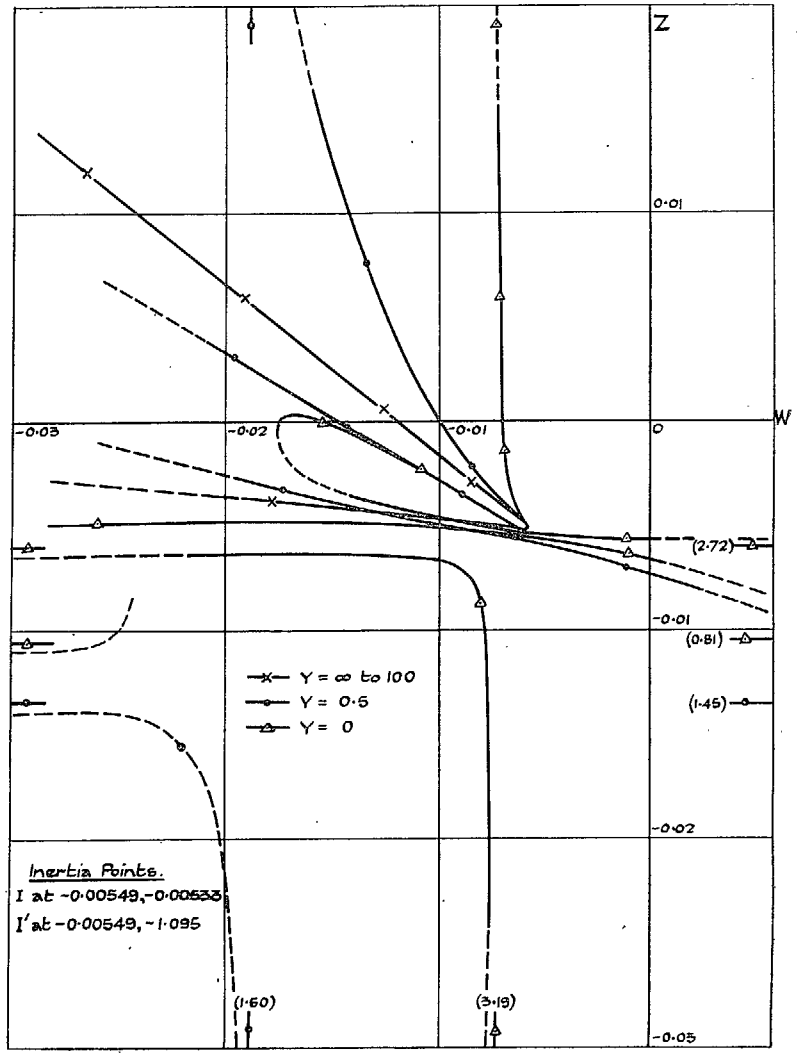

FIG. 25a. Torsion–aileron–tab inertia-stiffness diagram (aileron unbalanced).

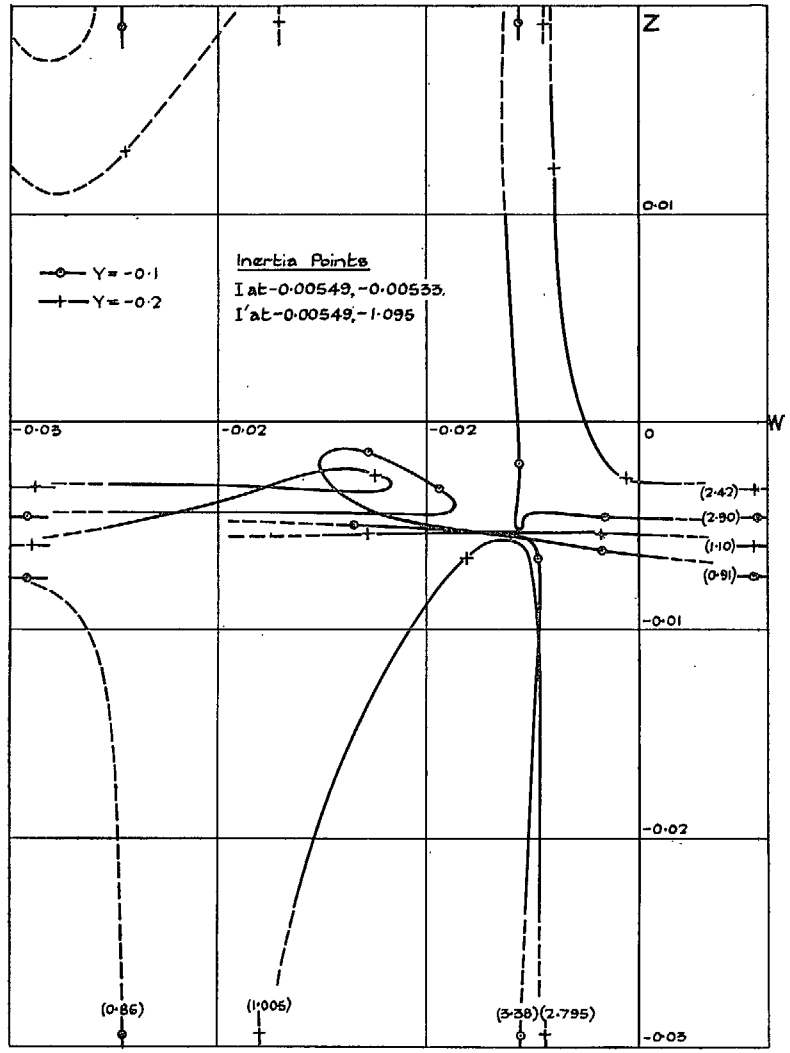

FIG. 25b. Torsion–aileron–tab inertia-stiffness diagram (aileron unbalanced)

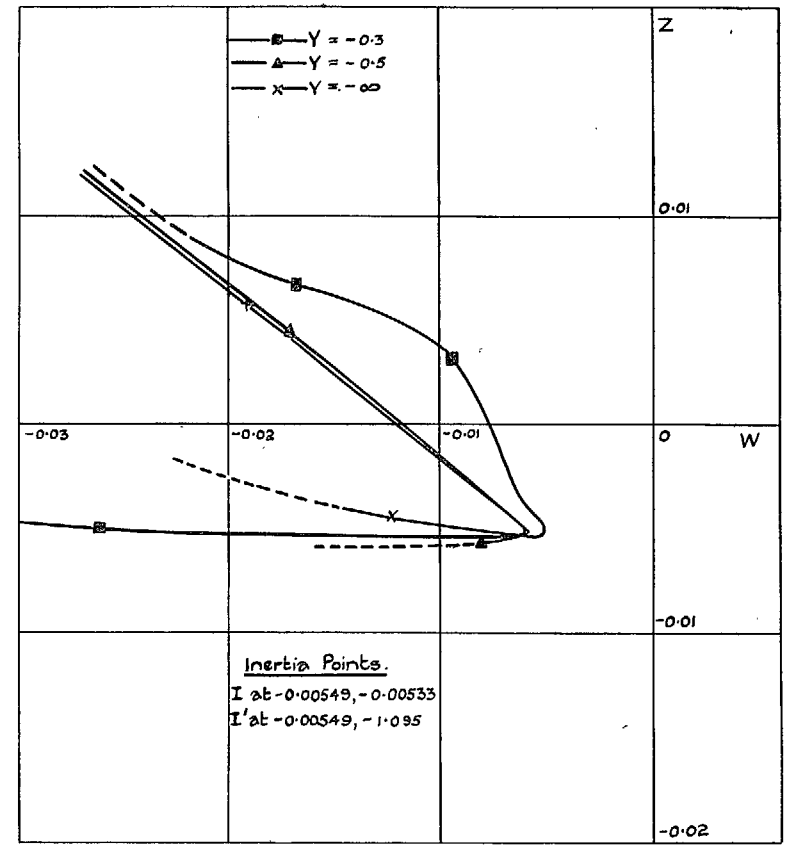

FIG. 25c. Torsion–aileron–tab inertia-stiffness diagram (aileron unbalanced).

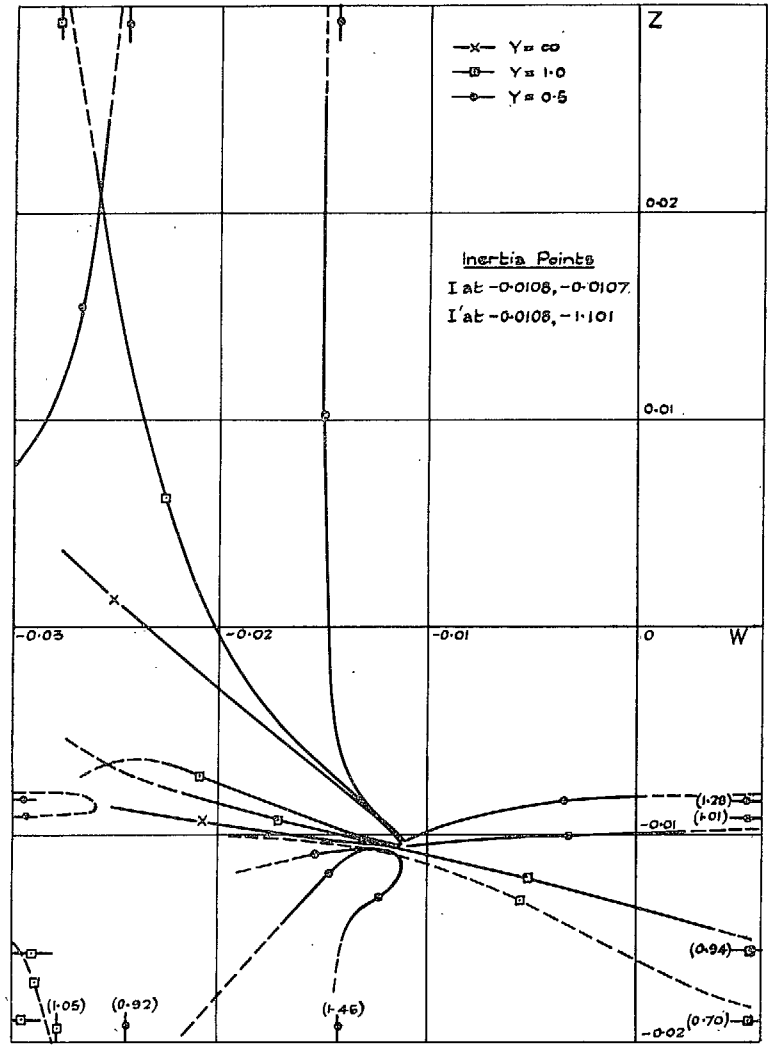

FIG. 26a. Torsion–aileron–tab inertia-stiffness diagram (aileron statically balanced).

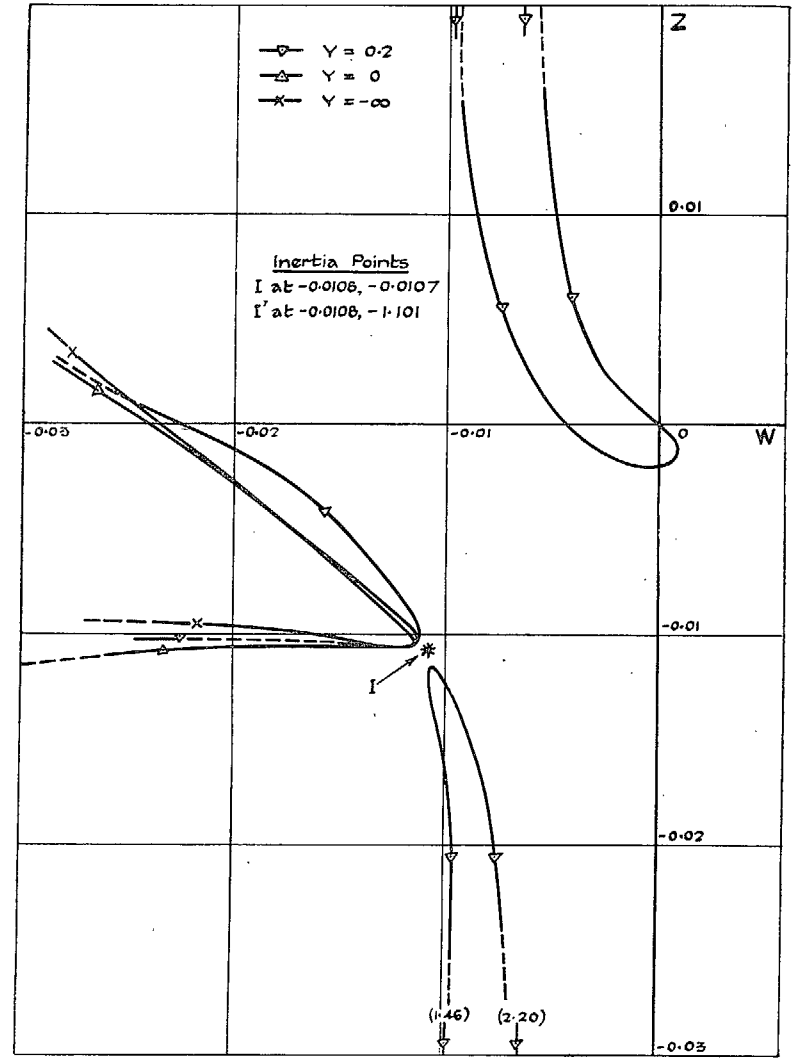

FIG. 26b. Torsion–aileron–tab inertia-stiffness diagram (aileron statically balanced).

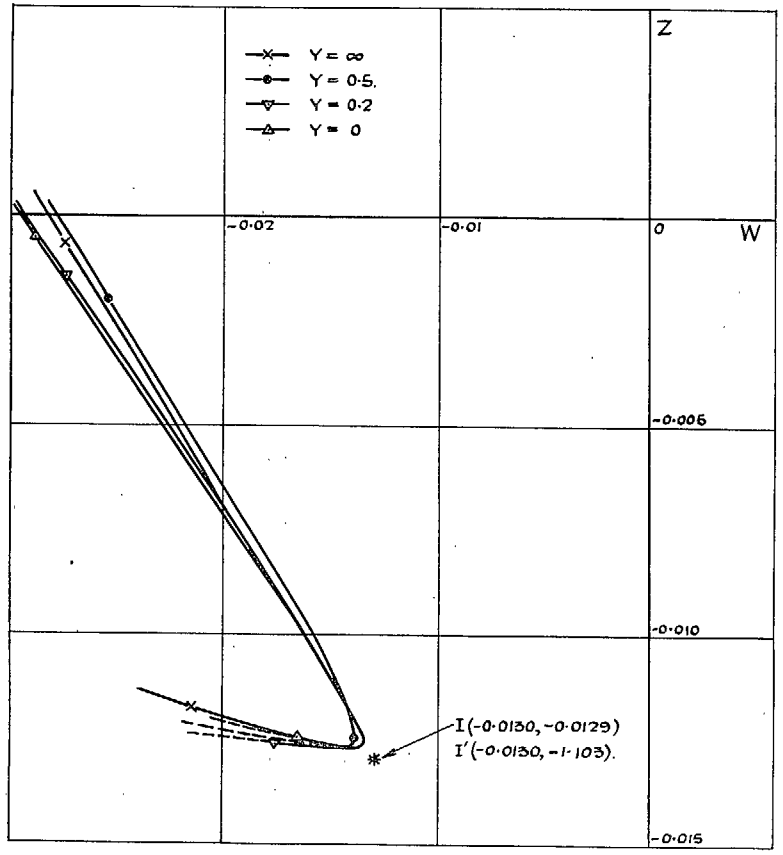

FIG. 27. Torsion–aileron–tab inertia-stiffness diagram (aileron dynamically balanced).

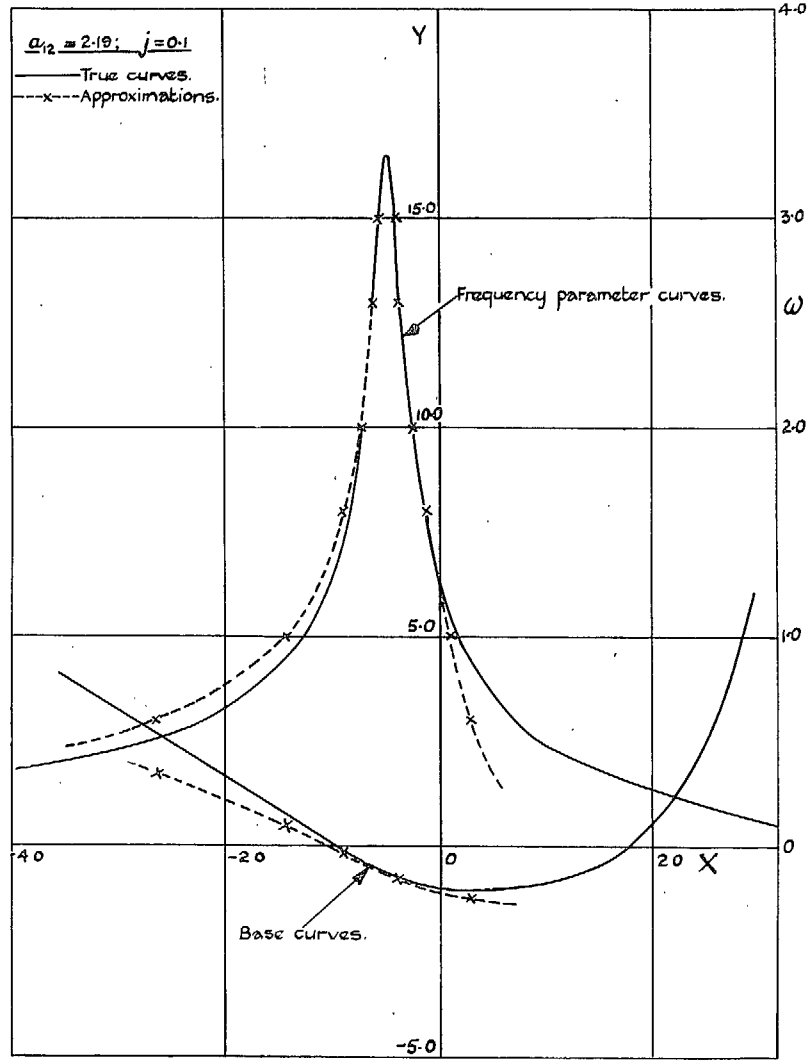

FIG. 28.—Flexure–torsion inertial-stiffness diagram with approximations.

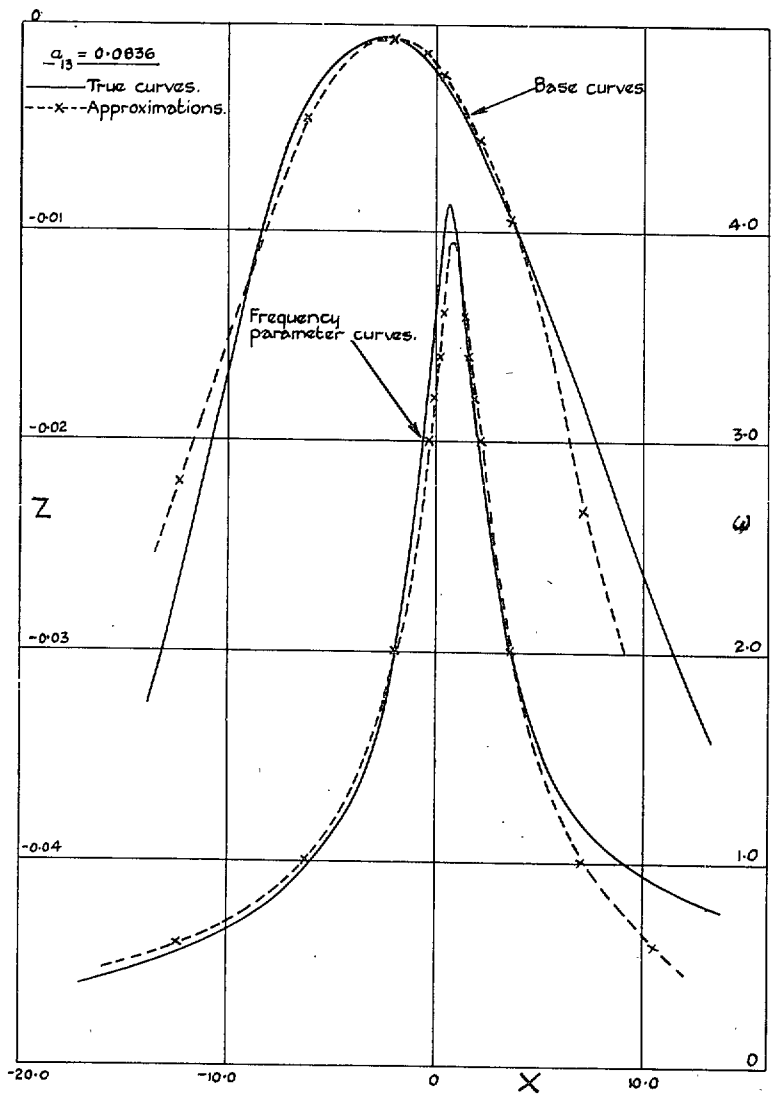

FIG. 29. Flexure–aileron inertia-stiffness diagram with approximations.

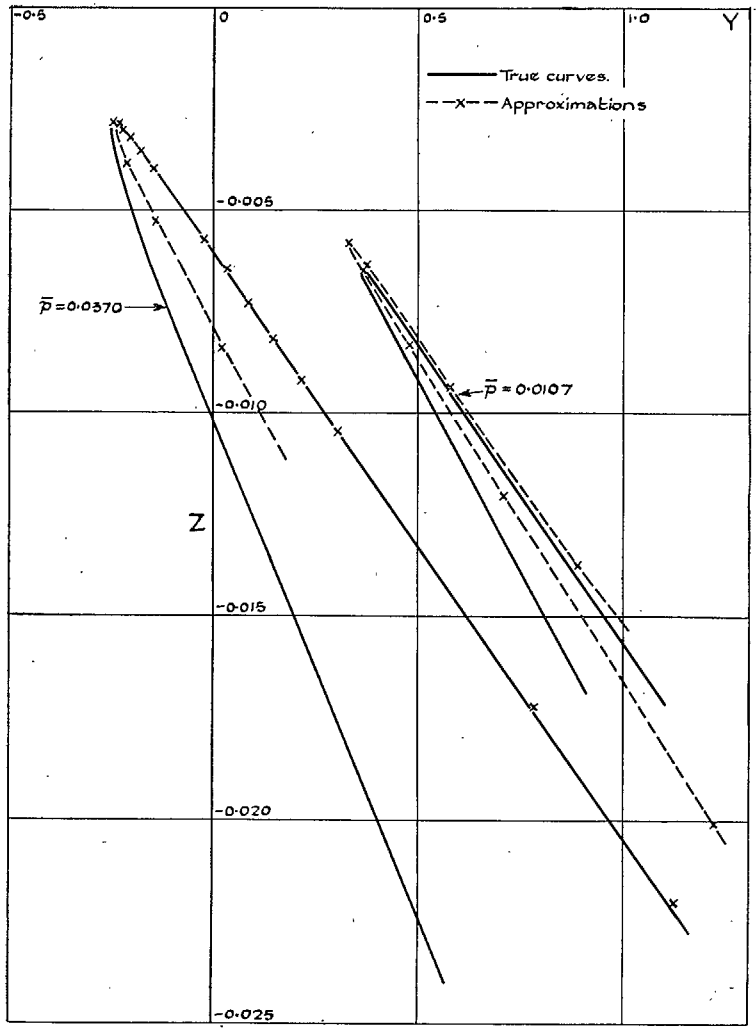

FIG. 30a. Torsion–aileron inertia-stiffness diagram with approximations. Base curves.

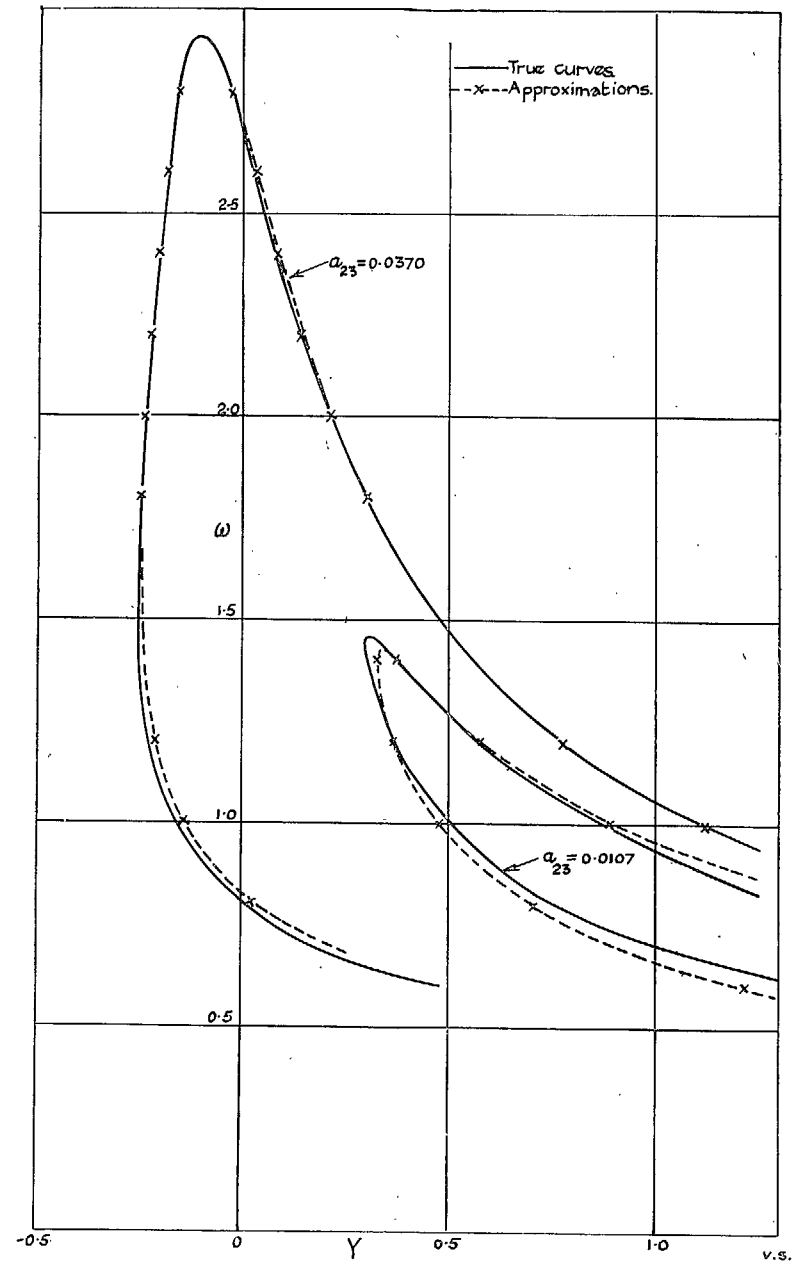

FIG. 30b. Torsion–aileron inertia-stiffness diagram with approximations. Frequency parameter curves.

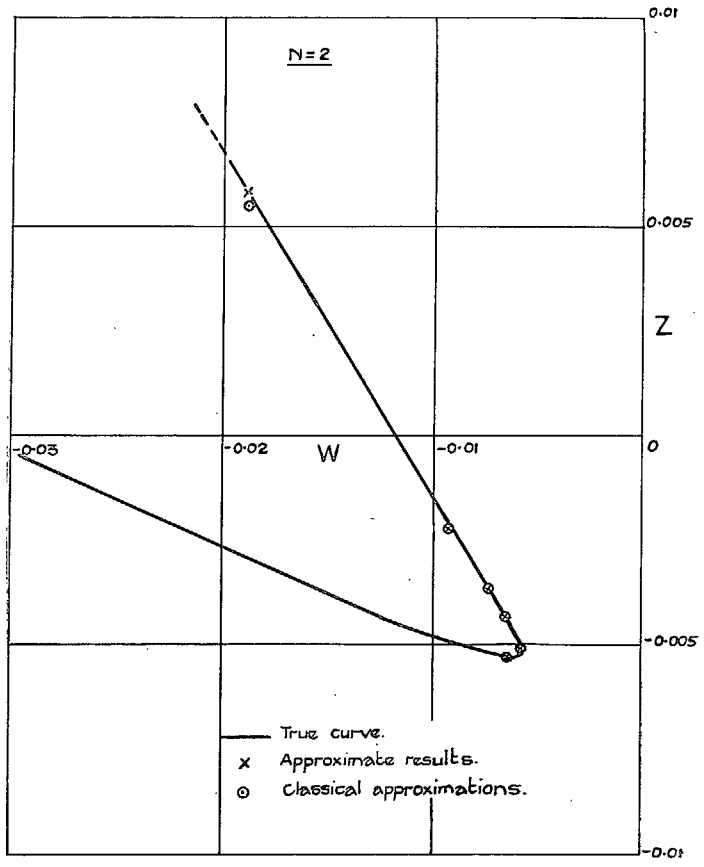

FIG. 31a. Aileron–tab inertia-stiffness diagram with approximations. Base curve.

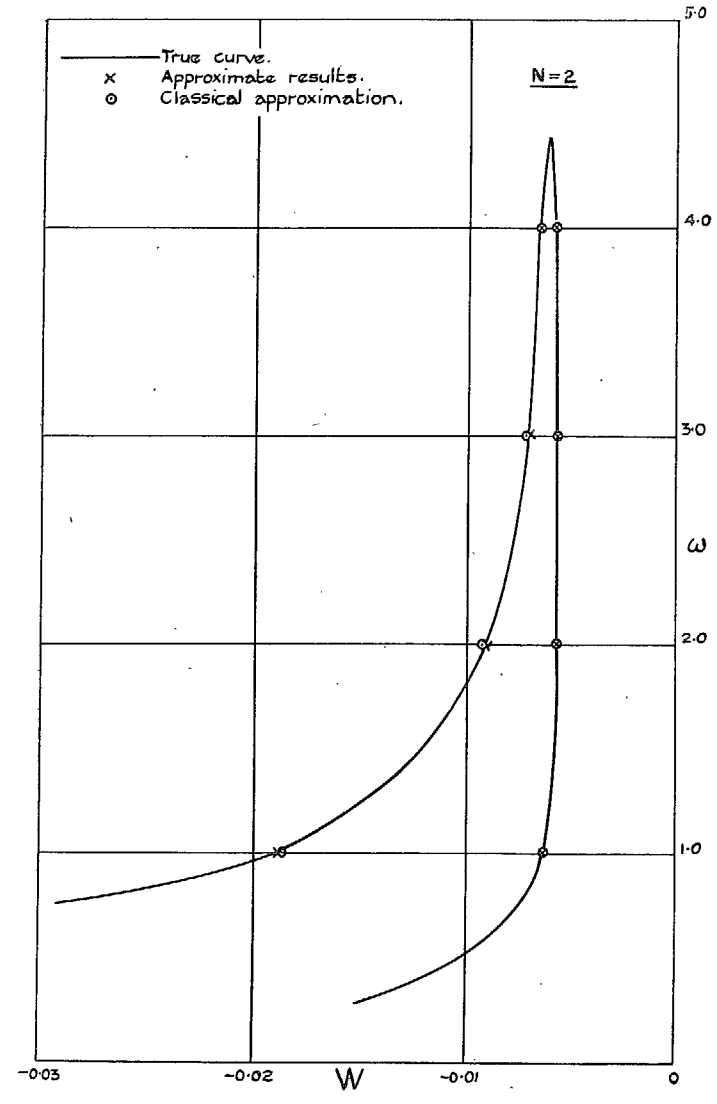

FIG. 31b. Aileron–tab inertia-stiffness diagram with approximations. Frequency parameter curve.

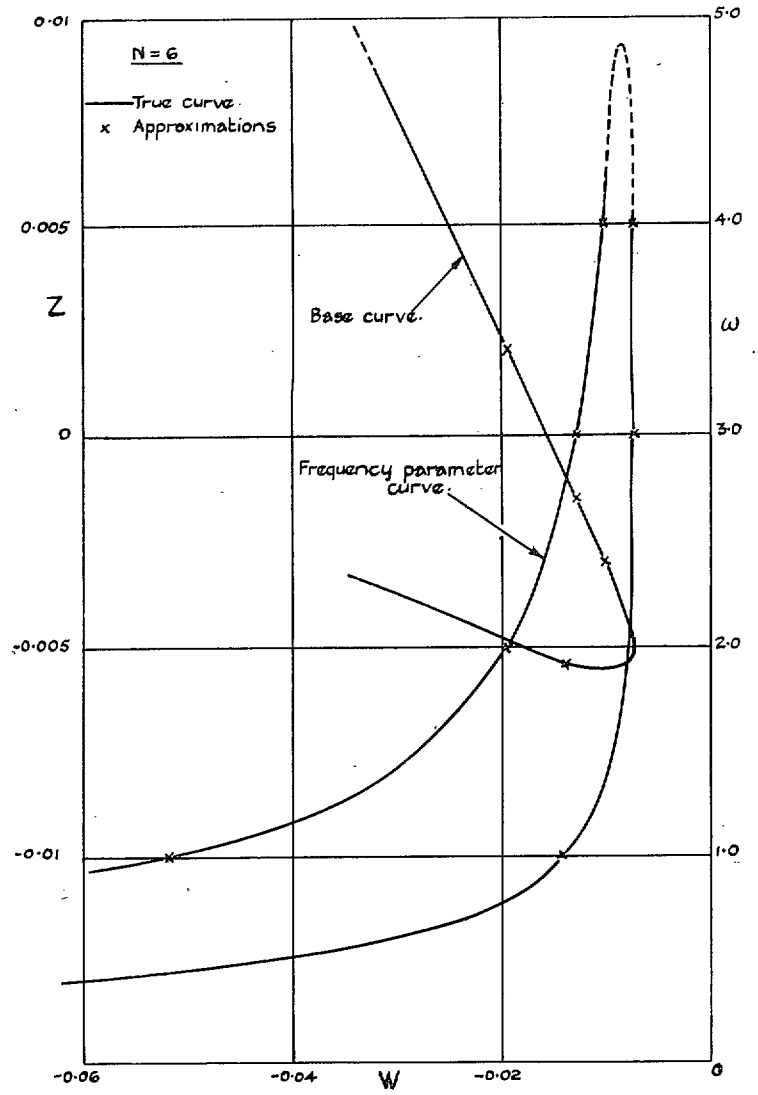

FIG. 32. Aileron–tab inertia-stiffness. Diagram with approximations.

PART II

Experiments on Binary Aileron-Tab Flutter

By

C. SCRUTON, B.Sc., J. WILLIAMS, B.Sc., and C. J. W. MILES

---

1. *Summary.*—A theoretical discussion of the effect of non-preloaded spring tab control on wing–aileron–tab flutter, in which the binary aileron–tab case is included, is given by Frazer and Jones in Part I. The experiments here described were made to test certain of their conclusions for binary aileron–tab flutter.

2. *The Model.*—The model was designed for tests in a 4-ft square wind tunnel. The wing (*see* Fig. 1), of 1·47-ft chord and 3-ft span and of NACA 2209 section, was rigidly constructed in wood. Fillets were fitted to the inboard end, where the wing was built into a plate for fixing to the tunnel floor.

Both aileron and tab were initially made of solid pine in order to obtain a density ratio (Δ)* of 1/1. Later this ratio was reduced by lightening holes in the aileron. The attachment of aileron to wing was by two small journal hinges and that of tab to aileron by two point and cup hinges. Balance arms, which were offset from the chord lines, were fitted to the aileron and to the tab, but subsequently that of the tab was changed to an arm with no offset and the necessary recess was cut from the aileron.

Details of the model representation of the elastic characteristics of the spring control are shown in Fig. 2. Here the flat spring (a), which represents the stiffness of the control circuit ($2\sigma_0$), is earthed at one end to the wing by an adjustable mounting and is fixed at the other end to the floating arm (b). The arm (b) is pivoted at the aileron hinge axis and is elastically connected to the aileron by means of the adjustable clamping link (d) and the piano-wire spring (c). Spring (c), which represents the stiffness of the tab mechanism spring (σ), is built into the aileron on the hinge axis. Connection between F at the top of arm (b) to M on the tab lever was made by a link of hypodermic tubing which was pin-jointed to F and M. It can easily be shown by comparison of the strain energies that this system is elastically equivalent to the spring tab control system of Fig. 1a, Part I. The equivalent leverages AF, AI and TM are similarly denoted in Fig. 2 of this Part and in Fig. 1a of Part I. For the model AF and TM were of fixed length such that $N = 6$, AI was variable to give values of n between 0 and 2.

No measurements of the inertial values were made when the aileron was of solid pine. After the aileron was lightened and without any additional masses the aileron and tab had the following inertial values.

$$\mu_a = 0{\cdot}39 \text{ lb}$$
$$\mu_t = 0{\cdot}02 \text{ lb}$$
$$A_{33} = 0{\cdot}93 \text{ lb/in.}^2$$
$$A_{44} = 1{\cdot}6 \times 10^{-3} \text{ lb/in.}^2$$
$$P = 3{\cdot}0 \times 10^{-3} \text{ lb/in.}^2$$

3. *Results.—Tests of Recommendations of Part I.—(a) The Effect of Density Ratio Δ.*—No systematic variation of Δ was attempted. Before the aileron was lightened the density ratio was approximately unity. No flutter within the speed range of the tunnel could then be obtained

---

* The symbols used accord with those used in Part I.

but successive additions of masses to the trailing edge of the tab progressively lowered the critical speed. The aileron was then lightened in order to obtain flutter without addition of mass to the tab and a critical speed within the tunnel range obtained. If the lightened aileron can be regarded as homogeneous the density ratio was then about 1/3.

(*b*) *The Effect of Addition of Mass to the Aileron* (*see Table*).—Addition of mass to the aileron invariably increased the critical speed. A comparison was made of the effect of equal additions to the moment of inertia of the aileron by masses added firstly to the aileron balancing arm and then to the trailing edge. The first method was slightly more effective than the second. This may have been due to very slight movements of the main wing.

(*c*) *The Effect of the Location of the Tab Balancing Mass.*—Tests were made with an offset balancing arm before the disadvantageous nature of such an arrangement was realised. In the Appendix it is shown that the neutral point (*i.e.*, the position forward of the hinge axis behind which mass has to be placed in order to be advantageous) recedes as the offset increases. The offset for the model arm was such that the neutral point was behind the rearmost tab balancing position available ($D/21$). It was found that any addition of mass to the arm reduced the critical speed.

The results of tests for $n = 0$ and $n = 2$ with the non-offset balancing arm are given in Fig. 3 and Fig. 4. Here the neutral point was distance $D/7$ forward of the tab hinge axis and the curves show that for $n = 2$ addition of mass was advantageous only when placed behind this position and that the addition of a mass at the neutral point which statically balanced the tab did not appreciably affect the critical speed. This conforms well with the theory but heavier masses added at the neutral point tended to decrease the critical speed. This decrease is more marked when $n = 0$ although the curves show the same general characteristics as those for $n = 2$. In both cases no flutter occurred within the tunnel speed range when the tab was statically mass balanced at position $2D/21$. Unfortunately no position intermediate between $2D/21$ and $D/7$ could be used but from the asymptotic trend of the curves it is probable that the system would be stable for all wind speeds if the tab were statically balanced by a mass rearward of the $2D/21$ position.

Fig. 4 shows the rate of increase of the critical speed with the addition of mass at the $2D/21$ position. If, as is deduced from Fig. 3, the system is stable when the tab is balanced by mass at the $2D/21$ position then it appears that a close approach to static mass balance is necessary to raise the critical speed appreciably.

Tests with Fluid Damping and Solid Friction.—Fluid damping and solid friction were applied separately between the floating arm (b) and the wing to represent such dampings on the spring casing of spring tab No. 1 of Part I.

Increase in damping or friction invariably increased the critical speed. The largest amount of fluid damping applied, that due to a 0·5 sq in. vane attached to the outer end of arm (b) and moving in heavy gear oil, only increased the critical speed from 44 to 48 feet per second. Solid friction, provided by a felt pad attached to the arm (b) and rubbing on a brass plate, was more effective. The critical speed increased with the pressure on the felt pad until there was no movement between the felt pad and the brass plate. In this condition flutter at a high speed was still possible because of flexibility in the connection of the felt pad to the arm.

4. *Conclusions.*—The recommendations (*a*), (*b*), (*c*) and (*d*) of para. 16 of Part I are confirmed by the model tests. In the application of recommendation (*c*) it is important to consider the dependence of the position of the neutral point on the offset of the balancing mass.

TABLE

The Effect of Addition of Mass to the Aileron

The inertial condition of model before the addition of masses is as stated in para. 3 for the lightened aileron

n	Mass added to aileron (lb) at		Added moment of inertia (lb in.^{2})	Critical speed (feet per second)
	Balancing arm	Trailing edge		
0	0	0	0	47·5
0	0·070	0	0·177	52·0
0	0	0·012	0·177	52·2
2	0	0	0	52·4
2	0·037	0	0·177	61·2
2	0	0·012	0·177	59·7
2	0·70	0	0·333	72·1
2	0	0·021	0·333	67·4
2	0·079	0	0·374	76·6
2	0	0·024	0·374	70·6

APPENDIX

The Position of the Neutral Point for an Offset Balancing Arm

Let a mass m be added to the tab at a distance λ forward of the tab hinge axis (*i.e.*, at a distance $D - \lambda$ behind the aileron hinge axis) but offset by a perpendicular distance $\lambda \tan \theta$ from the tab chord line produced, where θ is the angle between this line and the line which joins the tab hinge to the mass (*see* sketch which follows).

Then

$$\left.\begin{aligned} \delta A_{33} &= m(D^2 - 2\lambda D + \lambda^2 \sec^2 \theta) , \\ \delta A_{44} &= m\lambda^2 \sec^2 \theta , \\ \delta P &= m(\lambda^2 \sec^2 \theta - \lambda D) . \end{aligned}\right\} \quad \ldots \quad (1)$$

Hence

$$\delta \bar{A}_{44} = m\{\lambda^2 \sec^2 \theta (N+1)^2 - 2\lambda D(N+1) + D^2\} \quad \ldots \quad (2)$$

$$\delta \bar{P} = m\{\lambda^2 \sec^2 \theta (N+1)(n+1) - \lambda D(N+n+2) + D^2\} . \quad \ldots \quad (3)$$

From para. 16, Part I, the loading will be advantageous if $\delta \bar{a}_{44}/\delta \bar{p} < 1$ and $\delta \bar{p}$ is positive. ($\delta \bar{a}_{44}$ is always positive since $\sec^2 \theta > 1$.)

From (2) and (3) $\delta \bar{a}_{44}/\delta \bar{p} < 1$ if

$$\lambda^2 \sec^2 \theta (N+1)(N-n) - \lambda D[N-n] < 0 . \quad \ldots \quad (4)$$

For positions forward of the tab hinge axis $\lambda(N - n)$ is positive and condition (4) becomes

$$\lambda < \frac{D}{N+1} \cos^2 \theta . \quad \ldots \quad (5)$$

This condition determines the neutral point, provided $\delta \bar{p}$ is positive between $\lambda = 0$ and $\lambda = \{D/(N+1)\} \cos^2 \theta$. This is so since if the case of $\theta = 0$ is considered it is easily shown that $\delta \bar{p}$ is positive when $\lambda < D/(N+1)$ (or $> D/(n+1)$) and the effect of offset is to make $\delta \bar{p}$ more positive.

Thus, for a particular spring tab a circle $\lambda = \{D/(N+1)\}\cos^2\theta$ (as in sketch below) can be drawn which is the locus of the neutral points. Any tab balancing mass which is placed outside this circle will be disadvantageous.

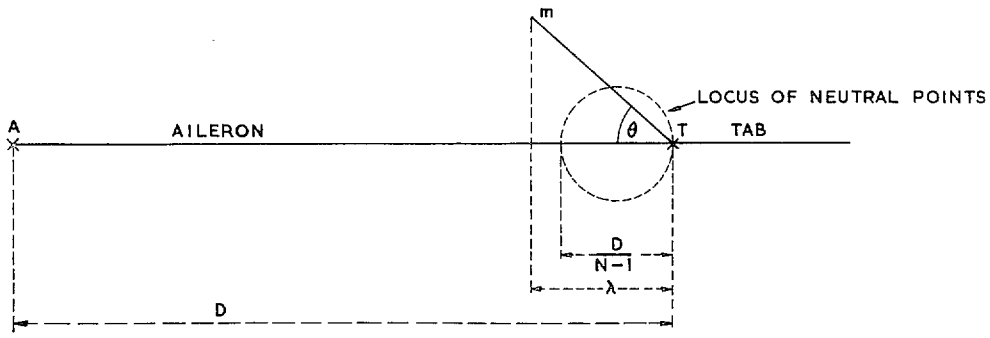

The following physical explanation of this rearward movement of the neutral point can be given. When λ is constant δA_{44} is increased by offset without any change in the mass moment about the hinge axis. The effect on the barred coefficients is immediately seen if equations (2) and (3) are written :—

$$\delta\bar{A}_{44} = (N+1)^2\delta A_{44} - 2(N+1)Dm\lambda + mD^2 \quad .. \quad .. \quad .. \quad (2a)$$

$$\delta\bar{P} = (N+1)(n+1)\delta A_{44} - (N+n+2)Dm\lambda + mD^2 \quad .. \quad .. \quad .. \quad (3a)$$

Hence, since $N > n$, $\delta A_{44}/\delta\bar{P}$ would increase with offset if λ were constant and to compensate it is necessary to reduce the value of λ.

In the case of a spring tab control on a *Spitfire* aileron the tab was fitted with balancing arms on the upper and lower surfaces of which the angular offsets were 60 deg and 50 deg respectively. The distance forward of the neutral point was thus only about one-quarter of the maximum possible distance.

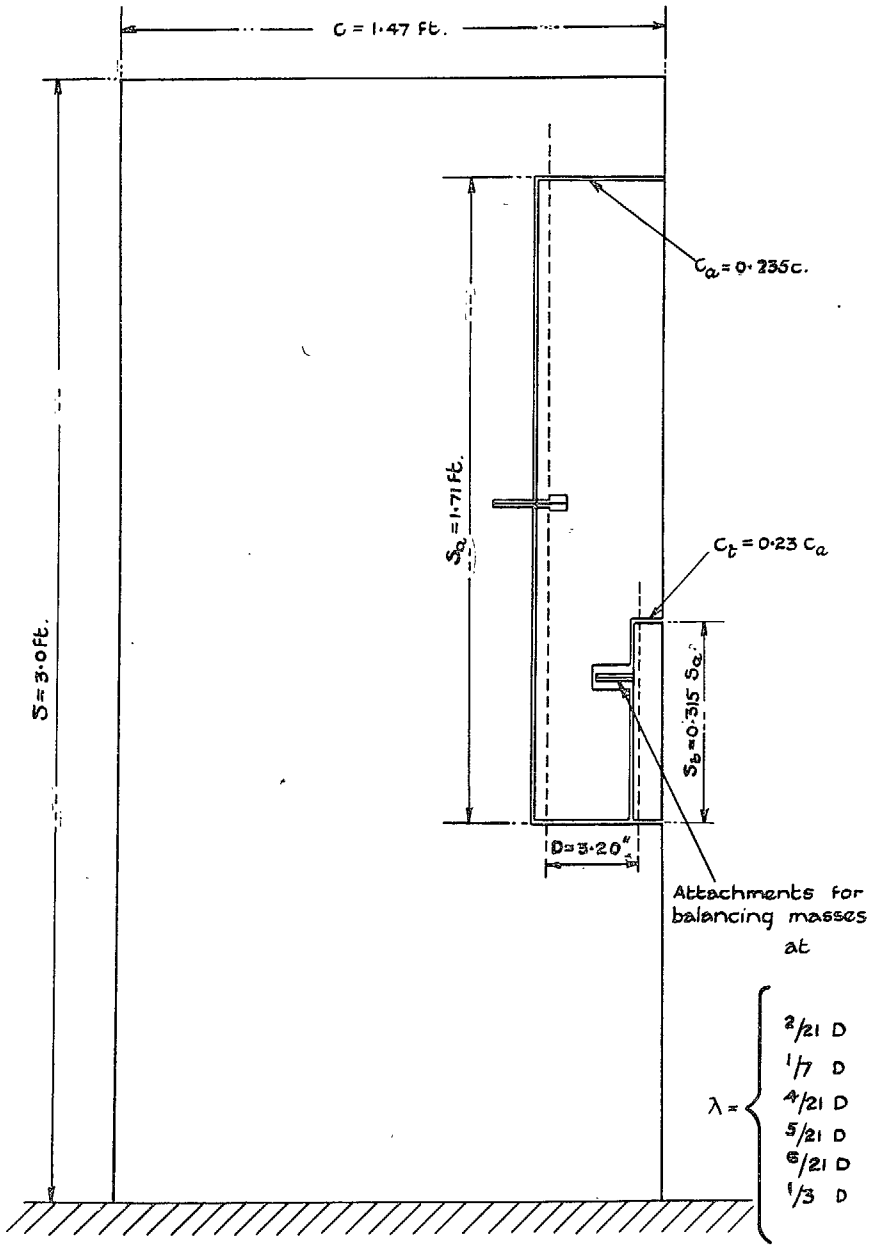

FIG. 1.

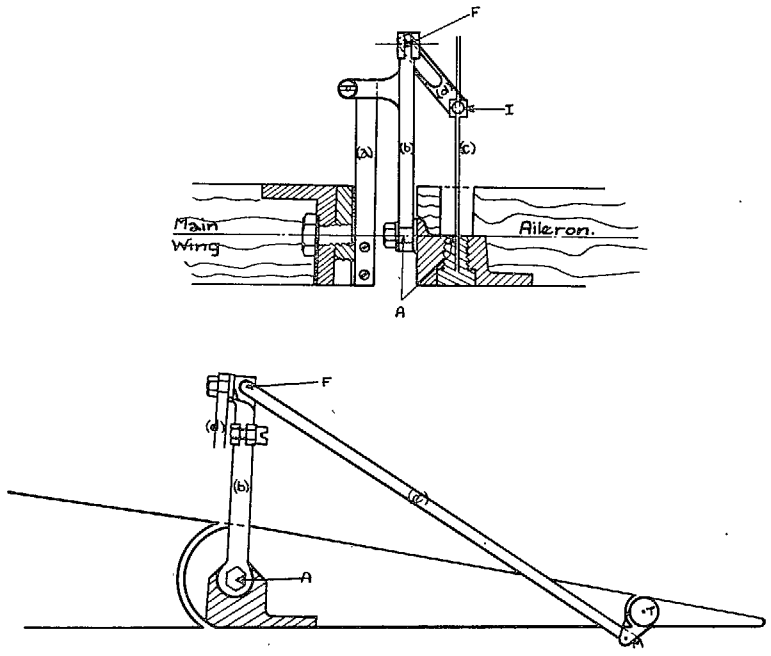

FIG. 2. Model representation of the elastic characteristics of a non-preloaded spring tab control.

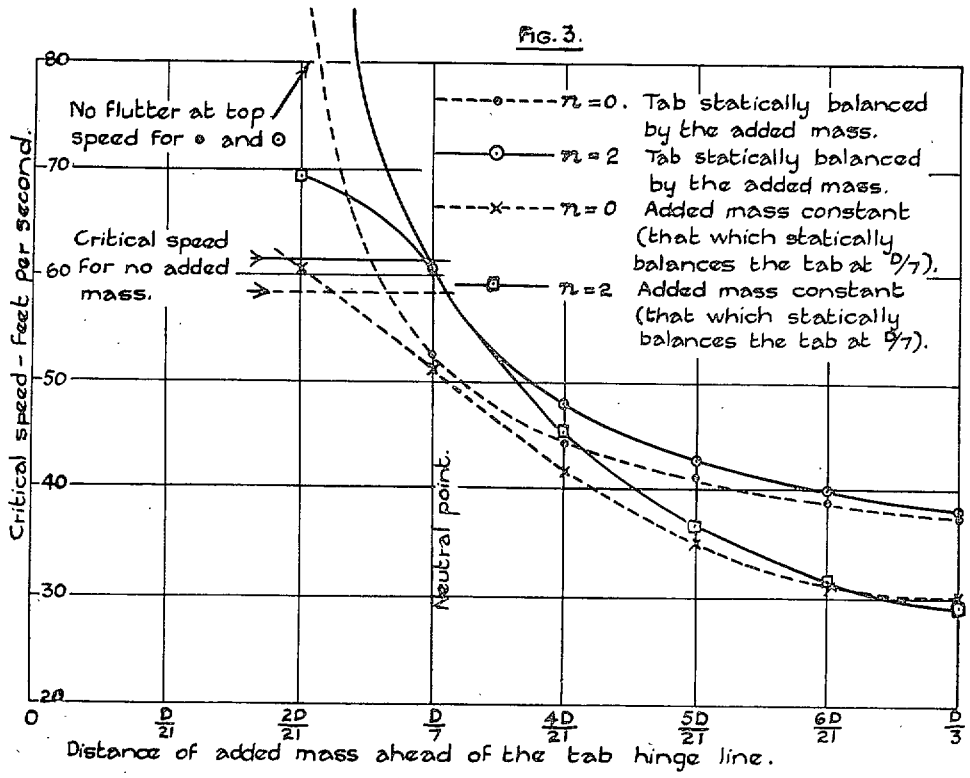

FIG. 3.

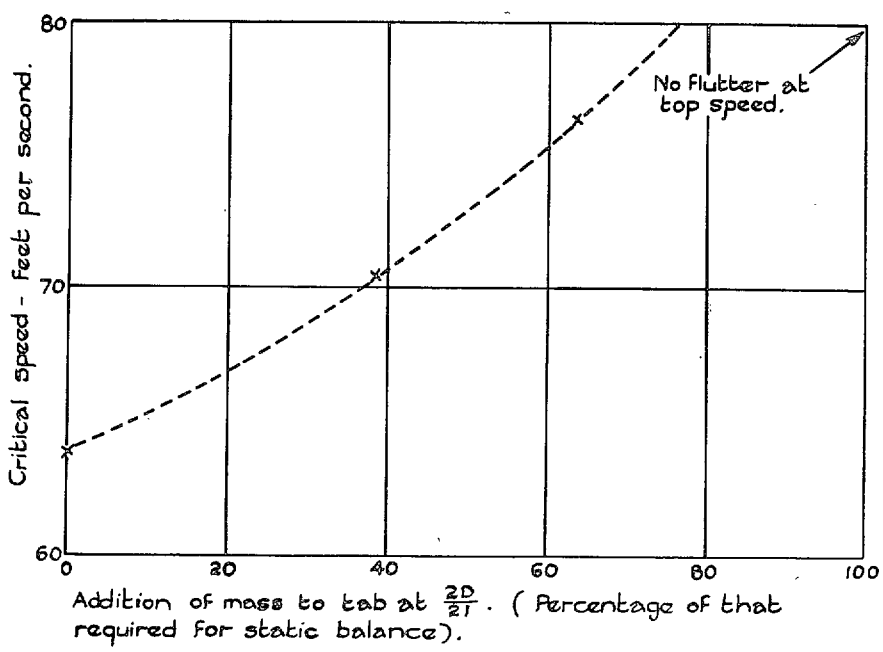

FIG. 4.

FIGS. 3 and 4. The effect of tab mass balance.

(1752) Wt. 18/9296 K5 12/55 Hw. PRINTED IN GREAT BRITAIN

Publications of the Aeronautical Research Council

ANNUAL TECHNICAL REPORTS OF THE AERONAUTICAL RESEARCH COUNCIL (BOUND VOLUMES)

1938 Vol. I. Aerodynamics General, Performance, Airscrews. 50*s.* (51*s.* 2*d.*)
Vol. II. Stability and Control, Flutter, Structures, Seaplanes, Wind Tunnels, Materials. 30*s.* (31*s.* 2*d.*)

1939 Vol. I. Aerodynamics General, Performance, Airscrews, Engines. 50*s.* (51*s.* 2*d.*)
Vol. II. Stability and Control, Flutter and Vibration, Instruments, Structures, Seaplanes, etc. 63*s.* (64*s.* 2*d.*)

1940 Aero and Hydrodynamics, Aerofoils, Airscrews, Engines, Flutter, Icing, Stability and Control, Structures, and a miscellaneous section. 50*s.* (51*s.* 2*d.*)

1941 Aero and Hydrodynamics, Aerofoils, Airscrews, Engines, Flutter, Stability and Control, Structures. 63*s.* (64*s.* 2*d.*)

1942 Vol. I. Aero and Hydrodynamics, Aerofoils, Airscrews, Engines. 75*s.* (76*s.* 3*d.*)
Vol. II. Noise, Parachutes, Stability and Control, Structures, Vibration, Wind Tunnels. 47*s.* 6*d.* (48*s.* 8*d.*)

1943 Vol. I. Aerodynamics, Aerofoils, Airscrews. 80*s.* (81*s.* 4*d.*)
Vol. II. Engines, Flutter, Materials, Parachutes, Performance, Stability and Control, Structures. 90*s.* (91*s.* 6*d.*)

1944 Vol. I. Aero and Hydrodynamics, Aerofoils, Aircraft, Airscrews, Controls. 84*s.* (85*s.* 8*d.*)
Vol. II. Flutter and Vibration, Materials, Miscellaneous, Navigation, Parachutes, Performance, Plates and Panels, Stability, Structures, Test Equipment, Wind Tunnels. 84*s.* (85*s.* 8*d.*)

Annual Reports of the Aeronautical Research Council—

1933–34	1*s.* 6*d.* (1*s.* 8*d.*)	1937	2*s.* (2*s.* 2*d.*)
1934–35	1*s.* 6*d.* (1*s.* 8*d.*)	1938	1*s.* 6*d.* (1*s.* 8*d.*)
April 1, 1935 to Dec. 31, 1936	4*s.* (4*s.* 4*d.*)	1939–48	3*s.* (3*s.* 2*d.*)

Index to all Reports and Memoranda published in the Annual Technical Reports, and separately—

April, 1950 — R. & M. No. 2600 — 2*s.* 6*d.* (2*s.* 7½*d.*)

Author Index to all Reports and Memoranda of the Aeronautical Research Council—

1909–January, 1954. — R. & M. No. 2570 — 15*s.* (15*s.* 4*d.*)

Indexes to the Technical Reports of the Aeronautical Research Council—

December 1, 1936 — June 30, 1939	R. & M. No. 1850	1*s.* 3*d.* (1*s.* 4½*d.*)
July 1, 1939 — June 30, 1945	R. & M. No. 1950	1*s.* (1*s.* 1½*d.*)
July 1, 1945 — June 30, 1946	R. & M. No. 2050	1*s.* (1*s.* 1½*d.*)
July 1, 1946 — December 31, 1946	R. & M. No. 2150	1*s.* 3*d.* (1*s.* 4½*d.*)
January 1, 1947 — June 30, 1947	R. & M. No. 2250	1*s.* 3*d.* (1*s.* 4½*d.*)

Published Reports and Memoranda of the Aeronautical Research Council—

Between Nos. 2251–2349	R. & M. No. 2350	1*s.* 9*d.* (1*s.* 10½*d.*)
Between Nos. 2351–2449	R. & M. No. 2450	2*s.* (2*s.* 1½*d.*)
Between Nos. 2451–2549	R. & M. No. 2550	2*s.* 6*d.* (2*s.* 7½*d.*)
Between Nos. 2551–2649	R. & M. No. 2650	2*s.* 6*d.* (2*s.* 7½*d.*)

Prices in brackets include postage

HER MAJESTY'S STATIONERY OFFICE

York House, Kingsway, London W.C.2; 423 Oxford Street, London W.1 (Post Orders: P.O. Box 569, London S.E.1); 13a Castle Street, Edinburgh 2; 39 King Street, Manchester 2; 2 Edmund Street, Birmingham 3; 109 St. Mary Street, Cardiff; Tower Lane, Bristol, 1; 80 Chichester Street, Belfast, *or through any bookseller*

S.O. Code No. 23–2952